Republic of Iraq
Ministry of Higher Education and
Scientific Research
University of Babylon
Collage of Engineering
Environmental Engineering Department

Organic Dyes Removal from Aqueous Solution Using Plant Waste

A Thesis

Submitted to the Department of Environmental Engineering of the College of Engineering in University of Babylon as Partial Fulfillment of the Requirements for the Degree of Master in Engineering / Environmental Engineering

By

Sammer Hussain Muhammed Jasim

Supervisor by

Prof. Dr. Isra'a Sadi Abdul-Amir Samaka

2023 A.D **1444 A.H**

بسم الله الرحمن الرحيم

((يَرفَعِ اللهُ الذِين امنُوا مِنكُم والذين
أُوتُوا العِلمَ دَرَجاتٍ واللّهُ بِما تَعمَلُونَ خَبِيرٌ .))

صدق الله العلي العظيم

سورة المجادلة

الآية

١١

Dedication

gift

To the symbol of devotion and sincerity, which showered us with her love and tenderness

Dear mother

To the source of goodness, sacrifice and altruism

My dear father

To the example of giving, pride and sacrifice

my brothers and sisters

To the great maqam with a fragrant biography

dear grandmother

To all who love me sincerely and sincerely

I dedicate my research to...

Sammer

2023

Supervisor's Certification

I certify that this thesis (Organic Dyes Removal from Aqueous Solution Using Plant Waste) and submitted by the student - Sammer Hussain Mohammed Jasim was prepared under my supervision at the Department of Environmental /College of Engineering /University of Babylon as a part of requirements for a master degree of science in Environmental Engineering .

Signature :

Supervisor : Prof. Dr. Isra'a Sadi Abdul-Amir Samaka

Date : / / 2023

I certify that this thesis mentioned above has been completed in Environmental Engineering in the College of Engineering /University of Babylon

Signature :

Head of Department : Asst. Prof. Dr. Hussein A.M. Al-Zubaidi

Date : / /2023

Examining Committee Certificate

We certify that we have read this thesis entitled (Organic Dyes Removal from Aqueous Solution Using Plant Waste) and as an examining cee examined that student (Sammer Hussain Mohammed Jasim) in its content and that in our opinion it meets a standard of a thesis for the degree of master in Engineering / Environmental Engineering

Signature:
Name:
Prof .Dr. Saif Salah Alquzweeni
(Chairman)
Data: / /2023

Signature:
Name:
Asst.Prof.Dr.Hussein A.M. Al-Zubaidi
(Member)
Data: / /2023

Signature:
Name:
Asst. Prof.Dr.Tariq J.Al-Musawi
(Member)
Data: / /2023

Signature:
Name:
Prof. Dr. Isra'a Sadi Abdul-Amir Samaka
(Supervisor)
Data: / /2023

Approval of Head of Department

Signature:
Name: Asst.Prof.Dr. Hussein A.M. Al-Zubaidi
Data: / /2023

Approval of the Dean of College

Signature:
Name: Prof.Dr. Hatem Hadi Obeid
Data: / /2023

Acknowledgement

"In the Name of Allah, the Most Gracious, the Most Merciful"

Praise to Allah his Majesty before anything and after anything and to the prophet “Mohammed and Ahl-Al-Bait” for the strength, courage, and wisdom that Allah gave me to complete this humble work and lengthy journey this degree.

I would like to express my deepest gratitude and respect to my thesis supervisor Prof. Dr. Isra’a Sadi Abdul-Amir Samaka. I am very grateful for her precious time spent and useful suggestions which provided valuable guidance and important role in the completion of thesis as well as the moral support continued for the duration of the search, calling God richly rewarded here.

I would like to thanks to Head of Environmental Engineering Department, Asst. Prof. Dr. Hussein A.M. for his help and he never saved an effort to help us and others.

I would also like to thank the staff of environmental engineering laboratory at the University of Babylon for their assistance in providing laboratory equipment's through this work.

I wish to express my deepest respect and sincere appreciation to my family especially my father and mother for their support and help during my study.

Also, I would like to thank all those who helped me in one way or another

Sammer

2023

Abstract

In this study, the ability of Leucaena leucocephala seeds pods to biosorp Janus Green B dye (JGBD) and Crystal Violate dye (CVD) from wastewater was tested as available in many sites of Iraq and low cost natural plant. A series of laboratory experiments divided into two parts, the first was batch experiments and the second was continuous flow experiments, which was used to evaluate treatments and variables that may affect the sorption of two dyes in aqueous solutions.

Various techniques have been used for characterization the used adsorbent, including Fourier Transform Infrared (FTIR), Scanning electron microscopy (SEM) and Scanning probe microscope (SPM). In the batch study, factors affecting the sorption of the two dyes were studied at room temperature. These factors are, the pH of dye solution, contact time, sorbent dose and the initial dye concentration. The optimum parameters were selected for sorption at pH 9 for each dye, the dose of LLSP is 0.08 g/100 ml and 0.3 g/100ml for JGBD and CVD, respectively. The contact time was 30 minute and 45 minute for JGBD and CVD, respectively.

Experimental data were analyzed by two isothermal models, which were Langmuir and Freundlich. Langmuir model agreed with the experimental data to be the best model to simulate the maximum sorption of each dye, where the Langmuir constant is related to the sorption capacity (q_{max}) of 142.85 mg/g and 45.45 mg/g with determination coefficient (R^2) of 0.9996 and 0.9906 for JGBD and CVD, respectively. The pseudo-second order model was the best kinetic model during kinetic study, indicated the chemical sorption as well as the intra-particle diffusion process. For continuous experiments, column parameters such as flow rate, bed height

and initial dye concentration were studied. The analyzed column data showed that the breakthrough curves were greatly affected by these factors. The bed depth service time model, Thomas and Yoon Nelson kinetic model were used to analyze the experimental column data.

High values of determination coefficient (R^2) were obtained for all kinetic models used, and the deviation between the experimental values and the values estimated by these models was very small. It was concluded that Leucaena leucocephala seeds pods is an sorbent with a high ability to remove JGBD and CVD from aqueous solutions.

Table of Contents

List of Tables

Table of Figures

List of Symbols

Symbol	Description	Unit
A	Cross section area of the column	m^2
C	Intraparticle Diffusion constant	mg/g
C_{ads}	Adsorbed concentration of dye onto biosorbent	mg/g
C_b	Breakthrough point concentration of dye	mg/l
C_e	concentration of dye at equilibrium	mg/l
C_o	Initial concentration of dye	mg/l
K_1	Pseudo-first-order rate constant	min^{-1}
K_2	Pseudo-second-order rate constant	$g.mg^{-1}.min^{-1}$
K_a	Langmuir sorption equilibrium constant.	1/mg
K_B	Sorption rate constant	1/mg.min
K_F	Freundlich constant related to relative sorption capacity of biosorbent	$(mg/g)(1/mg)^{1/n}$
K_{ip}	Intraparticle Diffusion rate constant	$mg.g^{-1}.min^{-1/2}$
K_{TH}	Thomas rate constant	1/min.mg
K_{YN}	Yoon-Nelson rate constant	min^{-1}
M_{total}	Total amount of dye inter the column	mg
n	Freundlich constant related to intensity	---------
q_B	Dynamic breakthrough sorption capacity per unit volume of biosorbent bed	mg/l
q_e	Amount of dye ions adsorbed per unit mass of biosorbent at equilibrium	mg/g
Q_{exp}	Experimental uptake or maximum capacity of the column	mg/g
q_m	maximum sorption capacity	mg/g
q_t	Amount of dye ions adsorbed per unit mass of biosorbent at time t	mg/g
Q_{th}	Maximum sorption per unit weight of biosorbent	mg/g
Q_{total}	Total quantity of dye ions adsorbed in column bed for a given inlet dye ions concentration and flow rate	mg
Q_{total}	Total quantity of dye ions adsorbed in column bed for a given inlet dye ions concentration and flow rate	mg

Q_V	Volumetric feed flow rate	ml/min
Q_V	Volumetric feed flow rate	ml/min
R%	The percentage of dye removal	-------
R_L	Separation factor	---
S_c	The column sectional area	cm^2
t	The time required for 50% adsorbate breakthrough	min
t_b	Time needed at which the sorption column reaches the breakthrough point with specific saturation percentage	min
t_e	Time needed to exhaust the bed of column	min
U_f	Linear flow velocity	cm/min
V	Volume of solution	l
V_b	Volume of effluent at breakthrough point	ml
V_{eff}	Volume of effluent at exhaustion	ml
w, m	Mass of biosorbent in batch and column system respectively	g
Z , H	Bed depth of column	cm
Z_c	Critical bed depth	cm
λ_{max}	The maximum wavelength	nm

List of Abbreviation

Abbreviation	Description
AC	Activated carbon
AFM	Atomic Force Microscopy
AIC	Akaike information criterion
AR	Acid red
ASS	Annona squmosa seeds
BDST	Bed-depth service time
BET	Brunauer, Emmet and Teller
CR	Congo red
CTDLP	hemically treated durian leaf powder
CVD	Crystal Violate Dye
EDS	Energy-Dispersive Spectroscopy
FTIR	Fourier-Transformed Infrared Radiation
IUPAC	International Union of Pure and Applied Chemistry
JGBD	Janus Green B Dye
JLP	Jackfruit leaf powder
LLSP	Leucaena leucocephala seeds pods
MB	Methylene blue
MG	Malachite green
MLP	Mango leaves powder
MTZ	Mass Transfer Zone
pH_{pzc}	The point of zero charge
R^2	Liner correlation coefficient
R_L	Separation factor
rpm	Revolution per minute
RSM	Reaction surface methodology
S.E	The Standard error of the estimate
S_{BET}	Specific surface area determined by BET method
SEM	Scanning Electron Microscopy
SPM	Scanning Probe Microscope
SPSS	Statistial Package for the Social Sciences
t_{cal}	Calculated time
t_{exp}	Experimental time

Chapter One

Introduction

Chapter One

Introduction

1.1 Introduction

Industrialization and modernization have generated many pollutants that have bad effects on the environment (Soylak et al., 2011; Jacob et al., 2018; Bushra et al., 2021). Water pollution on the global scale has posed challenges to environmental scientists because of continuous misuse of water from textile, rubber, pharmaceutical, dye industries, pesticides industries, and municipal wastewater.

Approximately 10,000 types of dyes are commercially available, and annually, about 1.6 million tons of dyes are produced for industrial uses (Kausar et al., 2007). Contamination of water resources with industrial dye, which is generally used to modify the color characteristics of different substrates is a severe threat to the ecosystem (Gupta et al., 2006; Gupta et al., 2007) due to its recalcitrant nature that made reluctant to aerobic digestion, heat, and light (Pearce et al., 2003; Ibrahim et al., 2010). This pollution is caused by the use of dyes in the clothing, paper, dyeing, and plastics industries. Because the dyes are very stable and solvable in water, failed dye treatment and disposal of these wastes into receiving waters causes huge damages to the environment, affecting photosynthetic activity (Regti et al., 2017), being toxic to aquatic life (Abdolali et al., 2014), and inherent toxicity, mutagenicity, and carcinogenicity (Asfaram et al., 2015).

In addition, overexposure to dyes has resulted in potentially life threatening complications such as skin harms, respiratory problems, and the probability of human carcinoma (Lellis et al., 2019). Due to toxicity of dyes, it is necessary to remove them from wastewater before discharge them to the natural environment. There are different treatment processes employed to complete degradation of the toxic textile wastewater components depending on the water

source and the application in the industry, physicochemical methods such as chlorination, coagulation-flocculation, adsorption, and advanced oxidation processes, such as ozonation, fenton treatments, electro-fenton methods, photo-fenton oxidation processes, photocatalytic oxidation/degradation, and membrane processes (Darwesh et al., 2021). This method is very dependent upon the type of the adsorbent used (e.g., activated carbon (AC), biomass, polymer, nanomaterial, etc.) (Moosavi et al., 2021). The cost of adsorbent production is not the only factor involved in developing an excellent adsorbent.

The adsorption performance, regeneration ability, and adsorbent separation are other important features of an effective adsorbent (Moosavi et al., 2020). Among the large number of adsorbents, activated carbon (AC) exhibited advantages over other adsorbents for their high surface area, microporous character, chemical nature of their surface, and high adsorption capacity when used on wastewater with different dye molecules, when activated carbon is deemed too expensive and the regeneration is difficult. So, there have been required for finding an alternative low-cost adsorbents (Moosavi et al., 2019). Recently, agricultural wastes have received considerable attention due to their abundant surface functional groups, porous structures, additional inorganic minerals, and high surface area. Many researchers studies the dye adsorption on various agro-waste materials such as oil cake (Ajmal et al., 2005), corn cobs (Milenković et al., 2013), tobacco residue white sugar (Ghaedi et al., 2014), sawdust (Suganya et al., 2017), sugarcane bagasse (Fideles et al., 2018), rice husk (Chen et al., 2019), gram husk (Gupta et al.,2019), pine cone (Pholosi et al.,2020), Astragalus bisulcatus tree (Jain et al., 2020), tea residue (Jain et al., 2020), vinasse (Li et al., 2021), groundnut shell (Alshabib et al., 2021).

1.2 Statement of problem

Problem in several countries of the world are the industrial processes that generate significant amounts of effluents containing heavy metals and dyes that affect the quality of water one of the resources most used by organisms. Water is a fundamental to the existence and maintenance of life and for this, it must be present in the environment in appropriate quantity and quality (Silva et al., 2019). When colorants are present in aquatic environments, color is generally the first impact to be recognized in an effluent because very small amounts of synthetic dyes in water interfere with the penetration of sunlight into the aquatic environment and thus retard photosynthesis, inhibiting the growth of aquatic biotics and interfere with the solubility of gases in bodies of water, It also causes many diseases in humans (Souza, 2013).

For agricultural waste, it is noteworthy that these plants are undesirable and most of the time they are extracted from nature and discarded or eliminated by chemical processes, which is observed two problematic: one is to give a useful end to vegetal species that in the majority of the times causes disorder to different human activities like agricultural, forestry, animal husbandry, ornamental, nautical, energy production between others (Silva et al., 2019). The other is chemical contamination of water which is a worldwide concern, in the case here specified by dyes. Compared with other methods, the removal of dyes from aqueous solutions by the adsorption process proved to be an excellent alternative for effluent treatment, as well as an economical technique (Crini, 2006).

1.3 The objectives of this Study

This work aims to investigate the removal of Janus green B dye (JGBD) and Crystal violate dye (CVD) from polluted water by sorption technique and take advantage of agricultural low-cost waste to remove organic dyes from aqueous solution instead of high-cost materials.

Chapter Two
Background and Literature Review

Chapter Two
Background and Literature Review

2.1 Introduction

Because of its critical role for the survival of many biota on our planet, water is the greatest gift from nature (Mikosch et al., 2020). Because it is one of the world's scarce natural resources, preserving its quality is a worldwide requirement that is growing by the day. Unfortunately, many crises, conflicts, and battles over limited water supplies have occurred in the new century. Moreover, several water contaminants are linked to numerous human activities that are discharged into water bodies at the same time, creating serious decline in water requirements (Richa and Roy Choudhury, 2020).

Clean water reduced will affect the agricultural, commercial, household, and industrial sectors. Water pollution is caused by a variety of sectors, including machinery manufacture, printing, textile (Yao et al., 2020), chemicals, electronics, and pharmaceutical industries (Özdemir et al., 2019). They are responsible for the seepage of several pollutants into the aquatic environment as byproducts, including dyes (Tonato et al., 2019), heavy metals, phenols (Mohammed et al., 2018), pesticides (Behloul et al., 2017), insecticides, and medicines (de Lima et al., 2018). These impacts can have negative consequences for human and animal health (neurotoxicity, carcinogenicity, and reproductive capacities) (Fontana et al., 2018). It may also lead to eutrophication and the suppression of photosynthesis (Nishikawa et al., 2018). This was owing to its inability to degrade and/or its significant accumulative effects (Novais et al., 2018).

2.1.1 Toxic organic pollution

In the future decades, growing urbanization, climate change, and human-caused demand on natural resources will provide new issues in preserving water supplies. Organic dye contamination of water resources is a rising problem.

organic pollutants such as dyes and phenolic compound are extensively used in the textile, paper, cosmetic, pharmaceutical, paint, leather, food, plastic, and etc. industries contributed to severe environmental contamination especially water pollutions. Every year, more than 7×10^5 metric tonnes of synthetic dyes are generated, and above 100,000 of dyes commercially available that have been reported. The textile wastewater discharge approximately 15% from the whole world production of dyes, with consume almost 97% of local dye wastewater are generated by the food, chemical, and textile industries. Yet, the bulk left–over dyes produced during dyeing and finishing process are released to the environment either with or without any further remediation, that might reflect to serious issue arises as these wastewater flow into natural waterbodies, due to the dyes are toxic, mutagenic, and carcinogenic (Muhammad and Norzahir, 2020).

Dyes are also harm to human body for examples, dysfunction of kidney, reproductive system, liver, brain and central nervous system. Other than that, even little amount of dyes such as below 1 ppm can be seen clearly in receiving waterbodies whereas can block sunlight from penetrate and prohibit the photosynthesis process of aquatic plants. Adsorption for the removal of organic micropollutants is still the method of choice in large-scale operations, such as drinking water treatment, since it works effectively for a wide range of chemicals (Westerhoff et al., 2012).

The global textile industry is estimated to be worth around $1 trillion USD and its contribution towards total world exports is around 7%, employing 35

million people worldwide (Desore and Narula, 2018). Thus, this industry has a high impact on the environment and human health in general, due to the pollution it causes. The most prominent and destructive form of pollution, caused by the textile industry, is the water pollution due to manufacturing of dyes. Textile effluents are both aesthetically polluted, and have high salinity, chemical oxygen demand, and ecotoxicity (Liang et al., 2020), and due to their increasing ubiquity in surface water, can lead to adverse effects to human and wildlife health and to aquatic ecosystems in general. Most synthetic dyes are highly toxic to humans and aquatic beings, and have acute and chronic effects. For example, reactive dyes are notorious, causing health issues such as, dermatitis, occupational asthma, rhinitis, and other allergic reactions for the workers involved in these dyes manufacturing (Chavan, 2011). Dyes are also mutagenic and carcinogenic in nature (Singh, 2018; Lellis et al., 2019), which leads to chronic effects, such as kidney, urinary bladder, and liver cancer in dye workers.

An xanthene dye called erythrosine is carcinogenic, neurotoxic and DNA-damaging for humans and animals alike (Pal, 2017). Metal complexed dyes, which are widely used for their resistance, have heavy metals, such as copper, nickel, and chromium. When discharged to aquatic environments, these metals can be taken up by fish gills and can be transferred to humans through the food chain (Lellis et al., 2019). Current treatment methods are inadequate to treat dye effluents effectively, because of their recalcitrant nature in aerobic environments (Vikrant et al., 2018), and thus, these substances can linger in soil and lead to bioaccumulation, leading to complications in organisms higher up the food chain 20 (Xiang et al., 2016). Thus, current effluent treatment techniques are inadequate for the dyeing industry and to prevent the further insemination of surface water with such mutagenic and carcinogenic molecules.

2.2 Health and environmental effects of dyes

The textile industry is one of the important industries that generates a large amount of industrial effluents. Color is the main attraction of any fabric. Manufacture and use of organic dyes for fabric dyeing has therefore become a massive industry. organic dyes have provided a wide range of colorfast, bright hues. However, their toxic nature has become a cause of grave concern to environmentalists. Use of organic dyes has an adverse effect on all forms of life. . These organic materials react with many disinfectants, especially chlorine, and form byproducts (DBPs) that are often carcinogenic and therefore undesirable. This effluent, if allowed to flow in the fields, clogs the pores of the soil resulting in loss of soil productivity (Manzoor and Sharma, 2020).

The industrial activities like textile industry has environmental problems, being one of the oldest and most technologically complex of all industries. A number of substances used in the textile industry can mean not only environmental, but also health problems. Among the many chemicals whose presence has been detected in textile wastewater, dyes are among the most important pollutants (Brillas et al., 2015; Mohamed et al., 2016; Zare et al., 2018). Worldwide environmental problems associated with the textile industry are mainly associated with water pollution caused by the discharge of untreated effluent, as well as those due to the use of potentially toxic substances, especially during processing (Khan and Malik, 2014; Pattnaik et al., 2018).

The scientific literature regarding potential adverse health effects of chemical substances in the textile industry is mainly related with human exposure during textile production. In contrast, the information about exposure of consumers is much more limited (KEM, 2014). There are numerous 3 activities involved in the textile and clothing industry, going from the treatment of raw materials to finishing activities such as bleaching, printing, dyeing, impregnating, coating, plasticizing, etc. As result of these activities, the main chemical pollutants are

dyes, which contain carcinogenic amines, metals, pentachlorophenol, chlorine bleaching, halogen carriers, free formaldehyde, biocides, fire retardants, and softeners (Brigden et al., 2012). Most research about health effects of chemicals in textiles concern allergic skin reactions. Disperse dyes, used for staining synthetic fibers have been reported to be the most common causes of textile allergy, being contact allergy to disperse dyes a clinically relevant problem (Ryberg et al., 2006, 2009; Malinauskiene et al., 2013; Coman et al., 2014).

However, contact allergy is not the only human health problem. It is well known that humans are exposed to toxicants mainly through the diet (food and drinking water) and breathing (air pollution). However, for some chemicals dermal exposure should not be minimized. In relation to dermal exposure, although most chemicals added during the processes of manufacturing clothes are rinsed out, residual concentrations of some substances can remain and can be released during the use by the consumers (Luongo et al., 2014).

2.3 Techniques for removal toxic organic

Efficient techniques for the removal of highly toxic organic compounds from water have drawn significant interest. A number of methods such as coagulation, filtration with coagulation, precipitation, ozonation, ion exchange, reverse osmosis and advanced oxidation processes have been used for the removal of organic pollutants from polluted water and wastewater. These methods have been found to be limited, since they often involve high capital and operational costs.

On the other hand ion exchange and reverse osmosis are more attractive processes because the pollutant values can be recovered along with their removal from the effluents. Reverse osmosis, ion exchange and advanced oxidation processes do not seem to be economically feasible because of their relatively high investment and operational cost (Nageeb, 2013). Among the possible techniques for water treatments, the adsorption process by solid adsorbents shows potential as one of the most efficient methods for the removal of organic contaminants in wastewater treatment.

Adsorption has advantages over the other methods because of simple design and can involve low investment in term of both initial cost and land required. The adsorption process is widely used for treatment of industrial wastewater from organic and inorganic pollutants and meet the great attention from the researchers. In recent years, the search for low-cost adsorbents that have pollutant–binding capacities has intensified. Materials locally available such as natural materials, agricultural wastes and industrial wastes can be utilized as low-cost adsorbents. Activated carbon produced from these materials can be used as adsorbent for water and wastewater treatment (Crini,. 2005).

Table (2.1): Various physical, chemical, and biological methods for the removal of dye from wastewaters (Kumar, et al., 2012).

Method		Advantages	Disadvantages
Physical	Adsorption	Good removal of wide variety of dyes	Nonselective to adsorbate
	Membrane filtration	Remove all dye types	Concentrated sludge production
	Ion exchange	Regeneration: no adsorbent loss	Not effective for all dyes
	Irradiation	Effective oxidation at lab scale	Requires a lot of dissolved O2
	Electro kinetic coagulation	Economically feasible	High sludge production
	Coagulation-flocculation	Good elimination of insoluble dyes	Cost of sludge treatment garbage dump
	Adsorption on active carbon powder coupled with coagulation process	Matter, organic matter, and low influence on color Fast fouling of suspended matter	Cost of actived carbon powder
	RO	Retention of mineral salt and hydrolyzed reactive dyes and auxiliaries	High pressure process, Fouling with high concentrations
	Nanofiltration	Separation of mineral salts, hydrolyzed reactive dyes and auxiliaries	Treatment for complex solution with a high concentration of pollutant
	Ultrafiltration / microfi Itra t ion	Low pressure process	Inadequate quality for reused the permeate
Chemical	Adsorption	Good removal of wide variety of dyes	Nonselective to adsorbate
	Fenton's reagent	Effective decolorisation of both soluble and insoluble dyes	Sludge generation
	Ozonation	Good elimination of color	No diminution of COD values. Extra costs
	Photochemical NaOCl	No sludge production Initiates and accelerates azo-bond cleavage	Formation of by-product release of aromatic amine
	Electrochemical destruction	Breakdown compounds are	High cost of electricity
Biological	Standard Biological degradation	Efficiency of oxidizable matter 90%	Low biodegradability of dye, the salt concentration stay constant

2.4 Adsorption

Adsorption is used as top quality treatment procedures for the removal of dissolved organic pollutants like dyes from industrial wastewater. Adsorption is the adhesion of atoms, ions or molecules from a gas, liquid or dissolved solid to a surface. This process creates a film of the adsorbate on the surface of the adsorbent. Adsorption is a surface phenomenon which deals primarily with the utilization of surface forces. When a solution having absorbable solute, also called as adsorbate, comes into contact with a solid, called as adsorbent, with highly porous surface structure liquid-solid intermolecular forces of attraction causes the solute to be concentrated at the solid surface. Adsorption is one of the unit operations in the chemical engineering processes used for the separation of industrial wastewater pollutants (Vital, et al., 2016).

Adsorbents are mainly derived from sources such as zeolites, charcoal, clays, ores, and other waste resources. Adsorbents prepared from waste resources used include coconut shell, rice husk, petroleum wastes, tannin-rich materials, sawdust, fertilizer wastes, fly ash, sugar industry wastes, blast furnace slag, chitosan and seafood processing wastes, seaweed and algae, peat moss, scrap tyres, fruit wastes, etc. (Cameselle et al., 2013).

2.4.1 General aspects of adsorption process

Heinrich Kayser (Choudhary, 2017), a German scientist, coined the word "adsorption" in 1881. Environmental adsorption research on the adsorptive removal of contaminants from the aqueous phase have exploded in the last decade. Because of its comparatively simple design, operation, cost effectiveness, and energy efficiency, it is favoured over other techniques (Tan and Hameed, 2017).

It is a mass transfer process in which a material (adsorbate) goes from a gas or liquid phase to a solid or liquid condensed phase and forms a surface monomolecular layer (substrate, the adsorbent). It frequently involves molecules, atoms, or even ions from a dissolved gas, liquid, or solid adhered to the surface. In practice, adsorption is carried out in a column filled with porous sorbents as a batch or continuous operation (Abebe et al., 2018). The term sorption is frequently used interchangeably with the phrase adsorption. Absorption and adsorption differ in that molecules penetrate a three-dimensional matrix in absorption, whereas molecules attach to a two-dimensional matrix in adsorption (Qi, et al., 2017; Al-Ghouti and Da'ana, 2020).

Because the process is frequently reversible (the opposite is termed desorption), sorption is responsible for both the extraction and release of chemicals. Adsorption can be caused by physical forces or chemical bonds, although it is most commonly caused by surface energy. Surface particles that are partially exposed tend to draw additional particles into place. There are numerous classifications for adsorption, and Figure (2.1) shows on the type of bond (physical or chemical) created between the adsorbent and the pollutant, as well as its features (Noble, et al., 2004).

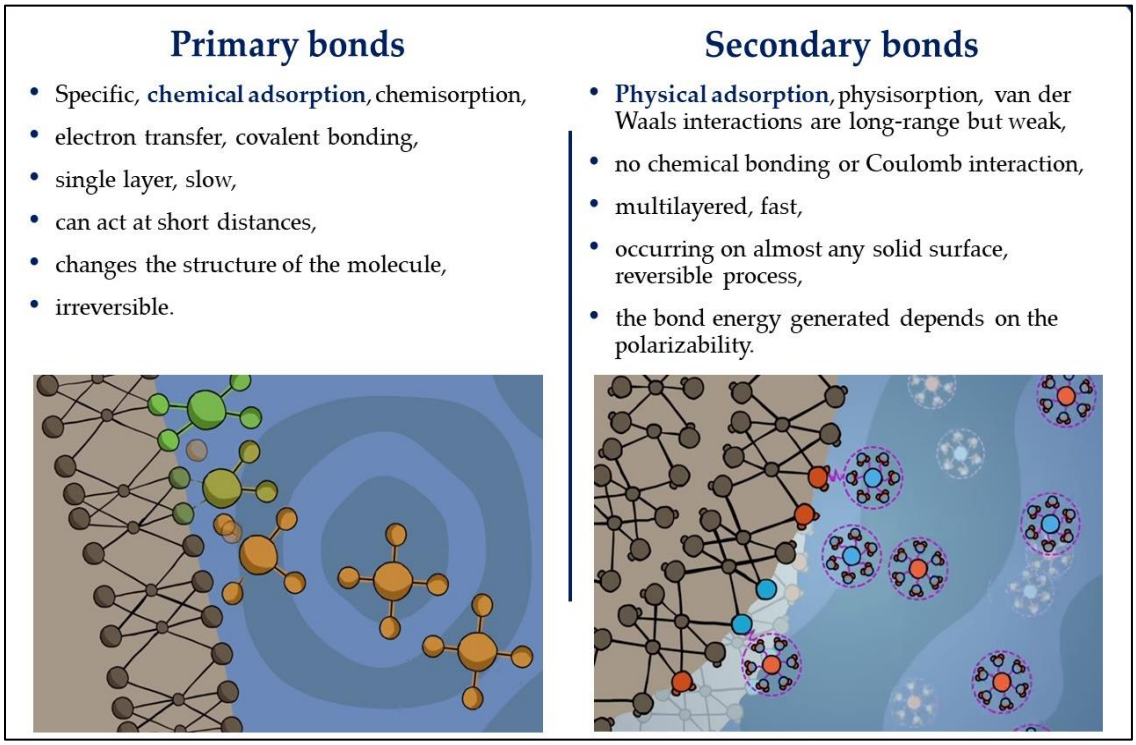

Figure (2.1): Types of adsorption bonds and nature of adsorption (Rápó, and Tonk, 2021).

Because adsorption occurs in a variety of natural, biological, physical, and chemical systems, humans often use it in industrial operations to reap the advantages. Due to its cheap cost and ease of operation, it is increasingly utilized for purification or separation purposes; it is also a wastewater treatment technology for the removal of a wide variety of substances from industrial wastewater (Guo and Wang, 2019; Al-Ghouti and Da'ana, 2020).

Adsorption is often used to remove low levels of non-degradable organic chemicals from groundwater, drinking water production, process water, or as a tertiary treatment, such as after biological water purification (Rápó and Tonk, 2021)

Adsorption, also known as surface enrichment, is the process of atoms, ions, and molecules binding to the active centers of a solid surface (surface binding). In most circumstances, the process does not need excessive energy

input; the removal rate is frequently dictated by the kinetic equilibrium, which is governed by the adsorbent's surface properties and composition. Adsorption progress is substantially determined by the adsorbent's affinity, capacity to react with the pollutant, and adsorption process between the sorbent and the pollutant's functional groups (Zhao, et al., 2020; Szende,et al., 2020). The concentration value at which equilibrium stability between the solid and liquid phase volumes is achieved is termed the end point of the adsorption process (Szende et al., 2020).

2.4.2 Types of adsorption

Physical adsorption and chemical adsorption are characterized by the nature of the forces responsible for the creation of the interfacial layer, and each has its own set of features (Brandani, 2021).

2.4.2.1 Physical adsorption

Physisorption or physical adsorption is a process characterized by relatively small force (Van Der Waals force) between the solid matrix and the material. The physical adsorption can be easily reversed because these forces are not strong (Parvathi et al., 2007).

The reversible physical adsorption is depending on the attractive forces strength between adsorbent and adsorbate. Therefore, when these forces are weak, desorption can be readily affected. In physical adsorption the adsorbed molecule is not fixed to a specific site on the surface, but it is rather free to undergo translational movement within the interface (Hameed, 2016).

Physical adsorption occurs rapidly and may be a mono-molecular (unimolecular) layer, or may be two, three or more layers thick (multi-molecular). If unimolecular, it is reversible; if multi-molecular, such that capillary pores are filled, hysteresis may occur. As physical adsorption happens,

it starts as a monolayer, progresses toward becoming multilayered, and afterward, if the molecules are close to the pore size, capillary condensation occurs, and the pores load up with pollutant (Seader and Henley, 1998).

2.4.2.2 Chemical adsorption

Chemical adsorption or chemisorption results from the formation of bonds between the adsorbent and the substrate. Compared to physical adsorption, it involves higher adsorption energies and the reaction may be irreversible. The heat of adsorption is significantly greater than for physical adsorption, ranging from 40 to 400 kJ/mol. The adsorbate frequently undergoes chemical change as a result of the reaction (Hameed, 2016).

Chemical adsorption usually contains only monolayer coverage and it is a site specific reaction and happening at the locations of specific functional group. Functional groups are usually have special arrangements of atoms in organic compounds that give the compounds their specific chemical and physical properties (Uddin et al., 2009). The most important characteristics of physical and chemical adsorption as listed in Table (2.2).

Table (2.2): Difference between physical and chemical adsorption (Lee and Lin, 2000).

Physisorption	Chemisorption
Van der Waals force between adsorbate and adsorbent	Include formation of chemical bonds between adsorbate and adsorbent
Low enthalpy of adsorption (20-40 kJ/mole)	High enthalpy of adsorption (40-400 kJ/mole)
Multi-molecular layer may formed	Monolayer is formed
Reversible process	Irreversible process
Occurs in many solid/fluid system	A highly specific process
Perturbation of the electronic states of adsorbent and adsorbate is minimal	Changes in the electronic states may be detectable by suitable physical means
Equilibrium can be quickly achieved	May take a longer time to achieve equilibrium

2.4.3 Factors affecting the adsorption process

There are many factors affecting the adsorption process, including pH, absorbent dose, contact time, etc., these factors have positive or negative effects, these factors will be identified in details.

2.4.3.1 Effect of solution pH

The pH of the dye solution is the most important factor in practically all adsorption methods. This component influences the adsorbent capacity as well as the process efficiency. The activity of functional groups in the adsorbent, competition with coexisting ions in the solution, and the surface charge of the adsorbent are all affected by pH. The characteristics of the adsorbent, the adsorption process, and dye molecule dissociation can all be influenced by the pH of the aqueous medium.

The pH of the solution can affect not just the adsorbent but also the chemical structure of the dye. The pH affects the adsorbed ion surface charge

and degree of ionization (Rápó et al., 2018; Brito et al., 2018; Khasri et al., 2021). Anionic dyes bind more efficiently to the adsorbent surface in acidic fluids, whereas cationic dyes bind more effectively in basic media.

The surface of the adsorbent in the solution is protonated when acidic solution is added to it, allowing the anionic dye to bind more efficiently on its surface due to electrostatic attraction. But, the addition of basic solution, deprotonates the biomass surface in basic media, resulting in a repulsive interaction between the anionic dye and the biomass. Cationic dyes, on the other hand, exhibit the opposite behavior.

2.4.3.2 Effect of contact time

The impact adsorbate / adsorbent contact time can help in determining the potential prompting of binding and the optimum time for the removal of contaminants. Also, the contact time is an essential factor which governs the kinetics of the adsorption process and oversees the inspiring use of an adsorbent for practical application and influences the economic efficiency of the adsorption (Das and Das, 2013). In general, removal efficiency rises quickly at first due to the availability of a large number of empty surface-active adsorbing sites but, as time passes, the adsorption process slows as the number of surface-active adsorbing sites decreases, forcing the molecule to go further and deeper through the pores, and the adsorption process eventually reaches an equilibrium (Mashkoor and Nasar, 2019).

2.4.3.3 Effect of biosorbent dose

Through the quantitative ratio of adsorbate / adsorbent, the amount of adsorbent is an essential parameter that controls the adsorption process. The dose of the adsorbent is an essential parameter since it impacts the adsorbent capacity for a particular initial concentration (sentürk and Alzein, 2020). According to Kroeker rule, the specific adsorbed volume decreases with increasing adsorbent mass for a fixed initial concentration (Pernyeszi et al., 2019). As a result, increasing the adsorbent dosage has a positive correlation with dye removal efficiency and performance. At constant contaminant concentrations, increasing adsorbent dose provides increased active surface area for adsorption and more active adsorption sites (Ma et al., 2020).

The effectiveness of pollutant removal improves as the concentration the quantity of adsorbent increases, but there is no direct correlation between the amount of adsorbent and the amount of pollutant eliminated. The quantity adsorbed per species decreases as the concentration of biosorbent increases. This is due to the fact that when the concentration of biosorbent increases, the shape of the sorption isotherm changes. In higher concentrated suspensions, portions of the surface or surface groups may not be saturated, resulting in a reduction in the specific adsorbed quantity (Neag et al., 2019; Dehghani et al., 2021).

The capacity of the dye removal process may be reduced for two reasons (Popa et al., 2021):

- adsorption sites remain unsaturated while the number of sites available for adsorption increases; or
- adsorbent particle aggregation or agglomeration occurs, reducing the available surface area and lengthening the diffusion path. In recent years, scientific investigations have looked into the removal of various dyes using various concentrations of broad-spectrum adsorbent.

2.4.3.4 Effect of initial contaminant concentration

The adsorbate uptake mechanism is particularly dependent on the initial concentration (Bouras et al., 2017). At low concentrations, contaminants are adsorbed by specific active sites, while at higher concentrations lower adsorption yield is due to the saturation of adsorption sites (El-Sayed et al., 2010). Initial concentrations increased the number of collisions between adsorbate and biosorbent, which could improve the sorption process (Ahmad et al., 2018). Hence, the removal of solute is strongly dependent upon the initial solute concentration. It is always necessary to identify the maximum saturation potential of a adsorbent, for which experiments should be conducted at the highest possible initial solute concentration (Vijayaraghavan and Yun, 2008).

2.4.3.5 Effect of particle size

Particle size can be an essential element in heterogeneous chemical reactions and adsorption (Stjepanović et al., 2021), despite the fact that it is rarely addressed in sorption investigations. Because of the tiny particle sizes, the specific surface area is increased. The total surface area of a solid substance per unit of mass, or specific surface area, is an important property for adsorption processes. The size of the particles, as well as the structure and porosity of the material, influence specific surface area (Šljivić-Ivanović and Smičiklas, 2020). The most frequent measuring unit is the m^2/g.

Two factors determine the link between adsorption capacity and particle size (Iqbal et al., 2011; Aljeboree et al., 2017):

- The chemical structure of the dye molecule (ionic charge) and chemistry (ability to generate hydrolyzed species); and
- The inherent property of the adsorbent (its crystallinity, porosity and rigidity of the polymeric chains).

Smaller particle sizes result in increased adsorption capacity and efficiency in static batch adsorption because there are more active sites for binding (Rápó and Tonk, 2021).

2.4.3.6 Effect of temperature

The uptake capacity of each contaminant differs from one to another species of adsorbent with different response to the temperature (Zeraatkar et al., 2016). Some available studies suggested that increasing the temperature of adsorbent culture could possibly increase the removal efficiency of contaminant known as endothermic, due to increase the active sites tendency to adsorb pollutants, change of complex formation constant with temperature, increased number of functional groups involved in contaminant uptake, mass transfer resistance is reduced in the diffusion layer by reduction the thickness of the diffusion boundary layer around the adsorbent groups, more diffusion of adsorbate molecules across the external boundary layer and internal pores of the adsorbent particle (Mehta and Gaur, 2005; Meena et al., 2005; Bayes et al., 2012; Bouras et al., 2017). Zaheer Aslam et al (2010) showed that the texture of biomass was changed, at higher temperature. Nevertheless, other studies submit that the uptake of contaminant by adsorbent biomass is exothermic and the removal efficiency increases with decreasing temperature (Cruz et al., 2004; El-Sayed et al., 2010). This is happened because of the weakness of sorption forces between the sorbents active sites and the sorbate species and also between the sorbed phase adjacent molecules, increasing in the relative escaping tendency of adsorbate from the solid phase to the bulk phase, and deactivating the biosorbent surface or destructing some active sites on the biosorbent surface due to bond ruptures (Meena et al., 2005; Sari and Tuzen, 2008). There is also an opinion that shows temperature has no important effect on the uptake of contaminant by adsorbent biomass (Tran et al., 2016).

2.4.4 Adsorbent materials for removal of pollutants from wastewater

Separation is defined in an adsorption-oriented process as a system that converts a mixture of components into two or more distinct products. The procedure is difficult to execute since it is the polar opposite of mixing, and advocated by thermocontinuous' second law. For many separation procedures, the separation occurs due to the action of a mass separating agent, a solid substance, or an adsorbent (Pirbazari and Saberikhah, 2014) . As a result, the quality of any adsorptive separation or purification procedure directly affects its performance. Thus, the first critical step toward developing an efficient adsorption process is identifying a solid material with high capacity, selectivity, and adsorption rate. Adsorption is a surface phenomenon, and so any porous substance with a large surface area can act as an adsorbent. Additional characteristics to consider when selecting a material include the following: low cost and availability, adequate mechanical qualities, high physical strength (not disintegrating) in solution, a long life, and the ability to be regenerated if necessary. According to the literature, the control of a solid material's adsorption performance in liquid-phase adsorption is dependent on the following factors (Park, et al., 2010; Crini et al., 2019) :

(1) The solid's origin and nature, including its physical structure, such as particle size, specific surface area, and porosity, as well as its chemical nature and functional groups, such as surface charge and pH at the interface, the charge zero point and mechanical properties of the raw solid.

(2) The activation conditions of the raw solid, such as physical treatment or chemical modification.

(3) The effect of process variables used in the contacting system such as contact time, initial pollutant concentration, solid dosage, and stirring rate;

(4) The chemistry of the pollutants, such as the pKa, polarity, size, and functional groups of a dye molecule; and finally.

(5) The solution conditions, such as pH, ionic strength, temperature, the presence of multiple pollutants or impurities, and their fluctuation.

2.4.5 Classification of adsorbent

Among several wastewater treatment process, adsorption have the potential in reducing water pollutants and dyes from textile industries. Adsorption is effective to be used in lowering dye concentration in the effluents. Figure (2.1) shows various type of adsorbent being studied in order to treat wastewater containing dye, pigments and other pollutants. Today, the most commonly adsorbent used for treatment is activated carbon and applied for various water pollutant removal such as dye and heavy metal. Activated carbon also known as solid sponge is a carbon form by using either physical or chemical treatment . Activated carbon have extended surface area, high capacity of adsorption, higher surface reactivity degree and also micro-pore structure which is suitable in eliminating dye from wastewater. However, treating wastewater by using conventional activated carbon that is available in the market are expensive and its regeneration are even costly. Therefore, various raw material have been examined to produce activated carbon and each presents different properties as some previous research of adsorbent (Mohammad Razi, et al., 2017).

2.4.6 Low cost adsorbents for the removal of organic pollutants from wastewater

As low cost adsorbents, many waste materials used include fruit wastes, coconut shell, scrap tires, bark and other tannin-rich materials, sawdust and other wood type materials, rice husk, petroleum wastes, fertilizer wastes, fly ash, sugar industry wastes blast furnace slag, chitosan and seafood processing wastes, seaweed and algae, peat moss, clays, red mud, zeolites, sediment and soil, ore minerals etc. These adsorbents have been found to remove various organic pollutants ranging from 80 to 99.9%. The present work describes the conversion of waste products into effective adsorbents and their application for water treatment, The diagram shows the types of organic pollutants in water (Ali et al., 2012).

The categorization and sorting of adsorbents has grown increasingly important as the number of adsorbents employed grows. Adsorbents can be categorised in a variety of ways; however, the most prevalent ones are mentioned below (Crini, et al., 2019):

- natural materials: sawdust, wood, fuller's earth or bauxite;
- natural materials treated to develop their structures and properties: activated carbons, activated alumina or silica gel;
- manufactured materials: polymeric resins, zeolites or alumino-silicates;
- agricultural solid wastes and industrial by-products: date pits, fly ash or red mud;
- biosorbents: chitosan, fungi or bacterial biomass.

2.5 Mechanisms of dye adsorption

The adsorption of dye from contaminated water on the surface of an adsorbent is achieved *via* various adsorption mechanisms, as schematically shown in Figure (2.2). It should be noted that the adsorption of water pollutants on adsorbents is mainly guided by electrostatic attraction, π–π interactions, van der Waals forces, hydrogen bonding, acid–base reactions, and hydrophobic interaction (Lu and Astruc et al., 2020). Shen and Gondal reported that electrostatic and intermolecular interactions govern the adsorption of Rhodamine dye on the surface of the adsorbent (Kai and Gondal, 2017). According to Zheng *et al.*, the adsorption of anionic dyes, such as CR and MO on GO–NiFe-LDH, is achieved by electrostatic attraction and ion exchange phenomena (Zheng et al., 2019).

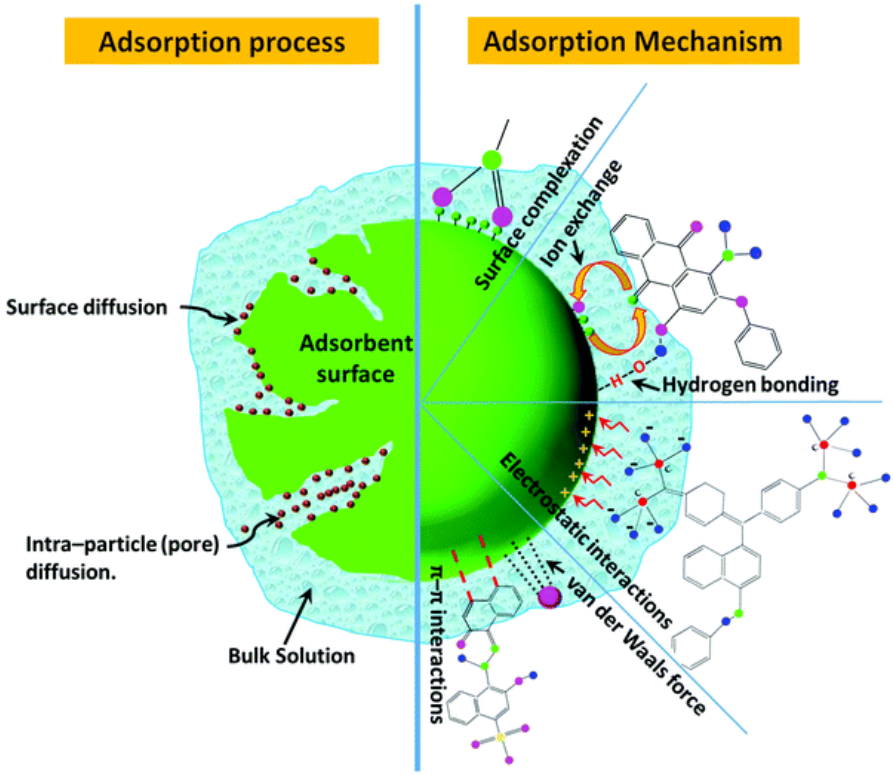

Fig. (2.2): Adsorption processes and mechanisms for dye removal from bulk liquid (Lu and Astruc et al., 2020).

Furthermore, the ion exchange mechanism involves the exchange of ions between a liquid (dye solution) and solid phase (adsorbent). Ebrahimian Pirbazari *et al.* suggested that two principal mechanisms are involved in removing the MB dye on NaOH-treated wheat straw impregnated with Fe_3O_4, namely the formation of a surface complex and ion exchange between the dye molecule and adsorption surfaces (Ebrahimian et al., 2014).

The formation of a surface complex is a mechanism associated with the adsorption process, which is described by the binding of ions to various surface functional groups available onto the surface of the adsorbent and electrostatic interaction between the adsorbent–adsorbate surfaces. Cojocaru *et al.* proposed that the formation of hydrogen bonds between Acid Orange 7 dye and adsorbents accounts for the adsorption process (Cojocaru et al., 2019).

According to Siddiqui *et al.*, H-bonds between MB and MnO_2/BC arise due to the interaction between the –OH groups present in MnO_2/BC and the acceptor present in MB molecules (Siddiqui et al., 2019). Similarly, π–π bonding/π-effects/π-interactions (non-covalent) involve π systems, where similar to electrostatic interactions, positively charged molecules interact with negatively charged surfaces. Further, the adsorption process can follow more than one mechanism simultaneously.

For example, the adsorption of Coomassie Brilliant Blue R 250 dye on the surface of adsorbents is governed by electrostatic interactions, π–π interactions, and intermolecular H-bonding (Thamer et al., 2019). The probable adsorption mechanisms involved in dye removal are shown in Figure (2.3), together with the various adsorption processes.

2.6 Equilibrium isotherms

Adsorption is usually described by isotherm. It is important for understanding the adsorption mechanism (Bouras et al., 2017). At a given temperature, equilibrium isotherm is the equilibrium relationship between the adsorbate concentration in the adsorbent particles and the adsorbate concentration in the fluid phase.

It is a plot of the contaminant concentration that remaining in solution at equilibrium against the amount of adsorbate per unit weight of adsorbent. An adsorption isotherm is described by specific constants, for example, values that express the properties and affinity of the surface and the adsorbents, respectively.

These isotherms can also be used to compare the adsorption capacity of adsorbents for various contaminants (Tran et al., 2016). Figure (2.3) shows some typical shapes of isotherm. Isotherm that is concave upward is a relatively low solid loading and it leads to quite long mass transfer zone in the bed, therefore, it is named unfavorable.

An isotherm that is convex upward is called favorable, because a relatively high solid loading can be obtained at low concentration in the fluid. The linear isotherm must go through the origin, and the amount adsorbed is clearly proportional to the concentration in the fluid. From these curves it will be noted that adsorption is a specific property depending upon the nature of the adsorbate-adsorbent system (Warren and Harriot, 1993).

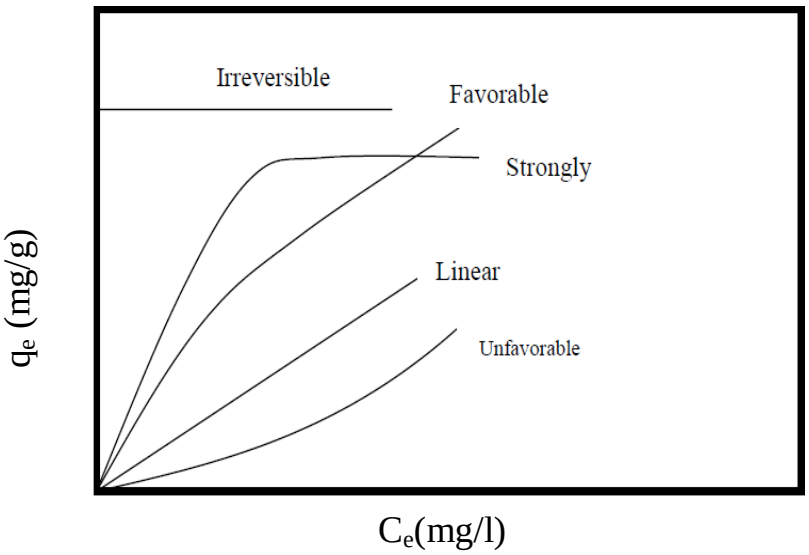

Fig.(2.3): The equilibrium isotherm relations (Warren and Harriot, 1993)

2.6.1 Langmuir isotherm

Equation (2.4) illustrates the Langmuir isotherm model of the nonlinear equation (Ayawei et al., 2017):

$$q_e = \frac{q_m * b * C_e}{1 + b * C_e} \qquad \text{……..……(2.1)}$$

Where q_m is the Langmuir constant related to the maximum capacity of adsorption (mg.g^{-1}), and b is the constant that denotes the adsorption energy (L.mg^{-1}). To estimate the adsorption capacity concerning a specific range of adsorbate concentration, the equation mentioned above [Eq. (2.1)] can be written as a linear form:

$$\frac{C_e}{q_e} = \frac{1}{q_m} * C_e + \frac{1}{b * q_m} \qquad \text{……..(2.2)}$$

The two constants (q_m, b) can be determined from the eq. (2.2) with a linearized type from the slope [1 /qm] and the intercept [1/ b q_m] of the linear plot of C_e/q_e versus C_e. A dimensionless constant, regularly known as a separation factor or an equilibrium parameter (R_L) c (Weber and Chakravorti, 1974), can be stated as:

$$R_L = \frac{1}{1+b*C_\circ} \quad \text{.....(2.6)}$$

C_o: is the adsorbate initial concentration (mg/l). The value of R_L indicates how favorable the isotherm is, as shown in Table (2.1).

Table (2.3): R_L value and isotherm kind.

Estimation of R_L	Kind of Isotherm
$R_L = 1$	Linear
$R_L > 1$	Unfavorable
$0 < R_L < 1$	Favorable
$R_L = 0$	Irreversible

2.6.2 Freundlich isotherm

The Freundlich isotherm is expressed as (freundlich, 1926):

$$q_e = K_F * C_e^{1/n} \quad \text{..... (2.3)}$$

The level of nonlinearity between solution concentration and adsorption demonstrates the n value. The circumstance of $n > 1$ is most expected. It might be because of the organization of surface sites or any factor, which diminishes the adsorbent adsorbate interaction with expanding surface density. The estimations of n inside the range of 1–10 demonstrate favourable adsorption (Al-Ghouti and Da'ana, 2020).

Eq. (2.3) can be rearranged into the linear form:

$$\log q_e = \log K_F + \left(\frac{1}{n}\right) \log C_e \quad \text{.....(2.4)}$$

Where: *(K_F, l/n)*: Freundlich constants related to adsorption capacity and adsorption intensity, respectively of the sorbent, and obtained from the linear plot of (experimental data) *log (q_e)* versus *log (C_e)* (Al-ghouti and Da, 2020).

2.7 Kinetic Adsorption

The sorts of adsorption techniques in a particular system must be understood in order to understand how the adsorption capacity develops over time according to the theory of adsorption kinetics. The following models are being used to describe the adsorption's kinetics trend (Patel, 2021).

2.7.1 Pseudo-first order model

Pseudo-first-order kinetics is used for determining the adsorption capacity in liquid- and solid-phase system (Singh, et al., 2021). To conduct linear fitting, the relationship between the adsorption capacity at a given adsorption time (q_t) and a given adsorption time (t) is plotted first. In a solid-liquid system, if the adsorption process follows the pseudo-first order model, it is primarily controlled by physical diffusion (Zhao et al., 2020). To choose the optimal model, the correlation coefficient (R^2) and standard error are employed. It's also crucial that the actual and theoretical values of the sorbate's adsorption capabilities (q_e) match (Fred-Ahmadu et al., 2020). The equation of pseudo first order:

$$\ln(q_e - q_t) = \ln q_e - 0.434 k_1 t \qquad \text{……..……. (2.5)}$$

Where :

q_e : the concentration of metal ion adsorbed after equilibrium (mg/g).

q_t : the concentration of metal ion adsorbed in time t (mg/g).

$K_1(min^{-1})$: is the Pseudo 1st order rate constant.

Values of q_e and K_1 can be obtained from the slope and intercept of the plot $\ln(q_e-q_t)$ versus t.

2.7.2 Pseudo-second-order kinetic model

The pseudo-second-order equation predicts the performance over the complete range of the adsorption process and seems to be controlled by the chemical sorption mechanism in the role of rate controlling step (Ahmad et al., 2018). In comparison with the initial rate of adsorption, the rate of adsorption is almost insignificant. The kinetic rate equation is given below (Ho and Mckay, 1999):

$$\frac{1}{(q_e - q_t)} = \frac{1}{q_e} + k_2 t \qquad \text{.....(2.6)}$$

Where : k_2 (g/mg. min) is the rate constant of pseudo second-order, q_e is the amount of contaminant sorbed at equilibrium, (mg/g), q_t is amount of contaminant on the surface of the sorbent at any time *t*, (mg/g). Equation (2.6) can be rearranged to obtain:

$$\frac{t}{q_t} = \frac{1}{k_2 q_e^2} + \frac{t}{q_e} \qquad \text{.....(2.7)}$$

K_2 and q_e are computed from the intercept and the slope of plotting (t/q_t) versus *t.*

2.7.3 Model of the intra-particle diffusion

The rate-limiting stage prediction is the best way to understand the mechanism of solid-liquid adsorption. The external mass transfer and the intra-particle diffusion or external or both are in charge of the mass transfer of solute. Mass transfer mechanisms include the adsorption on the particle diffusion, the porous adsorbent, and the film. Through batch adsorption, the adsorbate particle transfer into the pores of the adsorbent is the rate governing stage. The kinetic data of pollutant adsorption onto adsorbent subjected to intra-particle diffusion model given by Weber and Morris (1963) and is represented as shown in equation (2.8):

$$q_t = K_{ip} * t^{0.5} + C_i \quad \text{.....(2.8)}$$

Where:

q_t: is the amount of pollutant adsorbed at the time "t" (mg/g).

K_{ip}: is the rate constant for intraparticle diffusion (mg/g.min0.5).

C_i: is the intraparticle diffusion constant i.e. intercept of the line (mg/g).

directly proportional to the boundary layer thickness.

The values of Morris–Weber constants (K_{id} and C_i) were calculated from the plot of q_t versus $t^{0.5}$ which are equal to slope and constant, respectively.

Relying on such model, solute adsorbed plot versus the contact time square root must give a straight line passing through the origin (Weber and Morris, 1963). If the plot doesn't pass throughout the origin, it will yield a sign of a certain degree of the control of film diffusion, and the intra-particle diffusion isn't merely the stage of rate-limiting (Yadav, et al., 2015; Salahshoor and Shahbazi, 2016).

2.7.4 Elovich model for adsorption

The Elovich equation is a sort of model utilized in adsorption kinetics, and the equilibrium parameter of the Elovich equation (RE) was used to characterize the adsorption kinetics characteristic curves (Wu et al.,2009). where q_t (mg/g) represents the quantity of dye adsorbed at time t (min), a and b are constants, with being the initial sorption rate (mg/g min) and b being the extent of surface covering and chemisorption activation energy (g/mg) (Marcu et al.,2020). These constants' chemical relevance has yet to be determined (Wang et al., 2009). When graphing adsorption data using q_t vs ln t, every adsorption process that follows the Elovich kinetic model produces a straight line. The value of b is determined by the graph's slope, and the value of a may be estimated using the

value of b and the graph's intercept (Ray et al., 2020). The Elovich equation generally used is expressed as (Wang et al., 2009):

$$q_t = \frac{1}{b} ln(ab) + \frac{1}{b} ln\, t \qquad \text{……(2.9)}$$

where q_t (mg/g) is the amount of dye adsorbed at time t (min) and a and b are the constants. The chemical significance of these constants has not been clearly resolved (Wang et al., 2009). shows the plot q_t versus ln t having slope *1/b* and intercept *[(1/b) ln(ab)]*.

2.8 Continuous data analysis

The breakthrough appearance time and the curve shape are too significant to determine the process and the sorption column dynamic response. Breakthrough curves displayed the matter loading behavior for removing of dyes from the solution in a constant bed column, and they are frequently stated as adsorbed concentration (described as the ratio of the effluent concentration to the inlet (C_e/C_o) concentration as a function of time or the effluent volume for a certain height of bed (Singh et al., 2014). The area underneath the breakthrough curve determined via the integration of the adsorbed concentration (mg.l^{-1}) versus time (*min*) plot can be employed to find the total adsorbed quantity (the column maximum capacity) (mg) for which a certain feed concentration and a flow rate (Q) (*ml/min*) are calculated via Eq. (2.10) (Juela, 2020):

$$q_{total} = \left(Q * \frac{c_\circ}{1000}\right) \int_{t=0}^{t=t\ total} \left(1 - \frac{c_e}{c_\circ}\right) dt \qquad \text{……(2.10)}$$

Where: *Q* is the flow rate (*ml/min*) that can be calculated by dividing the effluent volume (V_{eff}, *ml*) by the total time (t_{total}, *min*.).

$$Q = \frac{V_{eff}}{(t_{total})} \qquad \text{……(2.11)}$$

And, the whole quantity of adsorbate that went throughout the column (mg) is computed by Eq. (2.12); likewise, the percent efficiency (%) of the total elimination is computed by Eq. (2.12):

$$M_t = \frac{c_\circ * t_e * Q}{1000} \quad \text{.....(2.12)}$$

$$\%R = \frac{q_t}{M_t} * 100 \quad \text{.....(2.13)}$$

Equilibrium uptake (q_{eq}) (or maximum column capacity) in the column is described via Eq. (2.14) as the total quantity of the sorbed (q_{total}) per (g) of sorbent (m) at the whole flow time end.

$$q_e = \frac{q_t}{m} \quad \text{.....(2.14)}$$

2.8.1 Continuous mode of sorption operation

Figure (2.4) schematically illustrated a typical fixed-bed sorption process operated in continuous flow mode, in which the input and output stream is continuously allowed to flow during the progress of the solute removal. In the fixed-bed column investigation, a definite amount of biosorbents are packed as a solid matrix in a column of defined length. The strainers are placed at the bottom of the column to prevent the run-off of the biosorbent along with the liquid phase. The biosorbent loaded column is kept in a thermostat to maintain the temperature uniformity and has been connected with a positive displacement pump with a flow regulator such as a peristaltic pump.

The solute (contaminants) rich liquid phase is allowed to pass through the fixed-bed column with the predefined flow rate. During this wetting of the solid bed, the solute from the liquid phase gets translocated and binds on the surface of the stationary matrix due to its relative affinity. This translocation and

surface binding of solute molecules continues till the pores or the functional moieties of the biosorbents attain equilibrium. After this point of saturation, the solute transfer process ceases at the solid-liquid interface and further adsorption is not practically feasible. Also, the transfer of solute across the phase boundary is facing a series of diffusional resistances offered by the surrounding film and intraparticle, sufficient time must be provided for the biosorbate molecules to reside inside the column.

The residence or retention time is a function of the volumetric flow rate of the liquid samples and hence it is one of the vital parameters in the optimal design of the continuous sorption process (Gan et al., 2012; Thirunavukkaras et al., 2018). In addition to this, other operational variables such as the bed length, temperature, contact time, packing volume and density etc. are also significantly affecting the solute removal process (Li et al., 2014; Chen et al., 2014; Calero et al., 2018). The prime advantage of dynamic sorption is to scale up the process using the data obtained from the continuous operation with the high degree of reliability. With the use of dimensional similarity approaches, either geometric or kinematic similitude, the scaling up of the sorption process can be effectively accomplished for the treatment of industrial effluents.

Unlike the batch mode of operation, the performance of the sorption process can be assessed with the aid of breakthrough curves which can be obtained from the plot of the ratio of the concentration of biosorbate at a time, t over the initial concentration C_0, (C_e/C_0) and time (t) (Fernandez et al., 2012; Abdolali et al., 2017). The breakthrough curves will provide vital information on the onset of the breakthrough point (breakthrough concentration) and saturation point (exhaust) of the process. Also, this curve can be used to predict the length of used and unused portion of the bed by determining the area under the curve regions. Mass Transfer Zone (MTZ) is a defined zone in the sorption column in which the solute transfer across the phase boundary is expected to occur. At the

solid-liquid interface, either physical or chemical or the combination of both interactions resulted in the surface binding of biosorbate molecules.

At the start of the process, the active binding sites in the biosorbent bed are completely free to access with the biosorbate and hence the solute transfer is rapidly attained. As the process proceeds, the available binding sites are pre-filled and hence the sorbate molecules need to move or diffuse along the length of the column to facilitate further binding. In other words, after the saturation of binding regions, MTZ moves down the length of the column Figure (2.5). The layer of the sorption bed which is above this MTZ can be considered as the saturated zone. As the complete sorption is expected at the start of the process, the concentration of the pollutant at the outlet stream was found to be zero. The longitudinal movement of MTZ, enlargement of saturation zone, diffusive resistances offered by the film and intraparticle, and non-ideal behavior of the solute molecules etc. are greatly affecting the sportive capability resulted in the increase in the value of C/C_0 against time (Fernandez et al., 2012; Abdolali et al., 2017).

The time at which this ratio attains a certain value, usually fixed by the researchers or threshold value of the pollutant specified by EPA is called breakthrough point (t_b) and the corresponding concentration is called breakthrough concentration. After the breakthrough point, the intensity of the diffusional resistances and the non-ideality of the solute molecules increases which results in a sharp rise in the concentration ratio values over time. The time at which the effluent concentration reaches the initial concentration, ie, the ratio, C_e/C_0 becomes one is called the exhaust time (t_e). Or otherwise, at the exhaust point, the sorption bed is completely saturated and further sorption is not feasible. Hence, the plot of C_e/C_0 vs t will form an 'S' shaped curve called breakthrough curve as illustrated in Figure (2.5) and the degree of steepness,

onset of tb and te will vary for the different fixed-bed column studies (Chowdhury and Saha, 2013; Hasanzadeh et al., 2016; Abdolali et al., 2017).

If an investigation is assuming the length of the MTZ in a column is uniform, the time required for (a) establishment of MTZ, (b) exchange of biosorbate at the interface and (c) rate of migration of MTZ along the bed length are the vital parameters affecting the design of a sorption process (Gupta and Ali, 2012). Besides, the significance of the operational factors includes the initial biosorbate concentration, solution pH, volumetric flow rate of the biosorbate, bed height, particle size distribution of the solid biosorbent and the operating temperature can also be studied with the help of breakthrough curves. Each of these variables can affect the efficacy of the sorption process significantly. For example, an increased amount of biosorbate molecules might result in the early onset of t_b and t_e due to the greater concentration difference that existed at the interface. The further increase would result in a decreased removal percentage as the available sites are saturated with the sorbate molecules (Moyo et al., 2017).

Likewise, an increase in the volumetric flow rate would result in the early onset of t_b and t_e as the retention time may not be adequate to make sorbate-sorbent interaction at the interface and hence it is obvious to operate the column with minimal flow rate to achieve the maximum efficiency (Rafiqueet al., 2009; López-Cervantes et al., 2018; Sheng et al., 2018). Conversely, an increase in bed height might favor the sorption efficacy as it can provide greater surface area for the biosorbate molecules to bind with them more efficiently (Elmholt et al., 2008; Fat'hi et al., 2014). The average particle size of the biosorbents should be minimal to offer improved surface area which in turn increases the efficiency.

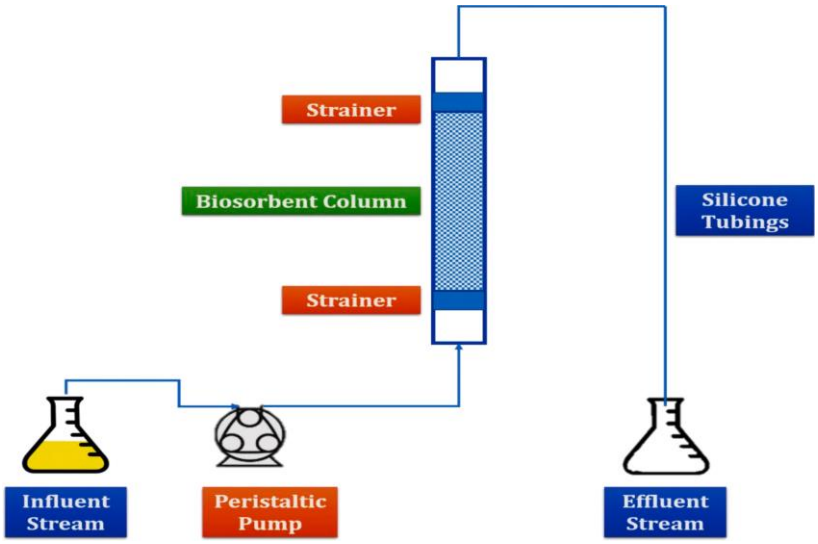

Fig.(2.4) Schematic illustration of a continuous flow sorption process (Thirunavukkarasu et al., 2021)

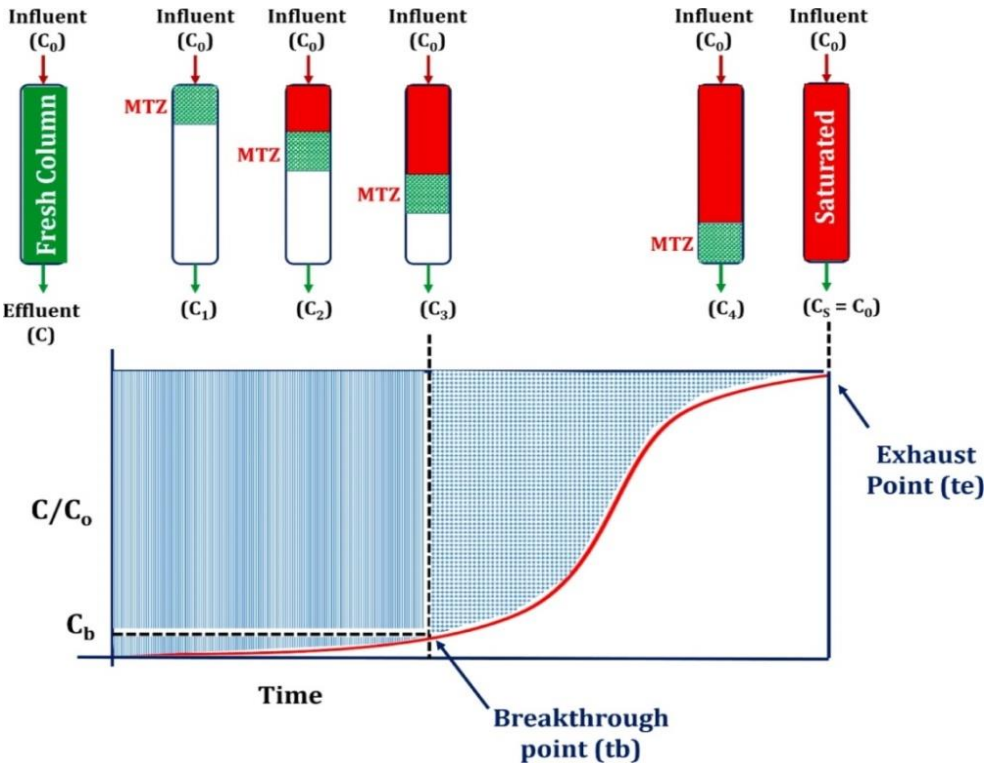

Fig. (2.5) Breakthrough curve from the plot of C/C_0 vs time and their correlation with the movement of MTZ along the length of the column (Thirunavukkarasu et al., 2021).

2.8.1.1 Bed depth service time model

BDST is another simple model which proposed there exists a linear relationship between the column bed height and service time in terms of the biosorbate concentration and sorption parameters. This model was initially derived from the Bohart-Adams model which was later modified by Hutchins (Hutchins, 1973). This model assumes that the resistances offered by the solid particle (intraparticle) and liquid phase (external diffusion) are negligible and the sorption kinetics is predominantly controlled by the chemisorption of sorbate and sorbent at the interface (Baral et al., 2009). This model can also be used to quantify and assess the sorption capacity of the different biosorbents. The mathematical linear form of the BDST model is given as:

$$t_b = \frac{q_B Z}{C_\circ U_f} - \frac{1}{K_B C_\circ} \ln\left[\left(\frac{C_\circ}{C_{te}}\right) - 1\right] \qquad \text{.....(2.15)}$$

Where, k_B is the BDST rate constant (l mg^{-1} min^{-1}), q_B is the maximum sorption capacity per unit volume of the sorption column (mg l^{-1}), Z is the bed height or depth (cm) and U_f is the linear velocity of the biosorbate solution (cm. min^{-1}). A plot can be drawn by taking time and bed height as their axis to determine the values of q_B and k_B.

2.8.1.2 Thomas model

The most fully studied Thomas model is intended to determine the sorptive capacity and to analyze the breakthrough curves by assuming the adsorptive equilibrium follows the Langmuir model and rate kinetics is governed by the reversible second-order equation (Ghasemi et al., 2011; Ghasemi et al., 2011; Vickers, 2017). Also, this model assumed that there will be no axial dispersion during the transit of solute molecules across the solid-liquid interface. This model can be used to estimate the sorption process where the externally driven and internal diffusive resistances are minimal (Konstantinos et al., 2004). As

this model is primarily considering the sorption process is being dominated by the mass transport phenomena at the interface, chemical-mediated sorption process could not be explained with a high degree of accuracy. The linear form of the Thomas model is given as:

$$\ln\left[\left(\frac{C_\circ}{C_e}\right)-1\right]=\frac{K_{TH}q_{TH}\,m}{Q_v}-K_{TH}C_\circ\,t \qquad \text{.....(2.16)}$$

Where, m is the amount of weight of the biosorbent loaded in the column (g), k_{TH} is the Thomas rate constant (ml min^{-1} mg^{-1}), C_0 and Ct are the initial and effluent concentration of the biosorbate (mg l^{-1}), Q is the volumetric flow rate ($ml\ min^{-1}$), q_{TH} is the sorptive capacity at equilibrium (mg g^{-1}). A plot can be drawn by taking ln [(C_0/C_t) − 1] on y – axis and time on x – axis to determine the slope (q_{TH}) and intercept values (k_{TH}).

2.8.1.3 Yoon-Nelson model

It is the simplest model as it does not concern with the physicochemical characteristics of biosorbate, type of sorbent and properties of the sorption column (Yoon and Nelson, 1984; Yagub et al., 2014). This model assumes that the declining sorption rate is directly proportional to the amount of sorbate adsorption and the probability of sorbate breakthrough on the surface of the sorbent (Yoon and Nelson, 1984). The linear expression of the Yoon-Nelson model can be described as:

$$\ln\left(\frac{C_e}{C_\circ-C_e}\right)=K_{YN}t-\tau K_{YN} \qquad \text{.....(2.17)}$$

Where, k_{YN} is the rate constant derived from the Yoon-Nelson model (min^{-1}), t is the time (min) and τ is the time required to achieve half (50%) breakthrough point (min). A plot can be constructed by taking $ln(C_e/C_0 - C_e)$ on x-axis and time on x-axis to obtain a straight line and the slope (k_{YN}) and intercept (τ) can be determined.

2.9 Previous studies of sorption of dyes using agricultural solid waste by batch and fixed-bed column study

Various biosorbents and sorbates were studied in batch and fixed-bed column study cited in the following review part:

Akar et al. (2009) studied a low-cost waste biomass derived from canned food plant, was tested for its ability to remove reactive textile dye from aqueous solutions. The batch sorption experiments were carried out at various pH, biosorbent dosage, contact time and temperature. Optimum decolorization was observed at pH 2.0 and 1.6 g dm^{-3} of biomass dosage within 20 min. The first-order and the pseudo-second-order kinetics were investigated for the sorption system. The applicability of the Langmuir and Freundlich isotherm models was examined. The thermodynamic parameters for the sorption were also calculated. The experimental results in this study indicated that this low-cost biomaterial was an attractive candidate for the removal of textile dye Reactive Red 198 (RR198) from aqueous solutions.

Reddy et al. (2012) studied the feasibility of using Indian Jujuba Seeds (IJS) (Zizyphus maruritiana), abundantly available in and around the Nallamalla forest in Andhra Pradesh, for the anionic dye (Congo red, CR) adsorption from aqueous solution, has been investigated as low cost and eco-friendly adsorbent. Adsorption studies were conducted on a batch process, to study the effects of contact time, initial concentration of CR, pH and temperature. Maximum colour removal was observed at pH 2. The equilibrium data was analyzed by the Langmuir, the Freundlich and the General isotherms. The data fitted well with the Langmuir model, with a maximum adsorption capacity of 55.56 mg g^{-1}. The pseudo-second-order kinetics was the best for the adsorption of CR, by IJS (Z. maruritiana) with good correlation. Thermodynamic parameters, such as standard free energy change ($\Delta G°$), standard enthalpy change ($\Delta H°$) and standard entropy change ($\Delta S°$), were analyzed. The results suggest that IJS (Z.

maruritiana) is a potential low-cost adsorbent for the CR dye removal from synthetic dye wastewater.

Sorption of dyes on shelled Moringa oleifera seed powder (SMOS) was investigated for the removal of methylene blue and Congo red from aqueous solution by Raj et al. (2013). Sorption studies led to the standardization of the optimum conditions: dye concentration (25 mg/l), contact time (40 min), particle size (105 μM), and volume (200 ml) at pH 6.5 and 2.5 for the removal of methylene blue (90.27 %) and Congo red (98.52 %). A single layer artificial neural network (ANN) model was developed to simulate the process and predict the removal efficiency of SMOS for the removal of dyes. Different ANN architectures were tested by varying network topology, resulting into an excellent agreement between the experimental data and the predicted values. The Levenberg–Marquardt algorithm was found best of BP algorithms with a minimum mean squared error for training and cross validation as 1.89E−09 and 0.145, respectively.

The removal of Novacron Golden Yellow (NGY) dye from aqueous solutions using peanut hulls was done by Nawaz et al. (2014). The experiments were performed with native, pretreated and immobilised forms of peanut hulls. The effect of various operational parameters (pH, biosorbent dose, initial dye concentration and temperature etc.) was explored during batch study. NGY showed maximum removal at low pH and low biosorbent dose. High initial dye concentration facilitated the sorption process. Maximum dye removal with native, pretreated and immobilised biomass was found to be 35.7, 36.4 and 15.02 mg/g, respectively. The experimental data were subjected to different kinetic and equilibrium models. The kinetic data confirmed the fitness of pseudo-second-order rate law for NGY biosorption. The equilibrium modelling was carried out by Freundlich, Langmuir and Temkin models. The isothermal data of NGY removal were best described by Freundlich adsorption isotherm.

Negative values of free energy change (ΔG_0) for NGY with native and pretreated biomass depicted the spontaneous nature of sorption process.

The removal of Congo red dye (CR) from aqueous solutions using a novel low-cost biological adsorbent, Stipa tonassicima fibers, was investigated by Chebli et al. (2015). Batch experiments were conducted to examine the effect of the main parameters, such as the initial CR concentration, the pH, and the temperature on the sorption of the dye. Maximum adsorption removal was observed at pH 4 and sorption capacity of S. tenassicima was enhanced by increasing the temperature. Rate constants of pseudo-first order, pseudo-second order, and intraparticle diffusion coefficient were calculated to analyze the dynamic of the sorption process; they showed that sorption kinetics followed an intraparticle diffusion model, while the two straight lines describing experimental data indicated that intraparticle diffusion was the limiting step for biosorption. Among the tested isotherm models, the Sips isotherm was found to be the most relevant to describe CR sorption onto S. tenassicima fibers. Thermodynamic parameters, such as changes in standard free energy, enthalpy, and entropy, were also evaluated and the results suggested that the sorption reaction was spontaneous and endothermic in nature. The potential of S. tenassicima fibers, an easily available and low-cost material, to be used as an alternative biosorbent material for the removal of a dye, CR, from aqueous solutions was therefore confirmed.

Temesgen et al. (2018) investigated the removing of reactive red dye (RRD) from textile industry wastewater by activated orange and banana peel. The textural characterization shows 336.224 m^2/g and 21.456 m^2/g (specific surface area) for orange and banana peels respectively. The experiment conducted in batch mode to optimize the maximum operating condition. The result shows maximum removal efficiency of 89.41% and 70.25% at pH of 4, initial dye concentration of 25 mg/l, adsorbent dosage 1 g/100 ml, and

temperature of 30 °C on the activate surface of orange and banana peels. The obtained results were well fitted with Langmuir and Freundlich isotherm model and adsorption process follows the pseudo second order model for both adsorbent. Overall both peels have good potential to reduce the dye from wastewater.

Residual chia-seed-oil-extraction biomass was studied as a biosorbent for removal of Reactive Yellow B2R textile dye from aqueous solutions in batch system by da Silva et al. (2019), to suggest an appropriate and eco-friendly application, other than incineration or landfill. This residue does not require previous treatment, sorption process responded very well at temperature of 303 K and time up to 60 min, characterizing a highly practical application in textile wastewater treatments. Sorption process was concluded effective by kinetic, thermodynamic and equilibrium studies. Efficiency was maximum at pH 2 and 150 rpm of agitation speed. Kinetic studies presented equilibrium time of and approximately 92% of dye removal from aqueous solution, and pseudo-second order was the best fit. To the adsorption isotherm indicated the maximum sorption capacity of 70.95 mg g^{-1} and the heterogeneity parameter of 1.2785, both suggesting good pollutant removal ability by biosorbent and a slight degree of heterogeneity of biosorbent surface, respectively, indicated also by the evaluation of the SEM images of the unloaded and dye-loaded biosorbent surface. Sorption process occurs favorably, spontaneously and possibly through physical adsorption, indicating possible dye recovery and reuse of the biosorbent, as concluded by thermodynamic studies.

Cellulose substrate waste was demonstrated great potential as a biosorbent of pollutants from contaminated water which was studied by Al-Ghamdi et al. (2020). In this study, Neriumoleander fruit, an agricultural waste biomaterial, was used for the sorption of methylene blue from synthetic solution. Fourier-transform infrared (FTIR) spectroscopy indicated the presence

of the main absorption peak characteristics of cellulose, hemicellulose, and lignin compositions. X-ray diffraction (XRD) pattern exhibited peaks at 2θ = 14.9° and 2θ = 22°, which are characteristics of cellulose I. Scanning electron microscopy (SEM) showed a rough and heterogeneous surface intercepted by some cavities. Thermogravimetric analysis (TGA) showed more than a thermal decomposition point, suggesting that Nerium fruit is composed of cellulose and noncellulosic matters. The pH_{pzc} value of Nerium surface was experimentally determined to be 6.2. Nerium dosage, pH, contact time, dye concentration, and temperature significantly affected the adsorption capacity. The adsorption capacity reached 259 mg/g at 19 °C. The mean free energy ranged from 74.53 to 84.52 KJ mol^{-1}, suggesting a chemisorption process. Thermodynamic parameters define a chemical, exothermic, and nonspontaneous mechanism. The above data suggest that Nerium fruit can be used as an excellent biomaterial for practical purification of water without the need to impart chemical functionalization on its surface..

Darwesh et al. (2021) tested four agricultural wastes, i.e., sugarcane bagasse, rice straw, cotton stalk, and corn stalk were experienced as low-cost lignocellulosic materials for their ability to adsorb reactive red dye from its contaminated solutions. Batch adsorption technology was carried out in order to analyze sorption behavior of dye-adsorbent systems at different wastes, initial dye concentration, and solution pH value. The acid pH treatment was detected to significantly enhance the adsorption efficiency of used lignocellulosic wastes to maximum removal efficiency (96%). Bioreactor technology was applied as up-scaling experiments using sugarcane bagasse (SCB) waste (the best adsorbent under batch experiments) with different adsorbent dosage and flow rates. The maximum removal efficiency (89.65%) was recorded by 448 g of SCB waste, hydraulic retention time of 24 h and 12.6 l/h flow rate. The SEM characterization illustrated accumulation of dye molecules onto lignocellulosic

structure. Also, elemental analyses by EDAX instrument confirmed absorption technology. Thus, the sugarcane bagasse wastes can be applied as low-cost and environmental safe absorbent for RR dye removal from its contaminated wastewater and introducing non-traditional water resource.

Costa et al. (2021) tested the sorption of the Reactive Blue 5 G dye (RB5G) in batch flow systems was investigated using brewery spent grains (BSG) as a biosorbent. The biosorbent was characterized by the point of zero charge, scanning electron microscopy, Fourier transforms infrared, and N_2 adsorption/desorption. A rotational central composite design was used in the batch sorption studies. This design generated a model with a determination coefficient of 0.98. The design results showed that the removal of the dye was favored by the increase in temperature and the pH and mean particle diameter reduction. Equilibrium was reached after 24 h, achieving a dye removal of approximately 94.5%. Batch sorption data fitted better to the pseudo-second-order kinetics and Langmuir isothermal model, indicating the prevalence of chemical biosorption. The maximum sorption capacity achieved was 83.42 mg g^{-1}.

Grabi et al. (2021) investigated a potential biosorbent is prepared from agricultural waste material (ash seed) without any treatment. This biomaterial could be successfully used as a low-cost adsorbent for the removal of an anionic dye named Cibacron Blue (CB), under optimal conditions. The prepared adsorbent was characterized by scanning electron microscope (SEM) coupled with EDX, Fourier transforms infrared spectrometer (FTIR), thermogravimetric analysis (TGA), and point of zero charge (pHpzc). The adsorption experiments were carried out in batch mode at room temperature. Results show that the rate of CB dye removal exceeds 95 % using a dose of 2 g/l ash seed at C_o = 25 mg/l and pH = 2.2. The kinetic data were analyzed using the pseudo-first-order, pseudo-second-order, Elovich's, Bangham, intraparticle diffusion, and Boyd

kinetic. Results show that the pseudo-second-order model fits better the experimental data. The isotherm data of the CB dye adsorption were analyzed with several theoretical models (Langmuir, Freundlich, and monolayer model coupled to real gaz (MMRG)). It was found that the adsorption process of the CB dye is well described by monolayer model coupled to real gaz (MMRG) compared to other models. The negative enthalpy (ΔH°) and free enthalpy (ΔG°) indicate the physical and spontaneous nature of CB adsorption. Therefore, the prepared material can serve as a potential adsorbent for removal of CB dye from industrial effluents.

Jainet al. (2022) focuses on the feasibility of elimination of Methylene Blue dye from the textile wastewater with the use of economical organic biosorbents like Sugarcane Bagasse (SCB), Peanut Hull (PHB) and Orange peel (OPB). Batch adsorption tests were performed based on pH, temperature, contact time, initial adsorbate concentration, and dose of biosorbents as independent variables by employing a central composite design (CCD) approach of response surface methodology (RSM). After 90 min of contact time, the dye adsorption equilibrium was reached. It was explained with the help of Langmuir and Freundlich adsorption isotherms for the full concentration ranges of 20–100 mg/l. RSM combined with CCD is used to optimize the experiments for achieving the optimum conditions for the removal of dye. The adsorption data are used for the kinetic modeling from the pseudo-first- and pseudo-second-order kinetic equations. Thermodynamic parameters such as changes in entropy (ΔS), enthalpy (ΔH), and free energy (ΔG) were investigated, also showed that the adsorption was natural and endothermic by removing the randomness of color at the solid and liquid interface. Biosorbent characterization was additionally performed by Fourier-transform infrared spectroscopy (FTIR) to study the adsorption of Methylene Blue before and after the tests. The dimensionless separation factor (R_L) and expected results

illustrated that SCB, PHB, and OCB could be used to substitute commercially available biosorbents for aqueous solutions and eliminate Methylene Blue dye from textile wastewater.

De Sá et al. (2022) studied a solid phase for fluorescein removal from water. The non-pretreated solid phase did not display any sorption properties for the chosen dye. However, interesting sorption properties were observed following a chemical derivative treatment with nitric acid. The study was carried out using both batch and column approaches. Regarding the batch study, all parameters that influence sorption capacity, such, as pH, adsorbent mass, ionic strength, temperature and contact time, were evaluated. A sorptive capacity of 36.80 mg g^{-1} was obtained in the optimized condition. Four different models, Langmuir, Freundlich, Temkin and Redlich-Patterson, were employed. The Akaike information criterion (AIC) was employed to rank the best equilibrium model, which was determined as the Freundlich isotherm. The method was applied to a real sample and the same removal rate was obtained, thus indicating its suitability to wastewater treatment.

Powdered pergularia tomentosa fruit used by Belmabrouk et al. (2022), as a locally available biomaterial, was characterized and used for the sorption of methylene blue in batch mode. FT–IR spectroscopy revealed that the hydroxyls (–OH) were the main groups responsible for the sorption of methylene blue. SEM depicted a rough and heterogeneous surface with the presence of some cavities. The thermal decompositions of pergularia fruit were observed at 233 °C and 393 °C which were ascribed to the decomposition of cellulose and non-cellulose constituents, and to the depolymerization process. The effect of the operational conditions such as pH, time, dye concentration, adsorbent dose, temperature, and ionic strength on the sorption performance was carried out. Several classical and statistical models were used to fit the experimental data. The monolayer model with two energies was the most appropriate. This

statistical model revealed that two functional groups of the pergularia tomentosa fruit surface contributed to the adsorption of methylene blue. Each group is characterized by a particular energy and a stoichiometric number. The pergularia tomentosa fruit could be anchored by one or more dye molecules per site. The adsorption energy is lesser than 20 kJ/mol. The results confirmed a physio-sorption process. The maximum sorption was 152 mg/g. The ionic strength disfavored the sorption system. The results demonstrated that pergularia tomentosa fruit is an attractive candidate for removing cationic dyes from contaminated water.

Various biosorbents and sorbates were studied in fixed-bed column are cited in the following review part:

Charola et al. (2018) studied the adsorption potential of empty cotton flower agro-residue based activated carbon (CFAC) to adsorb Reactive Orange 84 (RO84) dye from aqueous solution was studied using packed-bed adsorption column. The breakthrough curve characteristics were highly influenced by process variables like influent flowrate, inlet RO84 dye concentration and CFAC bed height. The findings indicated that higher value of dye concentration and bed height were favorable but high influent flowrates was unfavorable for adsorptive removal of RO84 dye. The maximum adsorption capacity of column was found to be about 720 mg of RO84 per 4.67 g of CFAC adsorbent for initial concentration, flowrate and bed height of 200 mg l^{-1}, 15 mL min^{-1} and 5 cm, respectively. Thomas, Yoon–Nelson and Bed Depth Service Time (BDST) models were applied to calculate kinetic parameters of the laboratory fixed-bed adsorption column. Based on error analyses, Thomas model and BDST model fitted well than Yoon–Nelson model. The study concluded that CFAC is an effective adsorbent for adsorption of RO84 dye using fixed-bed adsorption column. A continuous adsorption study in a continuous by Kumari and Dey,

2019 using coco-peat (CP) as an adsorbent was carried out for the removal of toxic malachite green (MG) from contaminated water. Continuous studies were carried out to check field application viability. Various parameters like particle size, pH, concentration, dose and interference were exercised to optimize dye removal. Data obtained from breakthrough column studies were evaluated using Thomas and BDST model. Thomas rate constants Kt (0.22 ml min^{-1} mg^{-1}) and adsorption capacity q_o (181.04 mg g^{-1}) were estimated and found to favor efficiency of CP. Thomas model was tested with several parameters like flow rate, concentration, and bed depth. Upon increase in input dye concentration, flow rate and bed height, adsorption coefficients increased. According to BDST model, maximum dye uptake of 468.26 mg/l was obtained with an input dye concentration of 5 mg/l. HYBRID and MPSD error functions were tested and found that Thomas model fits best. Dilute hydrochloric acid was found best for desorption. Real wastewater from textile industry was analyzed and confirmed the prospect of large-scale industrial application. In conclusion, coco-peat can be used as a promising bio-sorbent in column bed for scavenging of MG from contaminated water.

Abed et al. (2019) focused on the recovery of two agro-food waste available in our country with significant quantities olive pomace and date pits for the removal of a synthetic dye which is methylene blue. Both materials were used in their native forms separated and mixed to improve their adsorptive capacity. A range of physico-chemical analysis was performed to characterize adsorbents used, among them: the FTIR spectroscopy and the scanning electron microscopy. The ability of adsorbents prepared to adsorbe methylene blue (MB) from the aqueous solution was investigated in a continuous. The effects of several important parameters were studied, such as initial concentration of MB, flow rate and bed height. The corresponding breakthrough curves were calculated.

Thuong et al. (2019) investigated the elimination of methylene blue (MB) and crystal violet (VL) from wastewater using a fixed-bed column of pre-treated durian peel. Examined variables in the process are bed depths (2–6 cm), flow rate (5–20 ml/min), and influent dye concentrations (200–600 mg/l). The highest adsorption amount of pre-treated DP was 235.80 mg/g and 527.64 mg/g, respectively, on a 600 mg/l of methylene blue and crystal violet achieved within a bed height of 4 cm and a flow rate of 10 ml/min. Accordingly, the breakthrough curves were constructed and modeled using the relevant theoretical models under the effects of different experimental conditions. Pre-treated durian peel was found to exhibit high adsorption capacity for cationic dye in an initial concentration of 200–600 mg/l with complete removal being obtained.

The agricultural biomass from the Moroccan Sahara (ABMS) was investigated as an ecofriendly and low-cost biosorbent of textile dye by Abrouki et al. (2021). The effect of independent variables affecting the process fixed-bed adsorption such as inlet textile dye concentration (40, 80, and 120 mg l^{-1}), flow rate (2, 4, and 6 ml min^{-1}) and bed height (5, 10, and 15 mm), were modeled and evaluated by response surface methodology based on the Box–Behnken design. The kinetic models, Thomas and Yoon and Nelson model were applied to experimental data to predict the breakthrough curves using linear regression and to determine the characteristic parameters of the packed bed column. The data were in good agreement for both models with $R^2 > 0.95$. The maximum Methylene blue dye removal capacity was found to be 30.15 mg g^{-1}. These findings suggested that ABMS biosorbent without any activation in the column structure presents great potential in the removal of dyes from textile wastewater.

The adsorption of Congo red (CR), an azo dye, from aqueous solution using free and immobilized agricultural waste biomass of Nelumbo nucifera

(lotus) were studied separately in a continuous fixed-bed column operation by Parimelazhagan et al. (2021)

The N. nucifera leaf powder adsorbent was immobilized in various polymeric matrices and the maximum decolorization efficiency (83.64%) of CR occurred using the polymeric matrix sodium silicate. The maximum efficacy (72.87%) of CR dye desorption was obtained using the solvent methanol. Reusability studies of free and immobilized adsorbents for the decolorization of CR dye were carried out separately in three runs in continuous mode. The % color removal and equilibrium dye uptake of the regenerated free and immobilized adsorbents decreased significantly after the first cycle. The decolorization efficiencies of CR dye adsorption were 53.66% and 43.33%; equilibrium dye uptakes were 1.179 mg g^{-1} and 0.783 mg g^{-1} in the third run of operation with free and immobilized adsorbent, respectively. The column experimental data fit very well to the Thomas and Yoon–Nelson models for the free and immobilized adsorbent with coefficients of correlation $R^2 \geq 0.976$ in various runs. The study concludes that free and immobilized N. nucifera can be efficiently used for the removal of CR from synthetic and industrial wastewater in a continuous flow mode. It makes a substantial contribution to the development of new biomass materials for monitoring and remediation of toxic dye-contaminated water resources.

De Sá et al. (2021) studied the influence of particle size, flow rate and initial concentration of the dye in the fixed column bed and evaluated through breakthrough curves and a sorptive capacity of 4.35 mg g^{-1} was obtained. Thermodynamic studies revealed that the adsorption is exothermic and spontaneous. Four different models, Langmuir, Freundlich, Temkin and Redlich-Patterson, were employed. The Akaike information criterion (AIC) was employed to rank the best equilibrium model, which was determined as the Freundlich isotherm. The method was applied to a real sample and the same

removal rate was obtained, thus indicating its suitability to wastewater treatment.

Ghosh et al. (2022) studied the implement the continuous method to eliminate methylene blue (MB) by H_3PO_4 treated eucalyptus leaves. Characterization were used in study are SEM, FTIR, solid-state NMR, and BET surface areas. Initially, the batch experiments revealed that the maximum percentage removal of MB is obtained at pH 8. The column experiments are performed at pH 8 and 25 °C with a varying bed height (5–9 cm), rate of flow (10–20 ml min^{-1}), and MB concentration (10–50 mg l^{-1}). The column experimentation shows that the breakthrough and exhaustion times rise with the bed's height but decrease with the increasing rate of flow and MB concentration. Different well-known kinetic models are tested with the experimental results, which display that the Thomas model ($R^2 = 0.9969$, $\chi^2 = 0.0005$) fits better than others, so it is appropriate for the scale-up design. The Langmuir isotherm model ($R^2 = 0.9949$) is superior to the Freundlich model ($R^2 = 0.9516$). The Langmuir maximum adsorption capacity is 52.18 mg g^{-1}, which suggests monolayer adsorption. Desorption of MB from used adsorbents with CH_3COOH solution (0.4 N) suggests 55.10% regeneration efficiency. The used adsorbents are safely disposable after incineration at 800 °C. This innovative study suggests that the inexpensive H_3PO_4 treated eucalyptus leaves feasible to use effectively for MB removal from the wastewater. The modeling using multiple linear regressions shows a statistically good result. The applicability of GA-ANN modeling is also tested.

Chapter Three

Materials and Methods

Chapter Three
Materials and Methods

3.1 Introduction

This chapter describes the preparation and characterization of the biosorbent, LLSP. In a series of laboratory batch and continuous flow studies, the efficiency of LLSP in removing of Janus Green B dye (JGBD) and Crystal Violet dye (CVD) from colored industrial effluent was examined. Batch experiments for each dye at room temperature are based on study of the impacts of dye solution pH, contact time, biosorbent dosage, and initial dye concentration. Continuous flow tests have been conducted for each dye to determine the effect of dye solution flow rate, biosorbent bed depth, and initial dye concentration on dye removal efficiency.

3.2 Materials and methods

3.2.1 Adsorbate

3.2.1.1 Janus Green B dye

Janus Green B dye (JGBD), a basic dye and important stain in Several disciplines, including antimalarial agents, tissue culture monolayers, nucleic acids, staining chromosomes, yeast cells, and mitochondria, (Medjdoubi, et al., 2019). In this work, this dye was supplied from Iraqi markets.

The physical and chemical properties are listed in Table (3.1). Using a Shimadzu UV-VIS Spectrophotometer - 6800, the maximum wavelength was measured as λ_{max} of 611nm. Figure (3.1) shows the JGBD structural formula. By dissolving an adequate amount of dye powder in distilled water, a stock solution of dye with a concentration of 10^3 mg/l was prepared. To create different concentration of each dye solutions, the dilution method was utilized. The pH of each dye solutions was changed as needed using 0.1 M

HCl or NaOH.

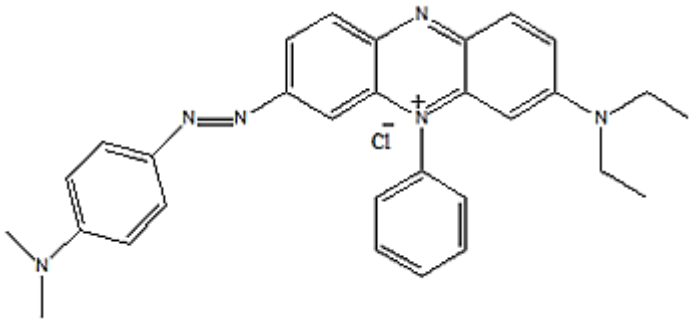

Fig. (3.1): JGBD structural formula (Bagher et al., 2010).

Table (3.1): Physiochemical characteristics of Janus Green B dye (Medjdoubi, et al., 2019).

Parameter	Value
Chemical name	3-(Diethylamino)-7 [{4-dimethylamino) phenyl} azo] -5-Phenylphenazinium Chloride
Synonym (s)	Diazin Green 5, Union Green B
Chemical formula	$C_{30}H_{31}ClN_6$
Molecular weight	511.07 g/mole
Absorption maxima ($\lambda_{max.}$)	611 nm
Nature	Cationic dye

3.2.1.2 Crystal Violet dye

A water-soluble, poisonous, recalcitrant organic, and cationic dye known as Crystal Violet dye (CVD) is responsible for serious health issues as well as environmental degradation. It is widely used in commercial textile operations, biological staining, and as a dermatological agent despite being known to be carcinogenic and mutagenic (Sarma, 2016). Figure (3.2) shows the CVD structural formula. The maximum wavelength was measured as λ_{max} of 591 nm and chemical formula is $C_{25}H_{30}N_3Cl$. Some of their physical and chemical properties are shown in Table (3.2). In distilled water, an amount of dye powder was dissolved, yielding a solution with a concentration of 10^3 mg/l. To get

varying dye concentrations, the dilution technique was applied. 0.1 M HCl and NaOH were used to adjust the pH of the dye solutions as needed.

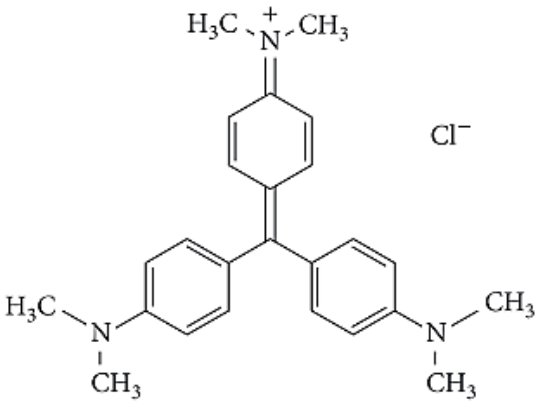

Fig. (3.2): chemical structure of the CVD (Safarik et al., 2016).

Table (3.2): The physical and chemical characteristics of CVD(Sarma, 2016).

Parameter	Value
Chemical name (IUPAC name)	4-{Bis[4-(dimethylamino)phenyl]methylidene}-N,N-dimethylcyclohexa-2,5-dien-1-iminium chloride
Synonym(s)	Gentian violet; Basic violet 3; Pyoktanin blue; s no 785;Violet 7b; Brilliant violet; Calcozine violet 6bn; Gram stain no 1; Gram stain.
C.I.No.	42555
Chemical formula	$C_{25}H_{30}N_3Cl$
Molecular weight	407.98 g/mole
Absorption maxima ($\lambda_{max.}$)	590 nm
Nature	Cationic dye

3.2.2 Biosorbent preparation

Leucaena leucocephala was selected as the biosorbent since it may be found locally in many locations around Iraq. The pods of the plant were collected and opened to get rid of the seeds and washed well in distilled water. They were then oven-dried for three days at 70 °C (Cimá - Mukul et al., 2020). Using a pestle and mortar, the pods were broken up into tiny pieces. Then, it was ground using a mechanical grinder. The created particle was sieved to get the appropriate particle size of 0.150 mm. In order to employ the generated biosorbent in the tests, it was stored in airtight containers. Leucaena leucocephala seeds pods powder sample, also known as LLSP, was collected. The stages of preparing of LLSP are shown in Figure (3.3 a, b, c).

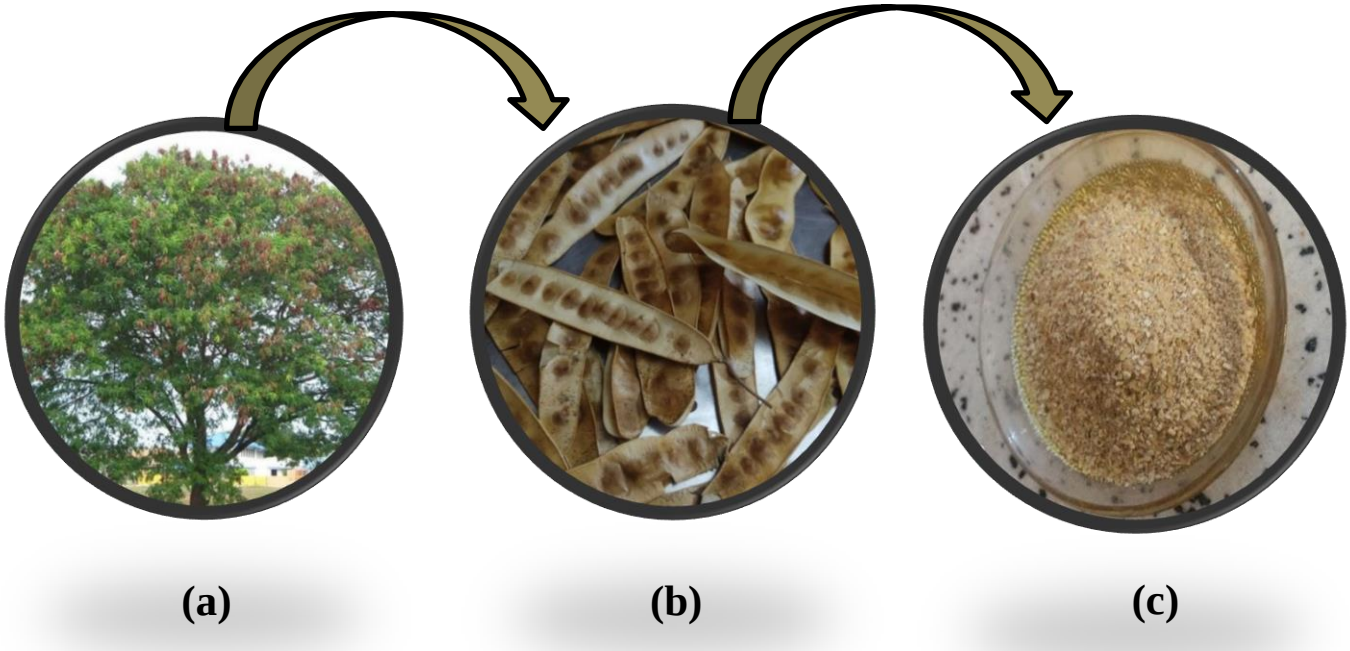

Fig. (3.3): (a) Leucaena leucocephala, (b) Leucaena leucocephala speed pods (c) prepeared adsorpent.

3.3 Characterization techniques of LLSP

3.3.1 Characterization of particular surface of LLSP

Based on the idea of adsorption - desorption isotherms observed of N_2 above the relative pressure (p/p^o) range from 0.01 to 0.991, the parameters of LLSP texture, including BET surface a and pore size distribution, were discovered utilizing a Micrometrics instrument firm, USA, ASAP2020. The BET method (Brunauer, Emmet, Teller) was used to compute the specific surface area, and the BJH techniques (Barrett, Joyner, Halenda) were utilized to define the pore diameter, size distribution of pore and total pore volume.

3.3.2 FTIR spectra

The surface functional groups on the LLSP sample were measured before and after the sorption of JGBD, using Fourier Transform Infrared (FTIR) spectroscopy (SHIMADZU, IRPRESTIGE 21, Japan) in the 4000-400 cm^{-1} range with KBr tablets type electron microscopy (SEM; TESCAN, Mira3, France).

These measurements were based on the surface morphology, crystalline structure, and direction of the LLSP sample. Thus, FTIR spectroscopy is a useful tool for identifying the distinctive functional groups that may bind dye ions. LLSP was subjected to FTIR spectroscopy before and after JGBD and CVD sorption in order to identify the locations of these active sites and how those locations changed as a result of JGBD and CVD biosorption.

3.3.3 Scanning electron microscopy (SEM)

Along with energy dispersive spectroscopy (EDS). SEM with various magnifications is used to test the surface texture, morphological, and to explain surface biosorbent before and after the sorption of JGBD and CVD using a high-resolution scanning electron microscope (SEM; TESCAN, Mira3, France).

3.3.4 Atomic force microscope (AFM)

The CSPM with AFM test (SPM AA300 Angstrom Advanced Inc., USA with AFM contact mode) was carried out to characterize and analyze the topography of LLSP surface before and after JGBD and CVD biosorption.

3.4 Experimental methods

In this study, the experimental procedure, batch and continuous experiments were used in this study. The continuous system of the sorption technique was carried out using fixed-bed columns.

3.4.1 Batch study

Conical flasks with a capacity of 250 ml were full with 100 ml of a dye solution with a predetermined concentration in order to create the right conditions for LLSP to remove JGBD and CVD. Each flask received a mass of LLSP, which was then added before the flasks were continuously stirred at an accelerating speed using an orbital shaker to provide LLSP enough time to reach equilibrium at room temperature (25±2 °C). Finally, the samples were taken out and filtered. Using a double beam UV-VIS spectrophotometer (UV/VIS-6800 JENWAY) with a maximum wavelength, for each dye to find the remaining concentrate of JGBD and CVD. The maximum wavelength of JGBD was determined to be 611 nm, whereas for CVD was 591 nm. An established calibration curve was used to determine the remaining dye

concentration throughout experimental procedure. Table (3.2) provide a list of the major various factors studied in batch investigations.

Table (3.3): The main different parameters used in batch experiments for JGBD and CVD**.**

Factor	Range	Purpose
pH solution	3 – 11	To identify the best pH
Contact time, min	5 – 90	Determining the optimal contact time for the removal of each dye
Dose, g/ 100 ml dye solution	0.05 – 0.8	To determine the optimum bisorbent quantity
Initial dye concentration, mg/l	10 – 100 30, 75, 150, 200	For isotherm analysis and study of kinetics.

The following equations were used to determine the removal efficiency and sorption capacity:

$$R\% = \frac{C_\circ - C_e}{C_\circ} \times 100 \quad \text{……..……(3.1)}$$

$$q_e = \frac{(C_\circ - C_e)V}{m} \quad \text{……(3.2)}$$

Where:

$R\ \%$ = Percentage removal

C_o = Initial concentration of dye (mg/l)

C_e = Concentration of dye at equilibrium time (mg/l)

V = Volume of dye solution (l)

q_e = Sorption capacity at equilibirum time (mg/g)

m = Sorbent mass (g).

3.4.1.1 Point zero charge (pH_{pzc}) of LLSP determination

An important characteristic that helps to determine which ionic species may be biosorbed utilizing LLSP at desired pH value at which the LLSP surface charge is neutral and named the pH_{pzc}, which is the pH value where the ending and beginning pH are equal. The earlier method is used to calculate the pH_{pzc} of LLSP (Mohseni et al., 2016). This approach has been explained as follows: 50 ml of 0.1 M NaCl with varied starting pH values (2-10) and ambient temperature (25±2 °C) were added to 0.5 g of LLSP. The suspensions were stirred for 24 hours before being emptied, then, the point of pH of each residual solution was measured. The point of intersection between the curve and zero that was created by plotting the initial pH against the ΔpH value yielded the value of pH_{pzc} for the LLSP.

3.4.2 Experimental and procedure setup for continous biosorption

Continuous experiments were conducted to study very important properties that are required to determine the dynamic and operational response of the sorption column. The time and shape of the appearance of the breakthrough curves were studied and determined in response to different operating parameters, where by the breakthrough curves were created by drawing C/C_0.

The Pyrex glass tube long is 750 mm that makes up the continuous system has an inner diameter of 20 mm. To make sure even distribution of the dye throughout the surface area, a layer of glass wool and glass beads measuring 5 mm in size was positioned close to the entry to the column. Glass wool was also added at the lowest of the column to prevent the a leak of the LLSP from the column and its loss. The system contains many parts that were drawn graphically and photographically as shown in Figure (3.2) and (3.3), respectively. A certain amount of LLSP was added to the fixed base column with different heights, which are 10 cm, 15 cm and 25 cm. Using a peristaltic

pump (model ISMATEC, IDEX, Corporation, Germany) the JGBD and CVD solutions were pushed down the column at a different flow rate of 8, 16, 25 ml/min.. Before starting the experiment, the LLSP is washed to remove the air between the particles of the substance and also to get rid of the original color of the substance. Experiments were carried out at room temperature (25±2 ℃). Samples were drawn every 15 minutes in all experiments until the sorption capacity of both dyes reached equilibrium and saturation. Table (3.4) lists the variables that were considered in achieving sorption of LLSP in continuous

Table (3.4): The main factors used in continuous experiments.

Factor	Range	Purpose
JGBD and CVD solution flow rate, ml/min	8, 16, 25	To assess the impact of various dye solution flow rates on breakthrough curves
LLSP bed height, cm	10, 15, 25	To investigate the effects of various biosorbent bed heights on breakthrough curves
Initial dye concentration of each dye, mg/l	25, 50, 75	To investigate the impact of various initial dye concentrations on breakthrough curves

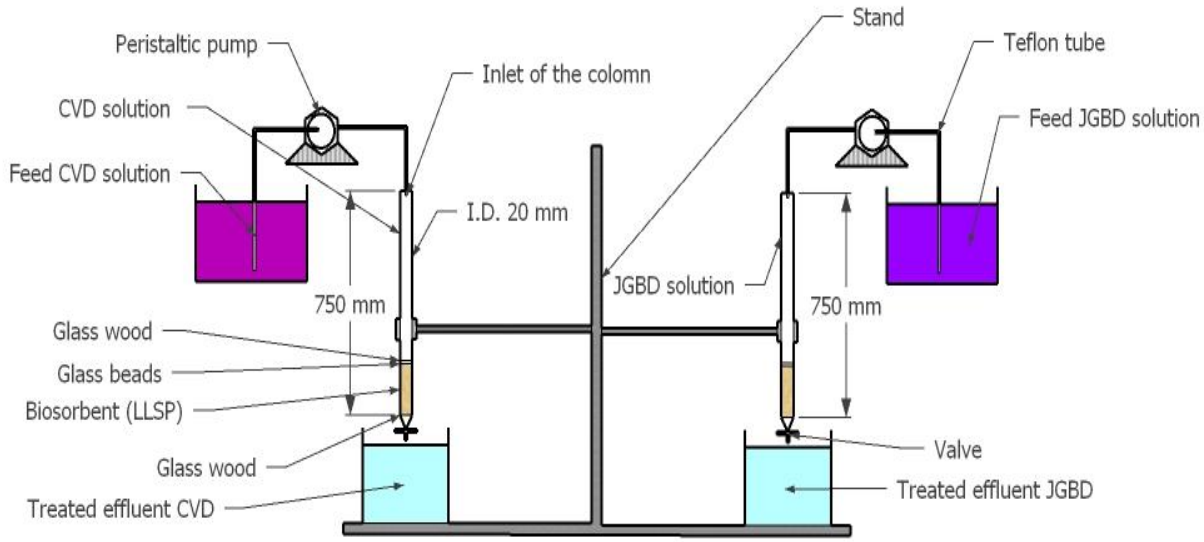

Fig. (3.4): The diagram of the fixed-bed column construction utilized in the investigation of dynamic sorption of JGBD and CVD.

Fig. (3.5): A fixed-bed column construction is set up in a lab for LLSP sorption tests.

Chapter Four

Results and Discussion

Chapter Four

Results and Discussion

4.1 Introduction

The efficiency of LLSP as sorbent for removing JGBD and CVD from aqueous solutions was tested using sorption technique in the batch and continuous test. The objective of the properties analysis is to show the importance of sorption properties such as surface area, topography, and active sites change before and after JGBD and CVD removal. Batch and continous systems are used to investigate LLSP sorption ability for JGBD and CVD removal. In batch test at room temperature (25 ± 2◦C), the influence of dye solution pH, contact time, LLSP dosage, and dye concentration on sorption capacity is examined. To understand the sorption isotherm of each dye and the nature of LLSP interaction, the equilibrim data were modeled using Langmuir and Freundlich isotherm models. To determine sorption kinetics and mechanism, batch experimental data was analyzed using pseudo first order, pseudo second order, intraparticle diffusion and Elovich models. The information is analyzed in a continuous flow system to examine the influence of operational factors on breakthrough curves.

4.2 Characterization of natural LLSP

4.2.1 Characterization of particular surface of LLSP

Table (4.1) shows the values of physicochemical parameters of natural LLSP biosorbent. The Brunauer-Emmett-Teller (BET) technique was used to find the S_{BET} of sorbent, which was based on the linear component of the N_2 adsorption-desorption isotherm.

Table (4.1): Physiochemical LLSP properties.

Property	Value
Moisture-content %	0.4
Bulk-density (g/ml)	0.342
Point-zero-charge (pH_{pzc})	4.2

In comparison to other absorbent, the LLSP sample has a significantly high percentage of carbon concentration. As a result, It may be found that the sample is dominated by carbon, indicating that it is carbonaceous and appropriate for sorption. The existence of a modest number of contaminants was suggested by the extremely low level of S. Table (4.2) lists the rest of LLSP elemental analysis.

Table (4.2): Elemental-analysis (%W/W) of LLSP.

Biosorbent	**C**	**O**	**N**	**H**	**S**	**Mg**	**Si**
LLSP	62.54	22.34	4.13	6.24	0.34	2.25	2.16

4.2.2 Characterization of porous properties

Figure (4.1) shows the isotherm of N_2 adsorption and desorption isotherms measured on LLSP which was used to get its characteristic structures when the hysteresis loops are related with the capillary condensation in mesopores. The expanding final parts of the isotherms display the formation of macropores in the pore structures of the considered sample. Table (4.3) summarizes the structural parameters of LLSP. The calculated micropore volume V_{micro} of the investigated sample shown that the participation of small pores to the total volume of pore is not important.

From Figure (4.1), it can be seen that a large uptake is observed near saturation pressure. As stated in the definition by the International-Union of Pure and Applied Chemistry (IUPAC), it can be noticed that LLSP sample is mesoporous adsorbent pores with an average diameter in a range of 2-50 nm (Kuila and Prasad, 2013). The biosorbent pore diameter (D_P) of LLSP was 4.364 nm.

Table (4.3): Parameters of LLSP structure.

Characteristic	**Value**
Specific surface area (S_{BET})[m^2 g^{-1}]	36.57
External surface area of pores (S_t) [m^2g^{-1}]	27.13
Total pore volume(V_t) [cm^3 g^{-1}]	0.16496
Volume of micropores (V_{micro}) [cm^3 g^{-1}]%	0.004
Volume of mesopores + macropores (V_{meso} + V_{mac}) [cm^3 g^{-1}]%	0.16096
BJH Adsorption cumulative volume of pores between 1.7000nm and 300.000nm width (cm^3 g^{-1})	0.312
BJH Adsorption cumulative surface area of pores between 1.7000nm and 300.000nm width (cm^2 g^{-1})	24.286
BJH Adsorption average pore diameter(nm) – D_p	4.364
BJH Adsorption average pore width (nm)	5.219

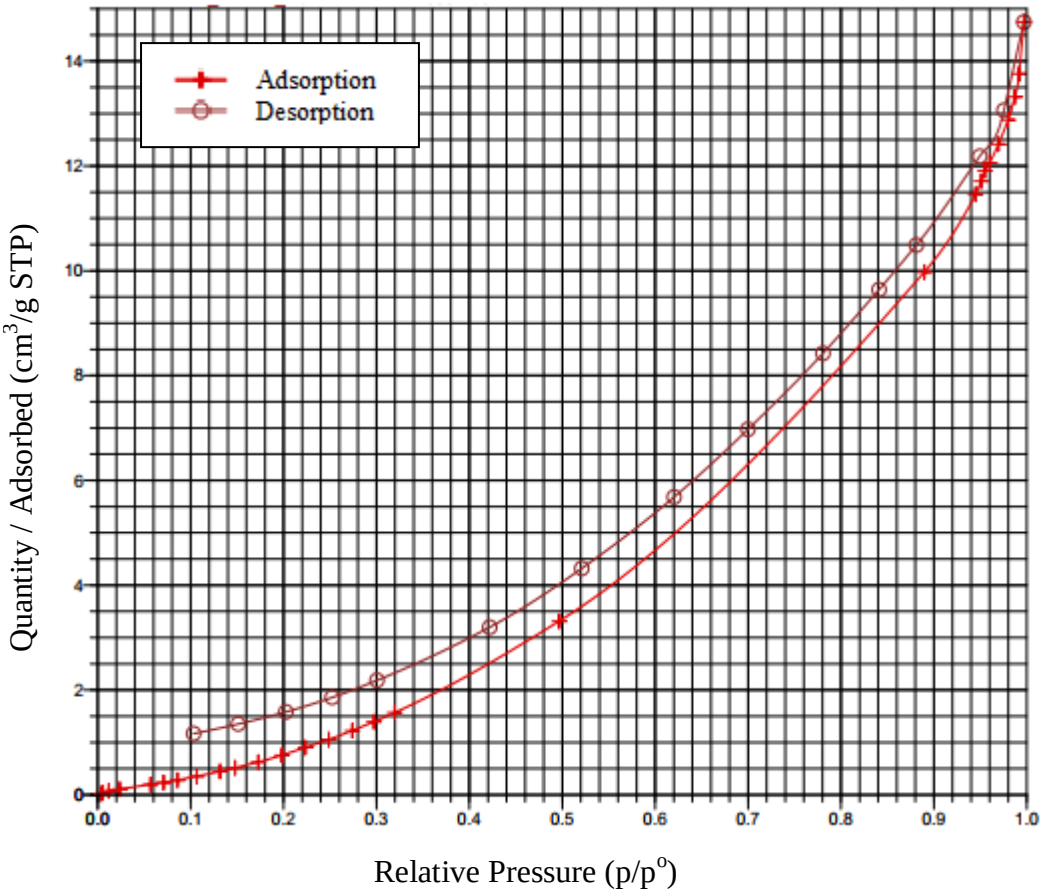

Fig. (4.1): Isotherm linear plot of LLSP.

4.2.3 FTIR analysis

In order to evaluate the mechanism of the sorption of JGBD and CVD also identify the functional groups current on the superficial of LLSP, which are able to biosorb dyes ions, the FTIR analysis was performed. The analysis of LLSP before and after sorption of each dye are shown in Figure (4.2a, b, c) and Table (4.4 and 4.5). The biosorbent material was lignocellulosic. It shows the characteristic broad and strong peaks at 3851.20 cm^{-1} and 3401.23 cm^{-1} which are ascribed to the presence of carboxylic acids group (-COOH), which overlapped with O-H stretching vibration of the hydrogen-bonded hydroxyl groups in the cellulose molecule and –NH groups (Kong et al., 2013). The band of 2922.77 cm^{-1} was corresponded to C-H asymmetric stretching vibrations in aromatic methoxyl groups, in the methyl and methylene groups of the side

chains (Álvarez et al., 2014; Kostic et al., 2014). The bands at 2356.51 cm^{-1} and 2326.94 cm are assigned to the C=C stretching vibrations in alkyne group.

The peak observed at 2028.96 cm^{-1} was assigned to the C=O stretching vibrations. At 1732.86 cm^{-1} appears C=O stretching vibrations of carboxylic groups (-COOH, $COOCH_3$) which can be ascribed to esters or carboxylic acids (Li et al., 2007; Patil and Shrivastava, 2012). The peaks at 1652.11 cm^{-1} and 1557.78 cm^{-1} are attributed to the stretching of C=O or C=C of aromatic bond and $–COO^-$ groups (Hanafilah et al., 2015; Mansur et al., 2020).

The peak experiential at 1538.54 cm^{-1} is assigned to the (N-H) bending of secondary amines (Hanafiah et al., 2015). The bands at 1505.26 cm^{-1}, 1489.31 cm^{-1} and 1463.69 cm^{-1} can be attributed to the presence of olefin v(C=C) vibrations. Whereas that shown at 1436.21 cm^{-1} and 1423.41 cm^{-1} are assigned to presence of the O-H bending (lactonic, ether, phenol, etc.).

The peaks at 1403.78, 1319.42 and 1292.07 cm^{-1} were associated with the C-H_2 rocking vibration were these peaks are referred to cellulose form of the carbohydrate (IIyas et al., 2017). The stretching vibrations of the C-O (ether) group around 1090.29-1196.90 cm^{-1} among others. Whereas that shown at 1046.34 cm^{-1} is assigned to the stretching vibrations of the C-OH bond (Cimá-Mukul et al., 2019). The appearance of bands at 667.96, 603.09, 588.01 and 568.35 cm^{-1} are attributed to presence of the phosphate and sulfur functional groups (Munagapat et al., 2010).

After the dyes-loaded LLSP, most absorption peaks are shifted, others are absent, and new peaks are appeared. These changes may be attributed to change in counter associated with groups suggesting that the each dye removal is controlled by hydroxyl, carboxyl and carbonyl and other active groups.

The JGBD and CVD sorption onto LLSP may be attributed to (i) chemical interaction between JGBD molecules and surface functional groups (ii) electrostatic interaction between the electron-rich sites on the biosorbent surface and dye molecules, and (iii) weak physical forces, hydrogen bonding and van der Waals interactions between the biosorbent and dye molecules. Therefore, the sorption of each dye onto LLSP surface occurs by the interaction between negatively groups of biosorbent and the positively charged of the each dye molecule. This means that a complicated pattern of both physical and chemical sorption are involved in two dyes biosorption.

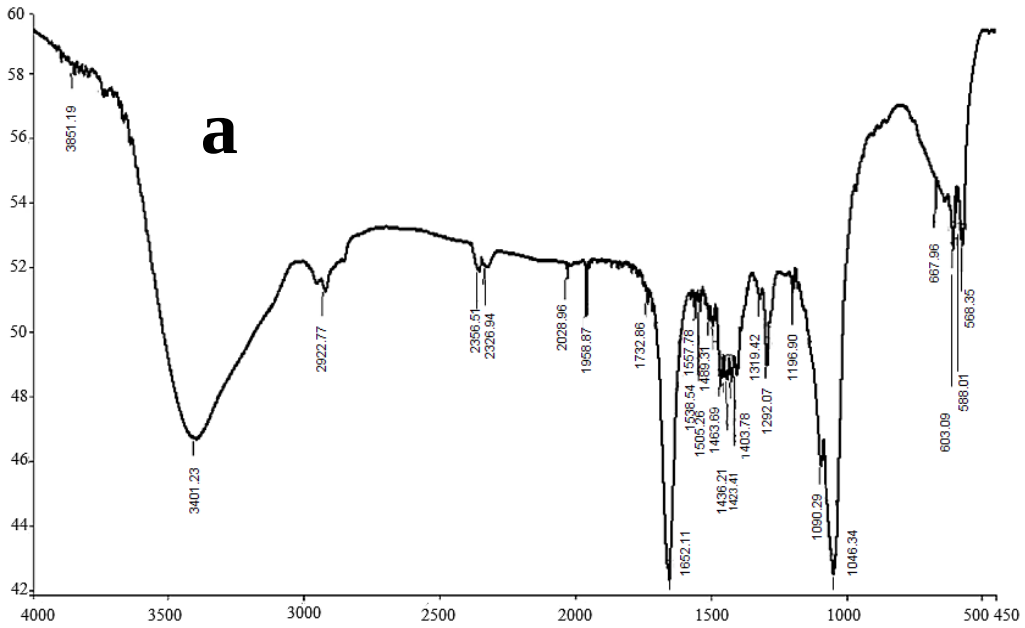

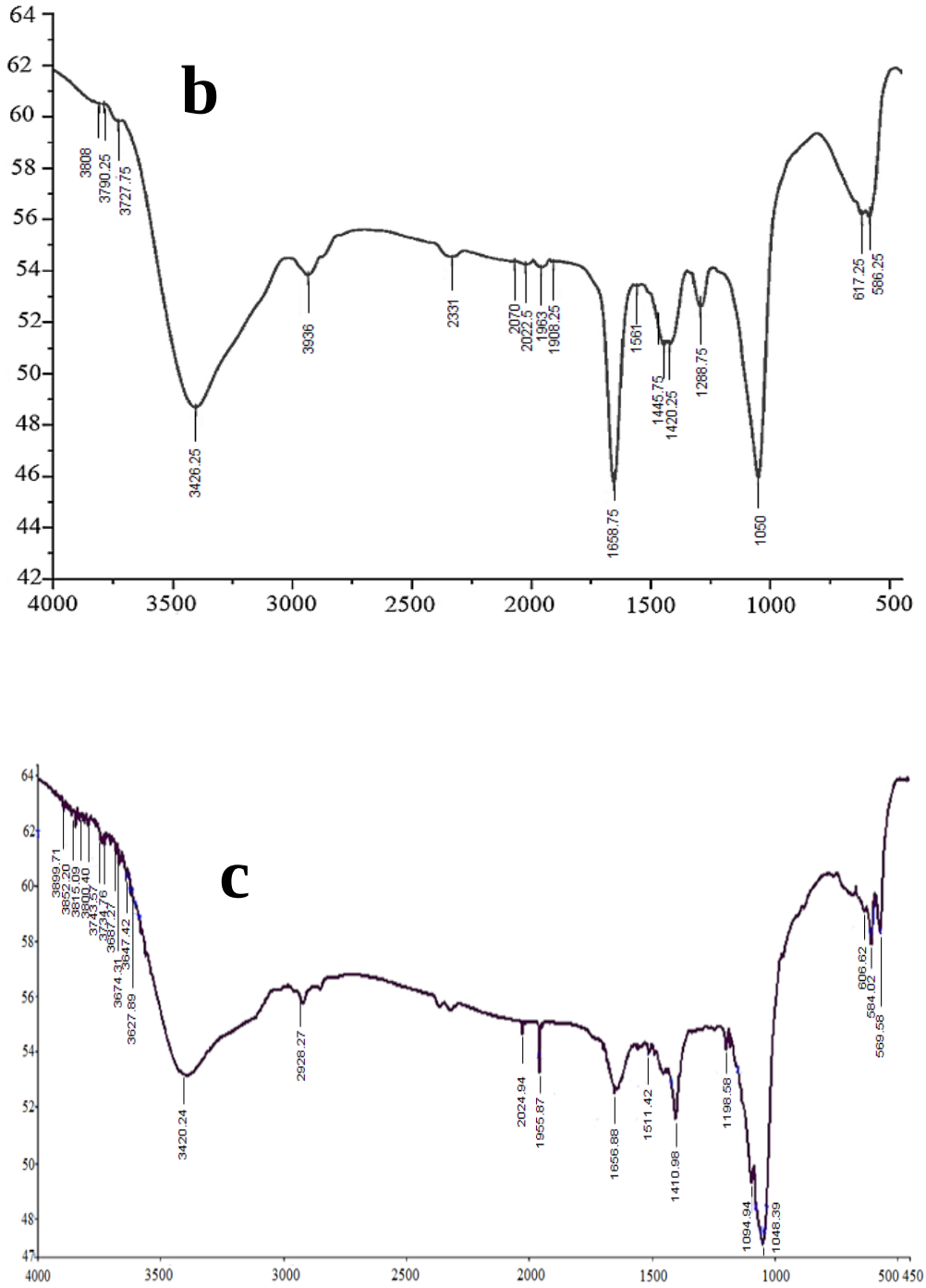

Fig.(4.2): FTIR test for: (a) LLSP (b) JGBD loaded LLSP (C) CVD loaded LLSP, initial dye concentration = 50 mg/l, at pH 9, 250 rpm using LLSP for 30 min. (b) for CVD using initial dye concentration = 50 mg/l, at pH 9, 250 for 45 min.

Table (4.4): FTIR analysis for LLSP before and after JGBD sorption.

Functional group	**Wavenumber (cm^{-1})**		**Differences**
	LLSP	**JGBD-loaded LLSP**	
Carboxylic acids group (-COOH), which overlapped with O-H stretching vibration of the hydrogen-bonded hydroxyl groups in the cellulose molecule and –NH groups	3851.19	3808	-43.19
	----	3790.25	----
	----	3727.75	----
	3401.23	3426.25	25.02
C-H asymmetric stretching vibrations in aromatic methoxyl groups, in the methyl and methylene groups of the side chains	2922.77	2936	13.23
C=C stretching vibrations in alkyne group	2356.51	2331	-25.51
	2326.94	----	----
C=O stretching vibrations of carboxylic groups (-COOH, $COOCH_3$) which can be ascribed to esters or carboxylic acids	----	2070	----
	2028.96	2022.5	6.46-
	1958.87	1963	4.13
	----	1908.25	-------
	1732.86	----	----
Stretching of C=O or C=C of aromatic bond and –COO- groups	1652.11	1658.75	6.64
	1557.78	1561	3.22
N-H bending of secondary amines	1538.54	----	----
Olefin v(C=C) vibrations	1505.26	----	----
	1489.31	----	----
	1463.69	----	----
O-H bending (lactonic, ether, phenol, etc.)	1436.21	1445.75	9.54
	1423.41	1420.25	-3.16

C-H_2 rocking vibration	1403.78	----	----
	1319.42	----	----
	1292.07	1288.75	-3.32
The stretching vibrations of the C-O (ether) group	1196.90	----	----
	1090.29	----	----
Stretching vibrations of the C-OH bond side groups	1046.34	1050	3.66
Phosphate and sulfur functional groups	667.96	----	----
	603.09	617.25	14.16
	588.01	586.25	-1.76
	568.35	----	----

Table (4.5): FTIR analysis for LLSP before and after CVD sorption.

Functional group	Wavenumber (cm^{-1})		Differences
	LLSP	**CVD-loaded LLSP**	
Carboxylic acids group (-COOH), which overlapped with O-H stretching vibration of the hydrogen-bonded hydroxyl groups in the cellulose molecule and –NH groups	3851.19	3899.71	48.52
	----	3852.20	----
	----	3815.09	----
	----	3800.40	----
	----	3743.57	----
	----	3734.76	----
	----	3687.27	----
	----	3674.31	----
	----	3647.42	----
	----	3627.89	----
	3401.23	3420.24	19.01
C-H asymmetric stretching vibrations in aromatic methoxyl groups, in the methyl and methylene groups of the side chains	2922.77	2928.27	5.5
C=C stretching vibrations in alkyne group	2356.51	----	----
	2326.94	----	----
	2028.96	2024.94	-4.02
	1958.87	1955.87	-3
	1732.86	----	----
Stretching of C=O or C=C of aromatic bond and –COO- groups	1652.11	1656.88	4.77
	1557.78	----	----
N-H bending of secondary amines	1538.54	1511.42	-27.12
Olefin v(C=C) vibrations	1505.26	----	----
	1489.31	----	----
	1463.69	----	----
O-H bending (lactonic, ether, phenol, etc.)	1436.21	----	----
	1423.41	----	----
$C-H_2$ rocking vibration	1403.78	1410.98	7.2
	1319.42	----	----
	1292.07	----	----
The stretching vibrations of the C-O (ether) group	1196.90	1198.58	1.68
	1090.29	1094.94	4.65
Stretching vibrations of the C-OH bond side	1046.34	1048.39	2.05

groups			
Phosphate and sulfur functional groups	667.96	----	----
	603.09	606.62	3.53
	588.01	584.02	-3.99
	568.35	569.58	1.23

4.2.4 Scanning electron microscopy (SEM) of LLSP

SEM images at various magnifications for LLSP before sorption process are shown in Figure (4.3a), but Figure (4.3b, c) shows the sorption state of JGBD and CVD, respectively, to investigate the surface morphology and form of the biosorbent surface. The produced LLSP has an indeterminate structure with holes of various sizes on its rough surface, as shown in Figure (4.3 a), which favors the sorption of both dyes. However, dye sorption caused some major alterations in sorbent structure Figure(4.3 b, c). Furthermore, the bserved pores on the surface of new LLSP are plugged, resulting in a buildup of occupied sorbent particles, a flat surface with white spots that shine. This statement is in agreement with Mohammed and Samaka; 2018 and Yusuff; 2019.

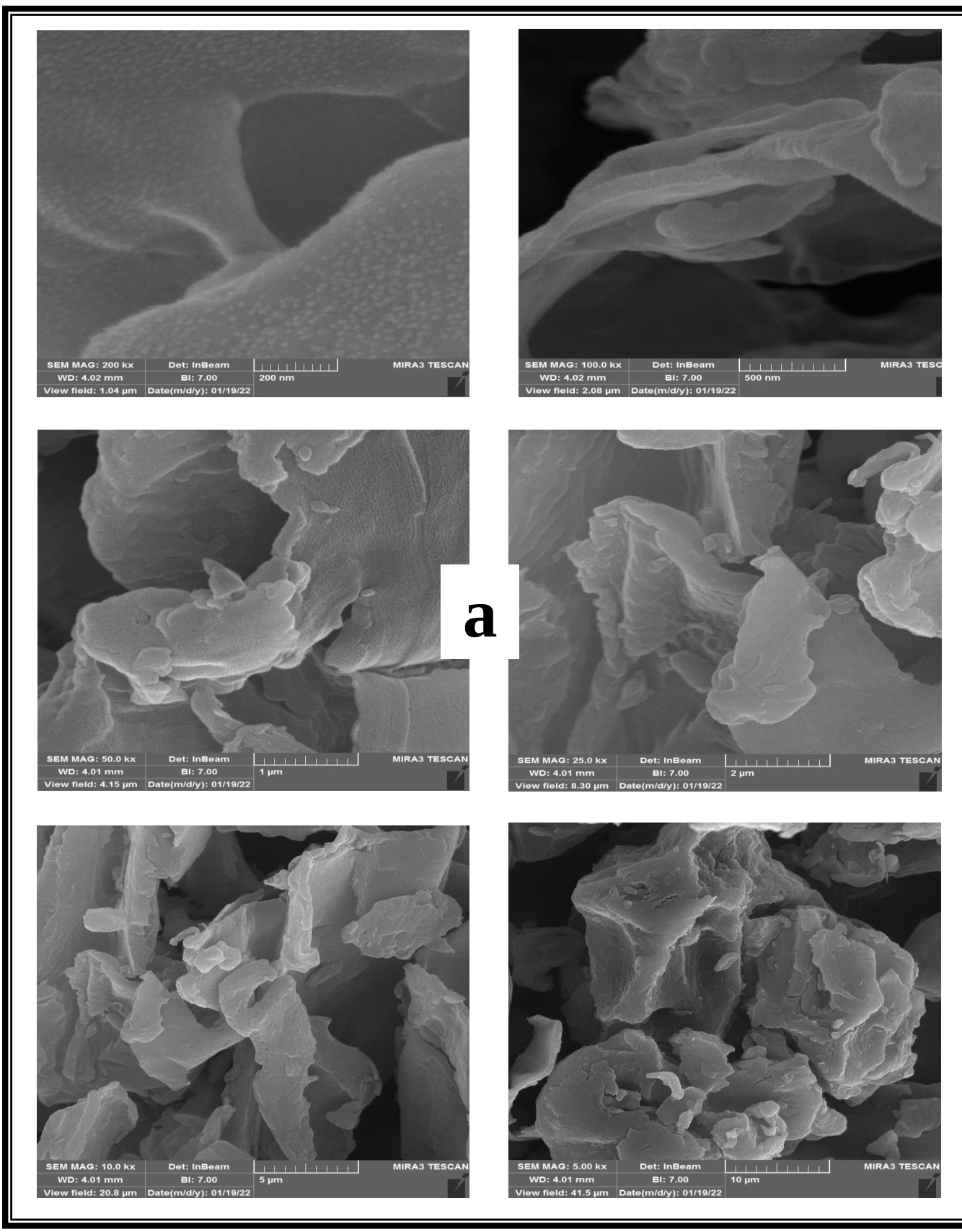
SEM MAG: 200 kx
Det: InBeam
MIRA3 TESCAN
WD: 4.02 mm
BI: 7.00
200 nm
View field: 1.04 µm
Date(m/d/y): 01/19/22
SEM MAG: 100.0 kx
Det: InBeam
MIRA3 TESC
WD: 4.02 mm
BI: 7.00
500 nm
View field: 2.08 µm
Date(m/d/y): 01/19/22
SEM MAG: 50.0 kx
Det: InBeam
MIRA3 TESCAN
WD: 4.01 mm
BI: 7.00
1 µm
View field: 4.15 µm
Date(m/d/y): 01/19/22
a
SEM MAG: 25.0 kx
Det: InBeam
MIRA3 TESCAN
WD: 4.01 mm
BI: 7.00
2 µm
View field: 8.30 µm
Date(m/d/y): 01/19/22
SEM MAG: 10.0 kx
Det: InBeam
MIRA3 TESCAN
WD: 4.01 mm
BI: 7.00
5 µm
View field: 20.8 µm
Date(m/d/y): 01/19/22
SEM MAG: 5.00 kx
Det: InBeam
MIRA3 TESCAN
WD: 4.01 mm
BI: 7.00
10 µm
View field: 41.5 µm
Date(m/d/y): 01/19/22

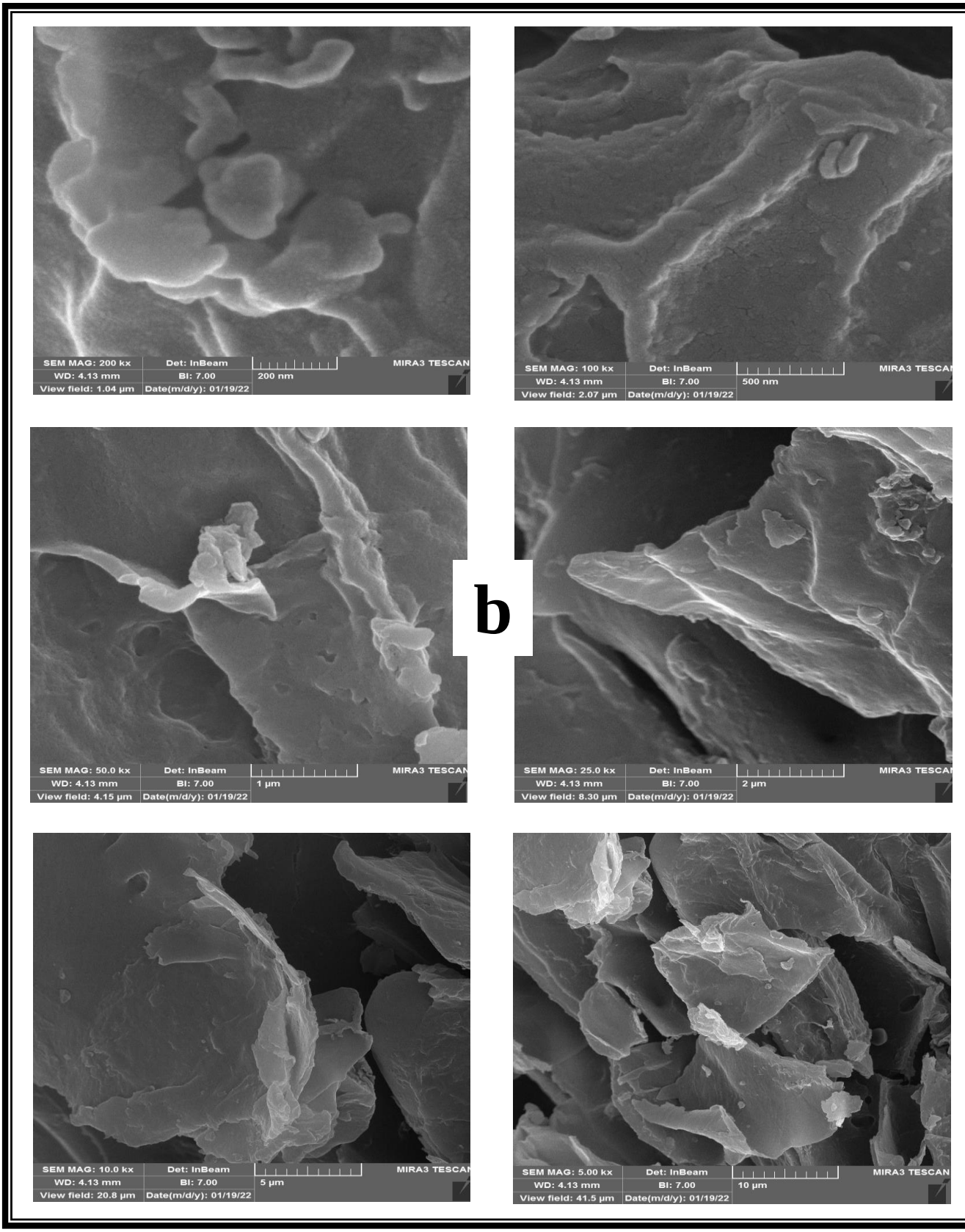
SEM MAG: 200 kx
Det: InBeam
MIRA3 TESCAN
WD: 4.13 mm
BI: 7.00
200 nm
View field: 1.04 µm
Date(m/d/y): 01/19/22
SEM MAG: 100 kx
Det: InBeam
MIRA3 TESCAN
WD: 4.13 mm
BI: 7.00
500 nm
View field: 2.07 µm
Date(m/d/y): 01/19/22
SEM MAG: 50.0 kx
Det: InBeam
MIRA3 TESCAN
WD: 4.13 mm
BI: 7.00
1 µm
View field: 4.15 µm
Date(m/d/y): 01/19/22
b
SEM MAG: 25.0 kx
Det: InBeam
MIRA3 TESCAN
WD: 4.13 mm
BI: 7.00
2 µm
View field: 8.30 µm
Date(m/d/y): 01/19/22
SEM MAG: 10.0 kx
Det: InBeam
MIRA3 TESCAN
WD: 4.13 mm
BI: 7.00
5 µm
View field: 20.8 µm
Date(m/d/y): 01/19/22
SEM MAG: 5.00 kx
Det: InBeam
MIRA3 TESCAN
WD: 4.13 mm
BI: 7.00
10 µm
View field: 41.5 µm
Date(m/d/y): 01/19/22

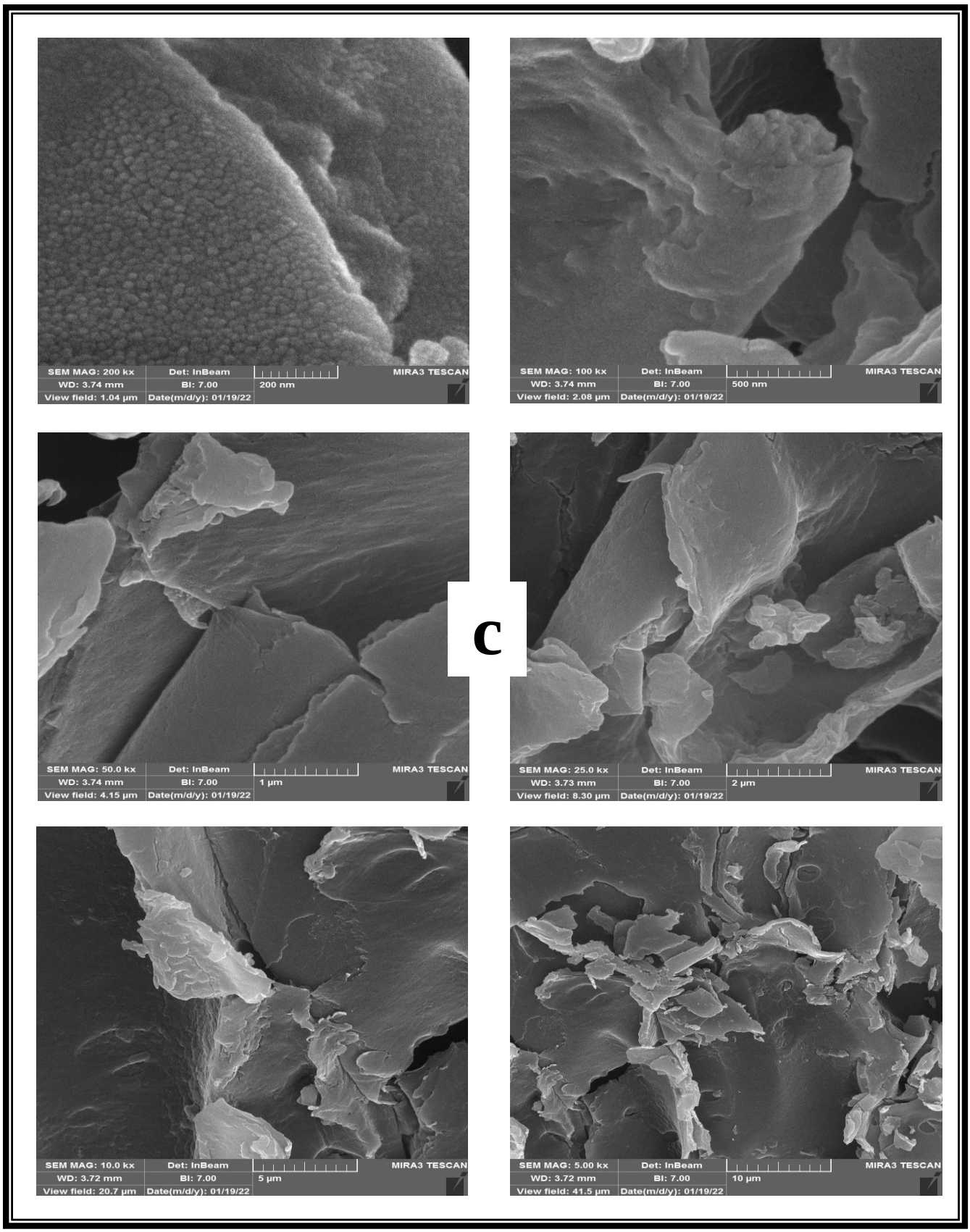

Fig. (4.3): The SEM micrograph pictures of LLSP were taken at various magnifications:
(a) before the sorption procedure (b) when JGBD sorption
(c) when CVD sorption.

4.2.5 Scanning probe microscope (SPM)

For identifying and investigation of topography of LLSP surface before and after the sorption process for each dye, the technique of SPM is used. Figure (4.4a) shows the LLSP before sorption process, while Figure (4.4b, c) shows the sorption of JGBD and CVD, respectively. Through Figure (4.4a), it is clear that LLSP has an irregular and distorted surface and the pores are rough and not homogeneous, suggesting the possibility of high sorption of the positive dye molcules.

After sorption of each dye, the LLSP surface has less roughness and surface area, and this is due to the difference in the number and shape of the dots according to the amount of JGBD or CVD dye ions deposited on the surface of the LLSP, which leads to a reduction in the surface roughness and porous structures (Jawad et al., 2018; Badr and Samaka, 2021). Table (4.6) lists the most findings of this test.

Table(4.6): LLSP characteristics before and after sorption of JGBD and CVD by SPM technique.

Character	Before biosorption	After loaded with JGBD	After loaded with CVD
Sa (roughness average) (nm)	11.78	3.477	4.399
Ssk (surface skewness)	1.336	2.735	1.888
Sz Ten point height (nm)	117	63.04	39.94
Sdr (surface area ratio)	99.29	16.91	26.53
Sk (core roughness depth) (nm)	26.13	9.614	9.861

(a)

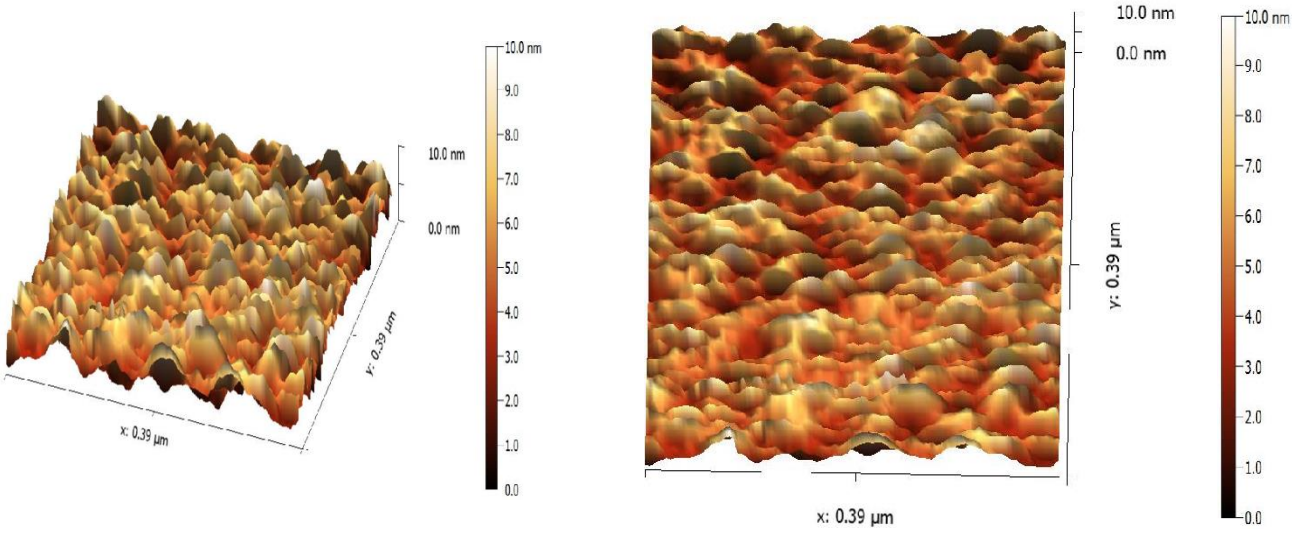
10.0 nm
0.0 nm
x: 0.39 µm
y: 0.39 µm
10.0 nm
9.0
8.0
7.0
6.0
5.0
4.0
3.0
2.0
1.0
0.0

(b)

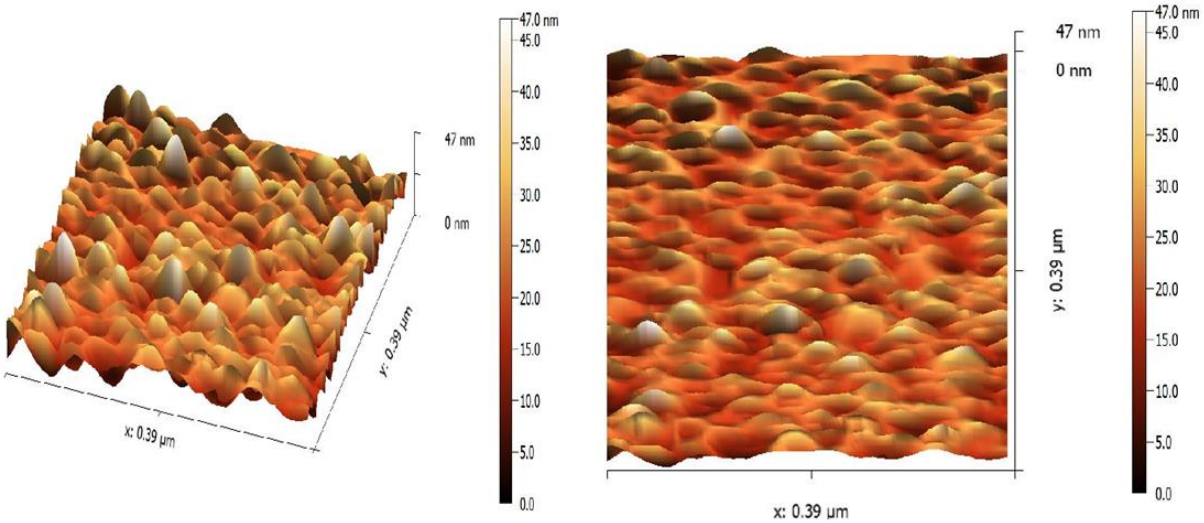
47 nm
0 nm
x: 0.39 µm
y: 0.39 µm
47.0 nm
45.0
40.0
35.0
30.0
25.0
20.0
15.0
10.0
5.0
0.0

(c)

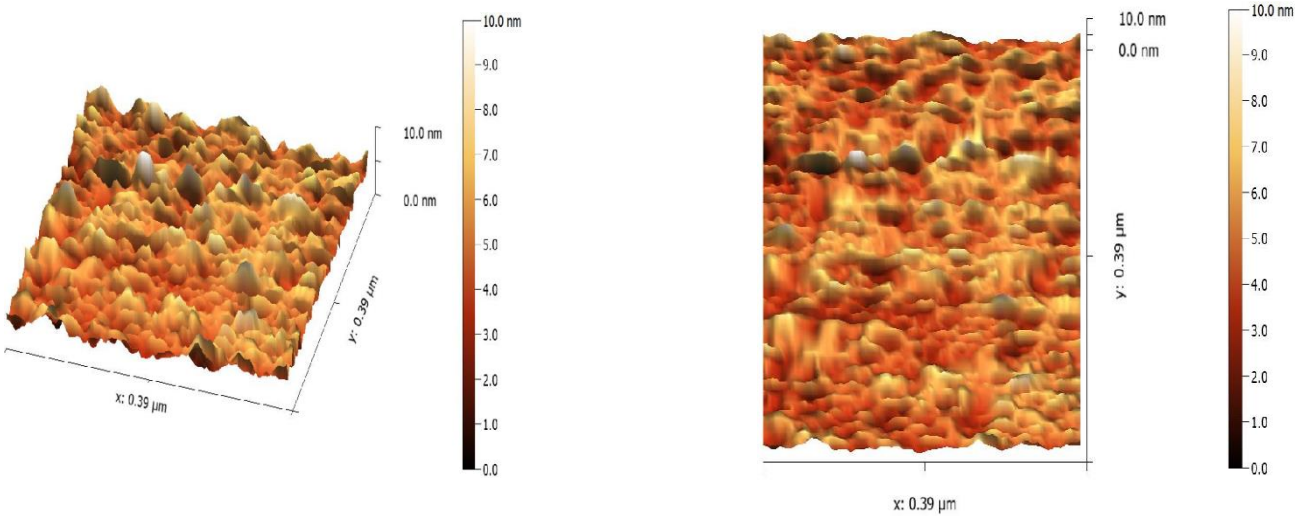

Fig.(4.4): Scanning probe microscope for LLSP: (a) before dyes sorption (b) after JGBD sorption (c) after CVD sorption, initial dye concentration = 50 mg/l, at pH 9, 250 rpm using LLSP for 30 min. (b) for CVD using initial dye concentration = 50 mg/l, at pH 9, 250 for 45 min.

4.3 The effects of experimental factors

4.3.1 Effect of solution pH

The pH of the dye solution is the most important parameter determining the adsorption process when compared to all other elements. The removal efficiency of LLSP as a function of JGBD and CVD solution pH is shown in Figure (4.5). The dye removal rises with increasing solution pH and reaches a maximum value at pH=9 for both dyes (98.75 % for JGBD and 97.25% for CVD), and the dye solution of pH was set in the following studies, but the fact that the water is mostly neutral at 7 pH, and since the change in the removal efficiency ratio is small, it can be considered that the neutral medium is preferred, to prevent the addition of any chemical compounds in the water to raise the pH value, because these compounds will affect the water quality.

This is due to the LLSP surface has more negatively charged sites, which promotes electrostatic interaction between the LLSP and the positively charged dye. Protons are present on the LLSP surface examined, causing electrostatic repulsion between the adsorbed H^+ and the cationic JGBD or CVD, which accounts for the limited removal at low pH. These findings are agreement with what has been found in the literature (Phuong et al., 2019; Sebeia et al., 2020). Figure (4.6) demonstrates that the point of zero charge of LLSP is 4.2, indicating that the LLSP surface is positively charged at pH lower than pH_{pze}. When pH exceeds pH_{pze}, the LLSP surface becomes negatively charged, which aids cationic JGBD or CVD sorption (Franca et al., 2009).

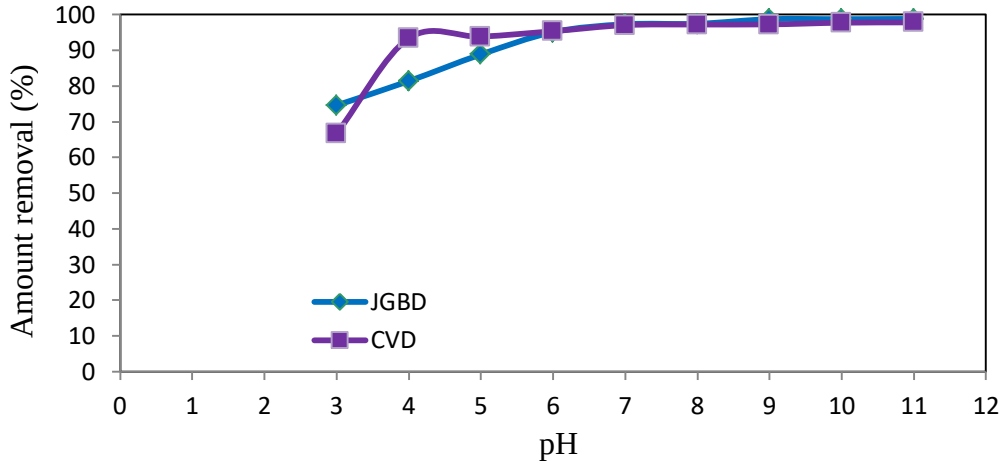

Fig. (4.5): Effect of the pH of the original dye solution on the effectiveness of JGBD and CVD removal from LLSP (LLSP dose = 0.08 gm for JGBD and 0.3 gm for CVD, initial dye concentration for each dye= 50 mg/l, and 250 rpm for 60 min.

Because the superficial area of LLSP is positive charge at pH < pH_{pzc} for two dyes, excess H^+ on the biosorbent surface repels cationic JGBD or CVD, resulting in poor dye sorption. The negatively charged surface of LLSP works as a cation attractor when the pH of the solution exceeds pH_{PZC} (pH > 4.2) for JGBD and CVD, generating high attraction between the biosorbent surface and the cationic JGBD or CVD, resulting in rapid dye sorption (Belhouchat et al., 2017).

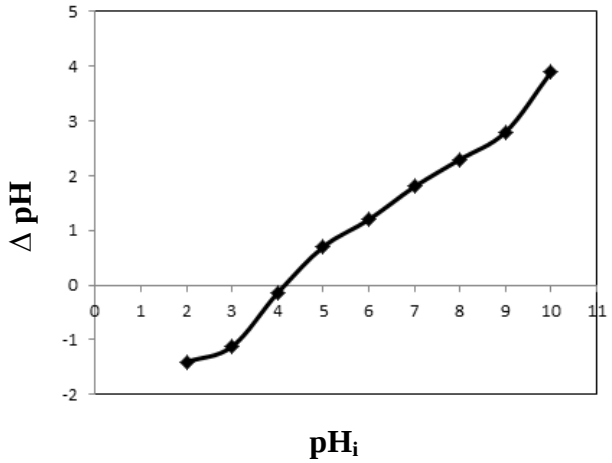

Fig. (4.6): Identification of point zero charge (pH_{pzc}) of LLSP.

4.3.2 The influence of contact time

The contact time factor, which is critical in the sorption process, used to determine the sorption equilibrium. Figure (4.7a) explains JGBD sorption was fast for the first 5 minutes and Figure (4.7b) shows sorption was fast for the period 5 minutes for CVD, because there are more potential sorption sites for JGBD or CVD molecules in the early phases of sorption, the adsorption rate for JGBD or CVD molecules is very high.

The sorption capacity at equilibrium was 61.3 mg/g and 16.1 mg/g for JGBD and CVD, respectively for C_o=50 mg/l, and the sorption rate gradually decreased and reached equilibrium in around 30 min for JGBD and 45 min for CVD. The period of 30 min. was designed in the next studies for JGBD and 45min. for CVD, when there was no significant increase uptake after this time. As a result, the JGBD or CVD aggregate at the LLSP surface, these sites gradually fill up, and sorption slows.

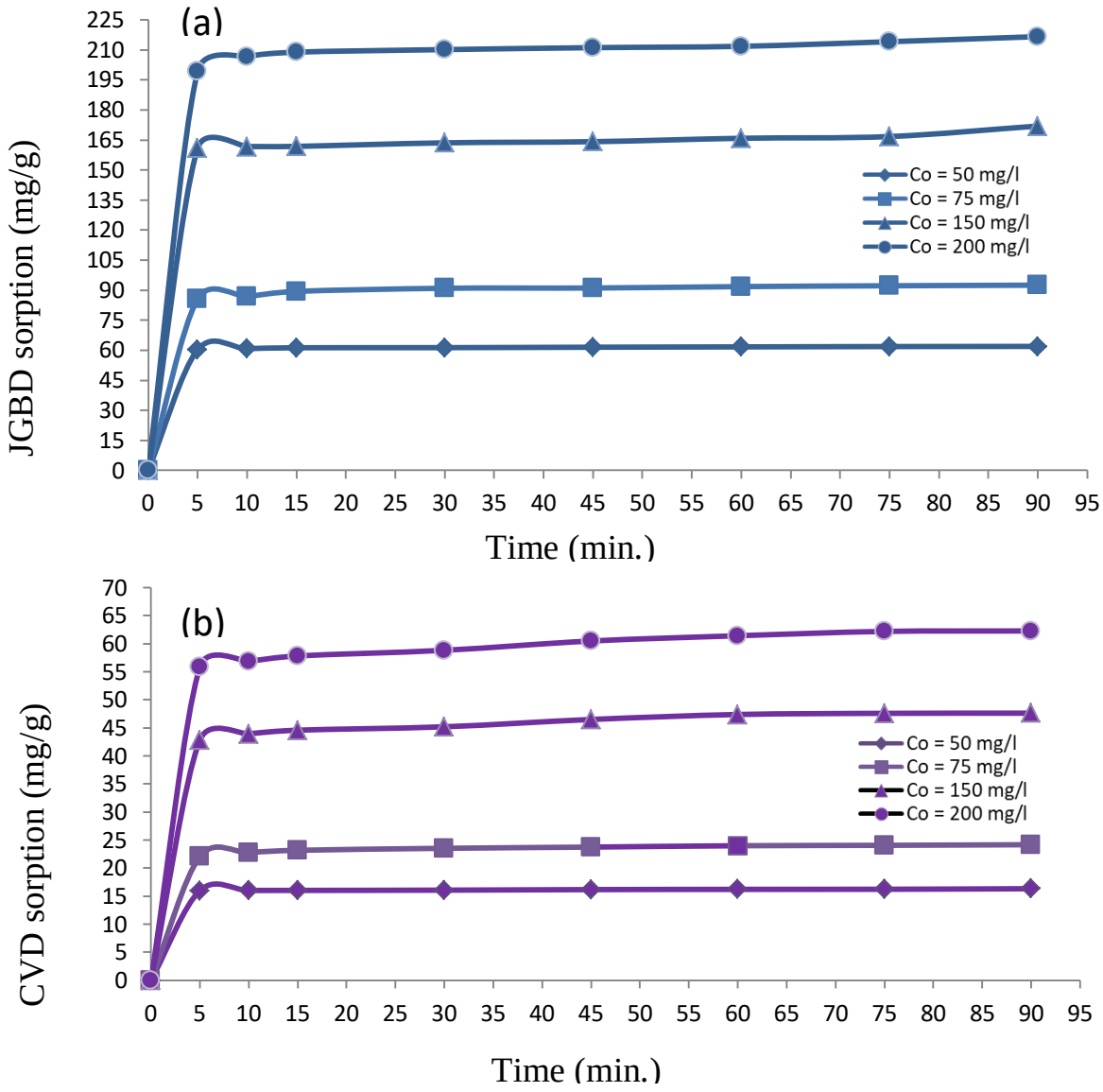

Fig. (4.7): Effect of contact time on sorption capacity (mg/g) of LLSP: (a) JGBD, (dose of LLSP = 0.08 gm , initial JGBD concentration = 50 mg/l, pH =9, 250 rpm for 30 min.). (b) CVD, (dose of LLSP = 0.3 gm, pH =9, 250 rpm for 45 min.

4.3.3 The biosorbent dose influence

The dose of biosorbent is an important parameter in the sorption process, as is determining the system adsorbent-adsorbate equilibrium (Deveci, 2013). To evaluate the effect of LLSP dosage on JGBD or CVD sorbed quantity and removal percentage, the amount of LLSP was changed between 0.05 and 0.8 g/100 ml of dye solution while keeping all other variables constant. Figure (4.8a, b) shows the effect of LLSP dosage on elimination percentage on JGBD and CVD, respectively. It is clear that as the LLSP dosage was increased, the removal efficiency of each dye increased and remained around 98% and 97% for JGBD and CVD, respectively at dose of LLSP of 0.08 g for JGBD and 0.3 g for CVD , but the dye amount biosorbed did not perform similarly to the sorption percentage, when the dye amount biosorbed decreased from 93.5 to 6.15 mg/g and 91.67 to 5.9 mg/g for JGBD and CVD, respectively.

As a result, 0.08 gm of LLSP was selected as the optimal dose for JGBD and 0.3 gm of LLSP for CVD. With an increase in the LLSP dosage in the range of 0.05–0.8 g/100 ml, the sorption capacity of JGBD or CVD dropped while the sorption percentage increased. Previous research revealed a similar pattern (Dawood et al., 2016; Yang et al., 2016). When the LLSP dosage is increased, the number of accessible sorption sites rises, resulting in an increase in JGBD and CVD elimination efficiency. However, increasing the LLSP dose can lead to particle interactions and sorption site aggregation (Chen et al., 2015), which could lead to a decrease in total LLSP surface area available to the JGBD or CVD and an increase in diffusion path length (Dotto et al., 2015).

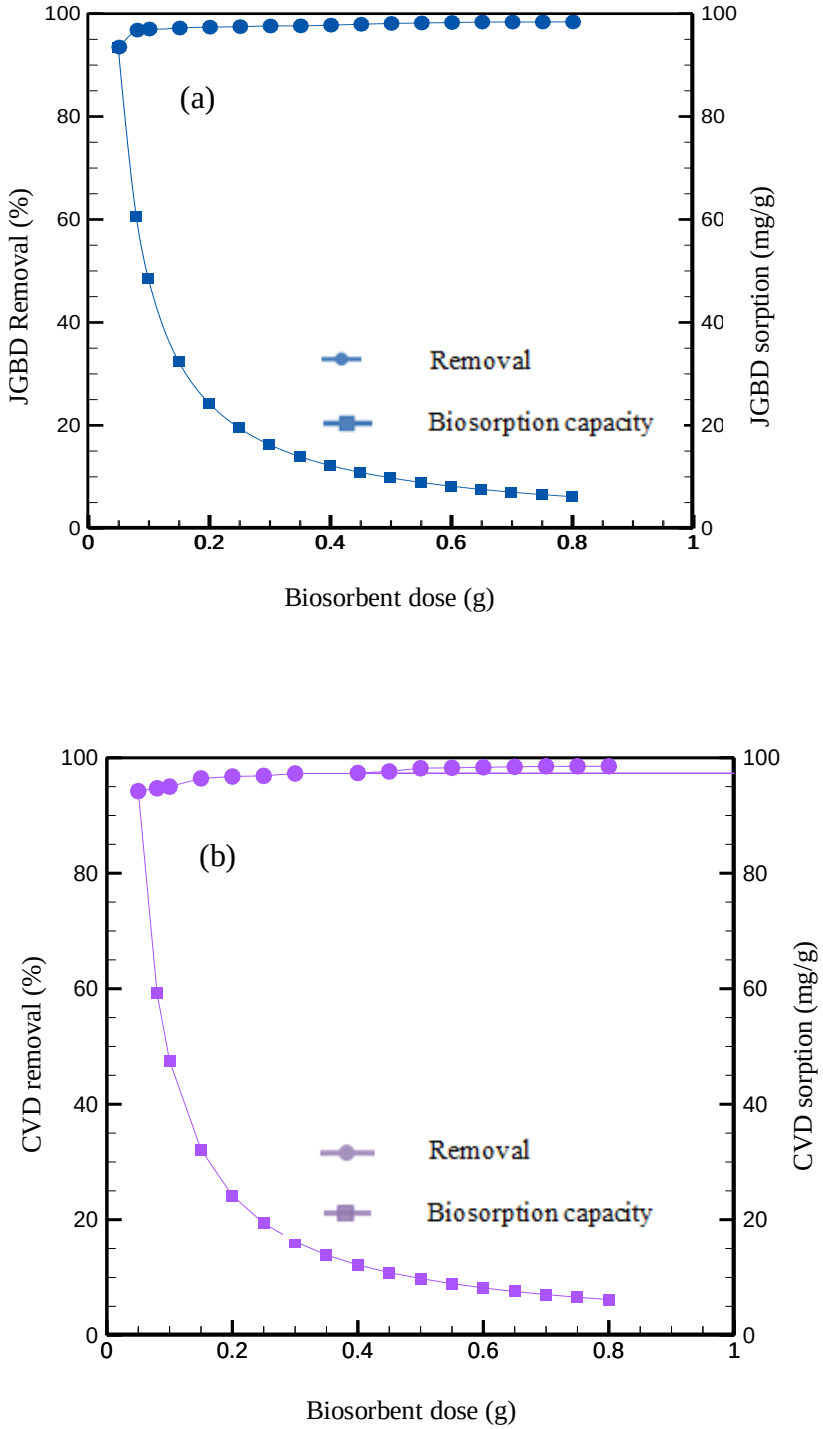

Fig. (4.8): Percentage removal and sorption capacity of dyes: (a) for JGBD using initial dye concentration = 50 mg/l, at pH 9, 250 rpm using LLSP for 30 min. (b) for CVD using initial dye concentration = 50 mg/l, at pH 9, 250 for 45 min.

4.3.4 Effect of initial JGBD and CVD concentration

The effects of initial JGBD and CVD concentration, fluctuating from 10 to 100 mg/l, were studied and are shown in Figure (4.9a, b) , respectively. The quantity of each dye sorbed increases from 12.40 to 119.71 mg per gram of LLSP and from 3.33 to 31.8 mg per gram of LLSP for JGBD and CVD, respectively, when the dye concentration is increased. This finding is explained by the fact that the contact between JGBD or CVD and LLSP rises when the concentration gradient between the aqueous solution and the solid phase increases (El maguana et al., 2018; Haddad et al., 2014). When JGBD or CVD concentration was raised from 10 - 100 mg/l, the quantity of LLSP remained constant, the dye removal efficiency was lowered, because the sorption sites available in LLSP got saturated more quickly, leaving no more sites to biosorp JGBD or CVD onto LLPS, lowering the removal efficiency (Geetha et al. 2015).

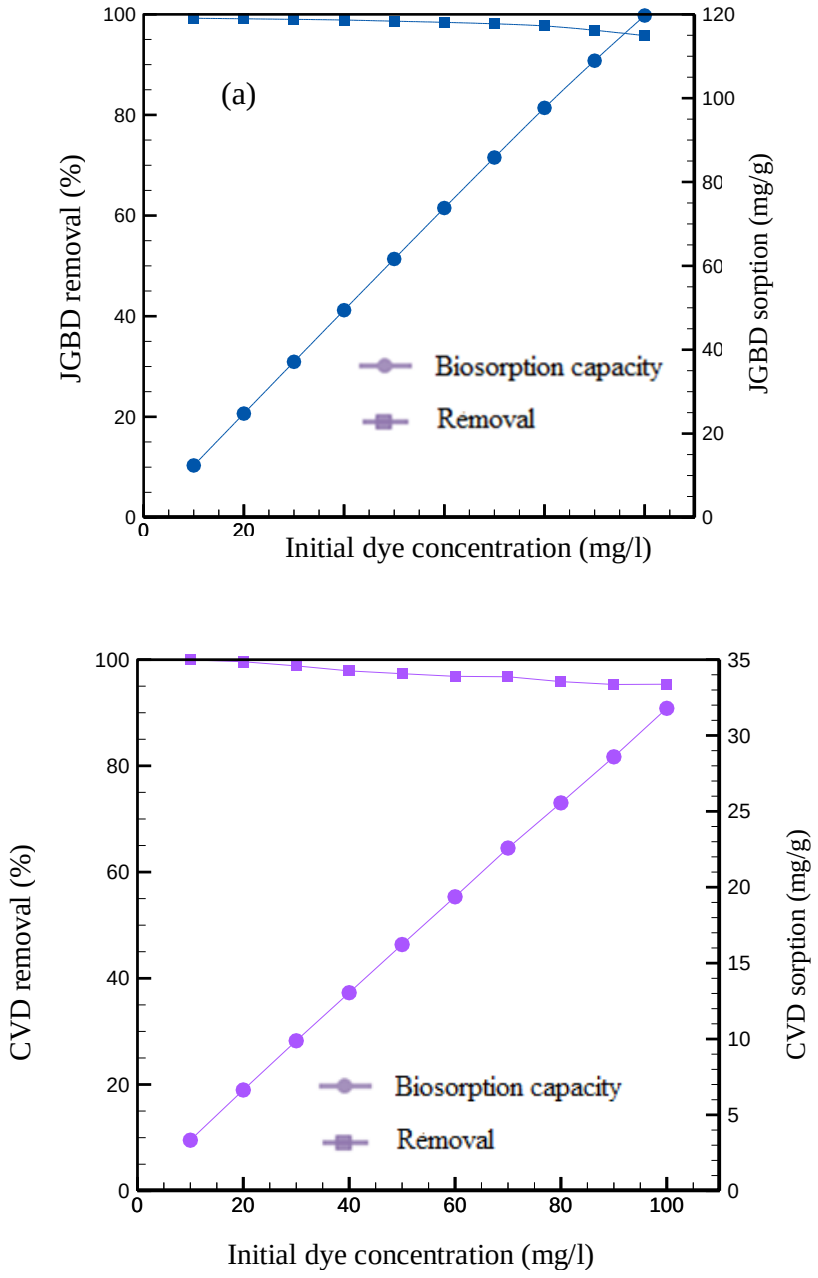

Fig. (4.9): Percentage removal and sorption capacity of dyes: (a) for JGBD at pH 9, 250 rpm using LLSP for 30 min. (b) for CVD at pH 9, 250 for 45 min.

4.4 Modeling and equilibrium sorption isotherms

Table (4.7) and Table (4.8) summarize the computed sorption isotherm constants and validation indices for two models of JGBD and CVD sorption onto LLSP. By comparing the R^2 and S.E. values, the validity of the isotherm model was established. As a result, the R^2 of the Langmuir model was closer to unity than the Freundlich model, and it accurately characterized the sorption isotherm with q_m of 142.85 mg/g for JGBD and 45.45mg/g for CVD. The values of R_L were ranged between 0 and 1, showing that JGBD and CVD sorption was respectable. The Freundlich constant may be used to evaluate the favorability of JGBD and CVD sorption using LLSP, since it has been discovered that n = 1.78 for JGBD, n = 2.94 for CVD suggesting advantageous sorption as n sits between 1 and 10 (Aljeboree et al., 2017).

As shown in Table (4.9) and Table (4.10), the sorption capacity of LLSP into JGBD and CVD were compared to that of other adsorbents, and they were discovered that the value of maximum capacity (q_m) of LLSP is greater, indicating that LLSP may be used as a sorbent to sequestrate JGBD and CVD from aqueous solutions. Figure (4.10 a, b) and (4.11 a, b) show linearized Langmuir and Freundlich isotherm model for sorption of JGBD and CVD, respectively using LLSP,

The sorption isotherms obtained by Langmuir isotherm and Freundlich isotherm models along with experimental data of JGBD and CVD are shown in Figure (4.12). It can be shown that the sorption capacity increased with an increase in the equilibrium concentration and it is shown that experimental data of sorption for JGBD & CVD onto sorbents could be well fitted by the isotherms. Clearly, the Langmuir equation provided better simulating in terms of and S.E. values from the Freundlich equation.

Table (4.7): Coefficients of sorption isotherm for JGBD using of LLSP.

Langmuir (95% Confidence level)		**Freundlich (95% Confidence level)**	
q_m (mg/g)	142.85	K_F (mg/g)(l/mg)$^{1/n}$	66.86
b (l/mg)	1.14	1/n	0.56
RMSE	5.68 mg/g	RMSE	130.53mg/g
MAE	2.18 mg/g	MAE	8.21 mg/g
R^2	0.9996	R^2	0.9584
S.E.	0.000207	S.E.	0.04522
R_L	(0.1716 - 0.9178)		
Equation	$q_e = 162.85\ C_e / (1+1.14C_e)$	Equation	$q_e = 66.86\ C_e^{0.56}$

Table (4.8): Coefficients of sorption isotherm for CVD using of LLSP.

Langmuir (95% Confidence level)		**Freundlich (95% Confidence level)**	
q_m (mg/g)	45.45	K_F (mg/g)(l/mg)$^{1/n}$	16.83
b (l/mg)	0.35	1/n	0.34
RMSE	1.18 mg/g	RMSE	7.08 mg/g
MAE	0.94 mg/g	MAE	2.15 mg/g
R^2	0.9906	R^2	0.9581
S.E.	0.00309	S.E.	0.06792
R_L	(0.4240 - 0.9982)		
Equation	$q_e = 15.9\ C_e / (1+0.35C_e)$	Equation	$q_e = 16.83\ C_e^{0.34}$

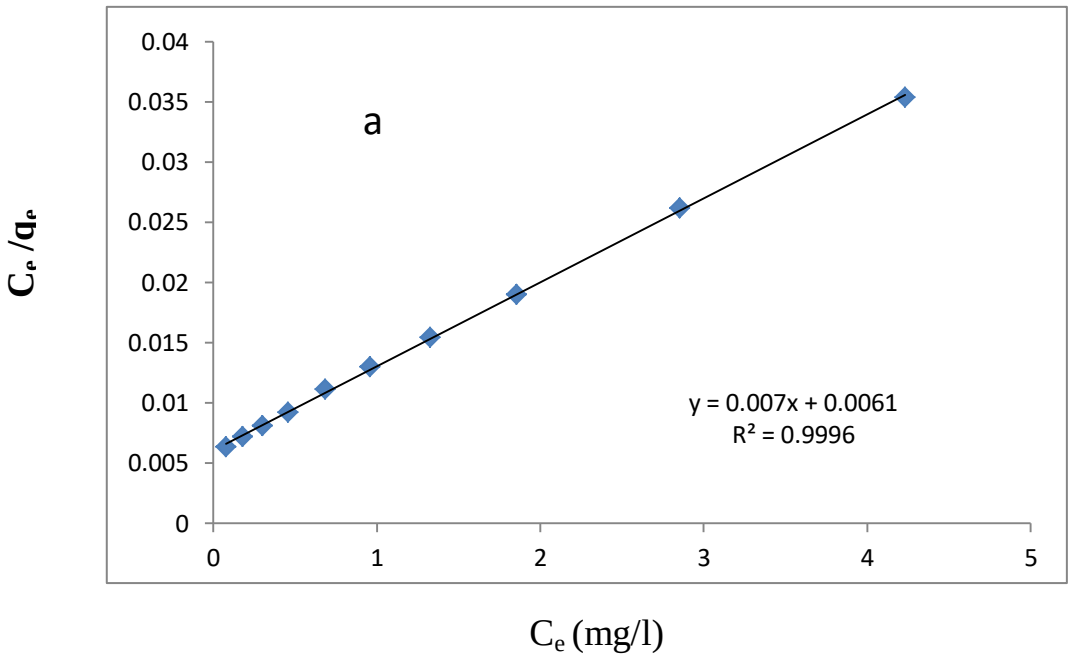

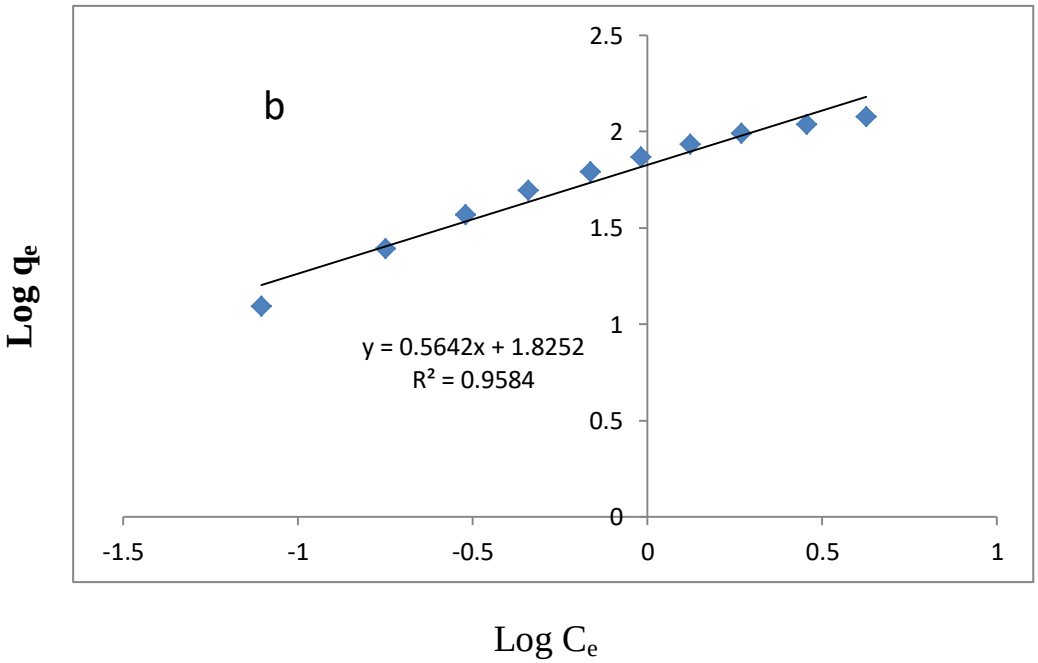

Fig. (4.10): (a) Linearized Langmuir isotherm model for sorption of JGBD using LLSP. (b) Linearized Freundlich isotherm model for sorption of JGBD using LLSP.

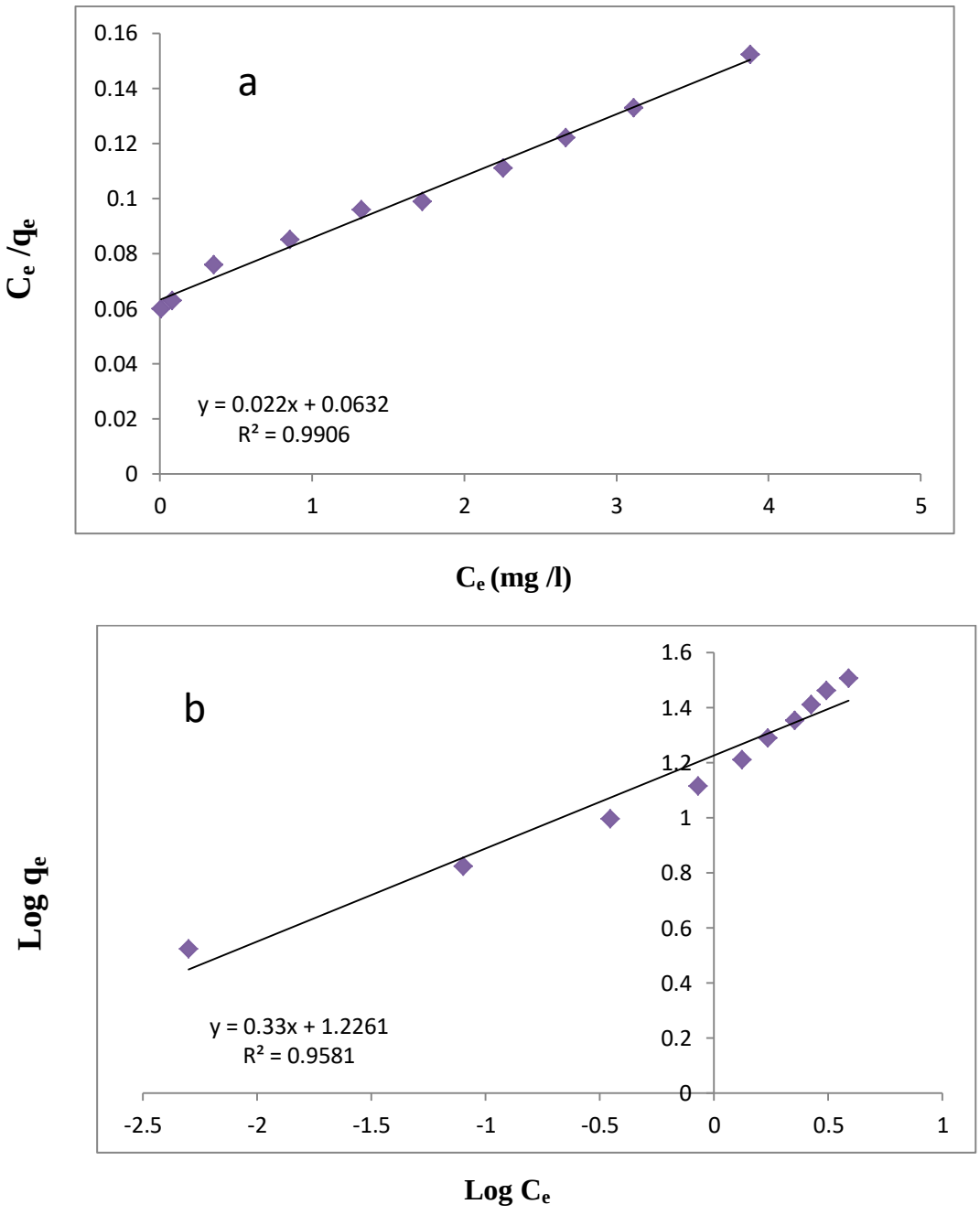

Fig. (4.11): (a), Linearized Langmuir isotherm model for sorption of CVD using LLSP. (b) Linearized Fruendlich isotherm model for sorption of CVD using LLSP.

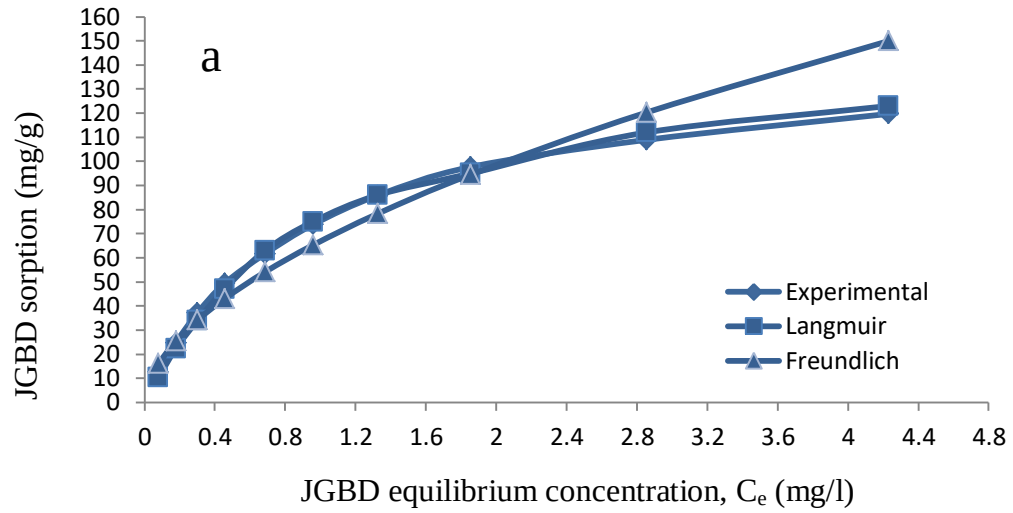

For JGBD Langmuir	For JGBD Fruendlich
RMSE: 5.68 mg/g; MAE: 2.18 mg/g	RMSE: 130.53mg/g; MAE: 8.21 mg/g

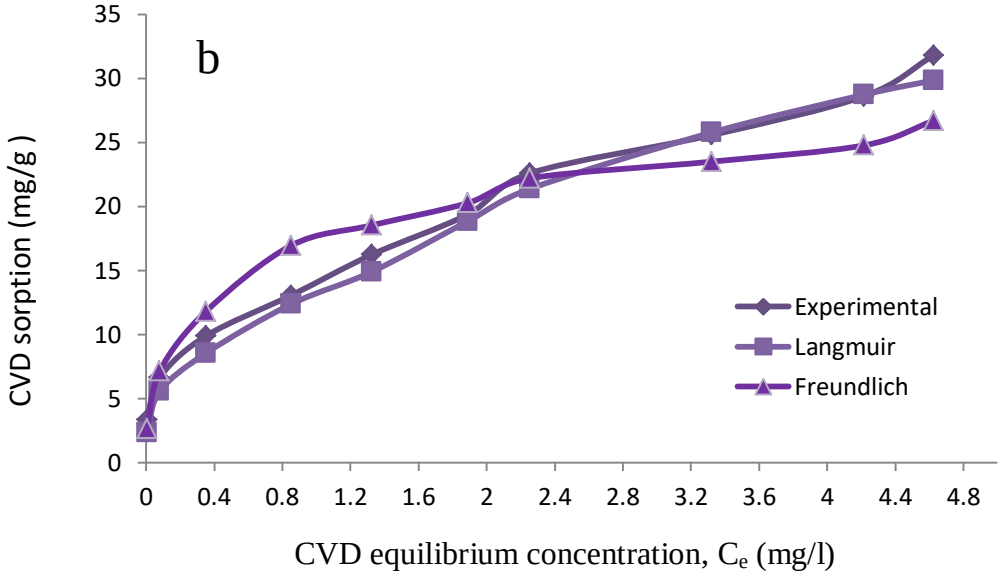

For CVD Langmuir	For CVD Fruendlich
RMSE: 1.18 mg/g; MAE: 0.94 mg/g	RMSE: 7.08 mg/g; MAE: 2.15 mg/g

Fig. (4.12): Assessment of experimental and modeled data using Langmuir and Freundlich: (a) for JGBD (b) for CVD.

Table (4.9): Assessment of the Langmuir uptake (q_m, $mg.g^{-1}$) for JGBD using LLSP with those of other adsorbents.

Adsorbent	**q_m(mg g^{-1})**	**Reference**
Walnut Kernel Shell	6.3051	Farhood et al., 2021
Tendu leaf waste	51.00	Nagda and Ghole, 2011
Oil palm frond	67 mg/g	Chew and Husni, 2019
Leucaena Leucocephala Seed Pods	142.85	**The present study**

Table (4.10): Assessment of the Langmuir uptake (q_m, $mg.g^{-1}$) for CVD using LLSP with those of other adsorbents.

Adsorbent	**q_m (mg g^{-1})**	**Reference**
Almond shell-based	12.2	Loulidi et al., 2020
Palm Kernel Shell-Derived Biochar	24.45	Kyi et al., 2020
Terminalia arjuna sawdust waste	45.99	Shakoor and Nasar , 2018
Leucaena Leucocephala Seed Pods	45.45	**The present study**

4.5 Kinetics of sorption study

4.5.1 Pseudo-first-order model

The pseudo first order kinetic model respected to varied concentrations of JGBD and CVD dye is shown in Figure (4.14). The experimental and anticipated qe, as well as the observed rate constants and corresponding correlation coefficient values, are shown in Table (4.11) for JGBD and Table (4.12) for CVD. There is a function of the process conditions called K_1, reduces as the dye concentration increases (Hu, et al., 2021; Fu et al., 2021; Singh, et al., 2021). The diffusion rate decreases due to the resistance of the boundary layers to LLSP, which increases with decreasing K1. It can be viewed in the following way: The time it takes for the process to achieve equilibrium is $1/k_1$, and if the initial concentration (C_0) is higher, it takes longer, therefore K_1 is lower.

The improvement in the concentration of the two dye solutions will lead to a linear rise in the continuous flow rate if the kinetics of sorption follow the PFO model (Hu, et al., 2021). The occupancy rate of sorption sites is proportional to the functional group, according to the pseudo first order model (Wang and Wang, 2018). Different adsorption models for diverse solutes have been established, but the applicability and consistency of their linear and non-linear forms must be verified (Kajjumba et al., 2018). The first-order equation does not always fit the entire range of reaction time and is only useful in the early stages of the adsorption process (Kassimi et al., 2021).

When the R^2 value for the PFO model was compared to the R^2 value for the second model, it was discovered that the bio-uptake of JGBD and CVD onto LLSP did not match this model. As a result, the bioabsorption of JGBD and CVD does not represent a regulated diffusion process since it does not follow pseudo first orde equation (Kajjumba et al., 2018).

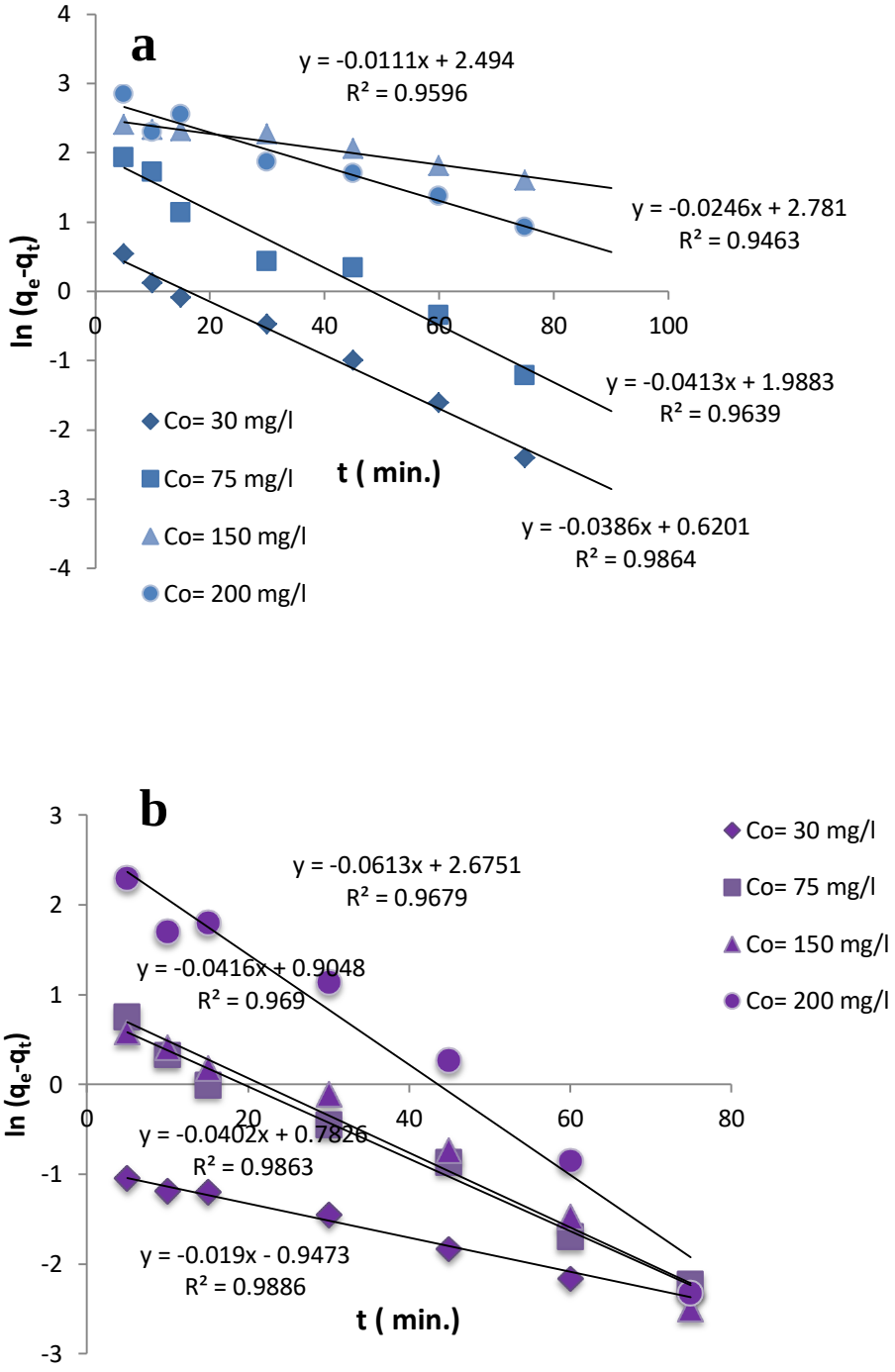

Fig. (4.14): Pseudo -first-order kinetic plots for sorption of dyes onto LLSP at different initial dye concentrations: (a) for JGBD (b) for CVD at pH 9, 250 rpm using LLSP for 30 min. and 45 min. for JGBD and CVD, respectively.

4.5.2 Pseudo second order model

The experimental results were tailored to a PSO adsorption model to better understand the process for adsorption kinetics (Ho and McKay, 1998). Figure (4.15a, b) shows the plots of the pseudo second order kinetic model at different dye concentrations of JGBD and CVD, respectively. The determination coefficient, R^2 of second-order kinetics is equivalent to 0.992 for JGBD and 0.998 for CVD. It implies that a second-order rate equation governs biosorption. Where q_t is the instantaneous adsorption capacity and k_2 is the pseudo-second-order rate constant. Sorption ability rises with increasing initial dye concentration, but k_2 for LLSP decreases with increasing initial dye concentration of JGBD and CVD, as shown in Tables (4.11 and 4.12).

This phenomenon can be explained by the fact that there is less competition for sorption sites at lower concentrations. At larger concentrations, competition for surface active sites would be strong, resulting in decreased sorption rates (Kassimi et al., 2021). If this model is correct, the electrostatic interaction and chemisorption process, which involves electron sharing and exchange between the adsorbate and biosorbent, is the rate-controlling phase (Sun et al., 2011), The PSO considers chemisorption to be in the lead and regulates adsorption as the rate-limiting step. (Eloussaief et al., 2011).

An increase in the initial adsorption rates (h) was observed with the increase of the dye concentration and this is due to the increase in the driving force for mass transfer, which allows more dye molecules to enter the surface of the adsorbent material in the shortest time (Hamza et al., 2018). The values of qe_{cal} and R^2 in the pseudo second order model were more close to the experimental values than the PFO model, this indicates that the PSO model is more compatible with the practical experiments and this is listed in Table (4.11) and Table (4.12).

Straight lines generated from PSO kinetic plots in compared to PFO kinetic model, indicate that the PSO kinetic model will fit the experimental data across all phases of the sorption period (Hossain et al., 2021). As shown by a high association coefficient suggesting a chemisorption mechanism (Hamza et al., 2015; Asfaram et al., 2018) and a type of adsorption that may be the result of electron transfers or sharing between the functional groups and the JGBD, CVD dyes, it can be determined that the PSO model is more reliable for determining the instruction of kinetics of JGBD and CVD removal by LLSP. Electrostatic contact and the chemisorption process may be the phase that controls the rate. Similar results were observed by the other researchers that investigated the elimination of organic substances using adsorption kinetics. (Milenkovic et al., 2013; Roosta et al., 2014; Saad et al., 2017).

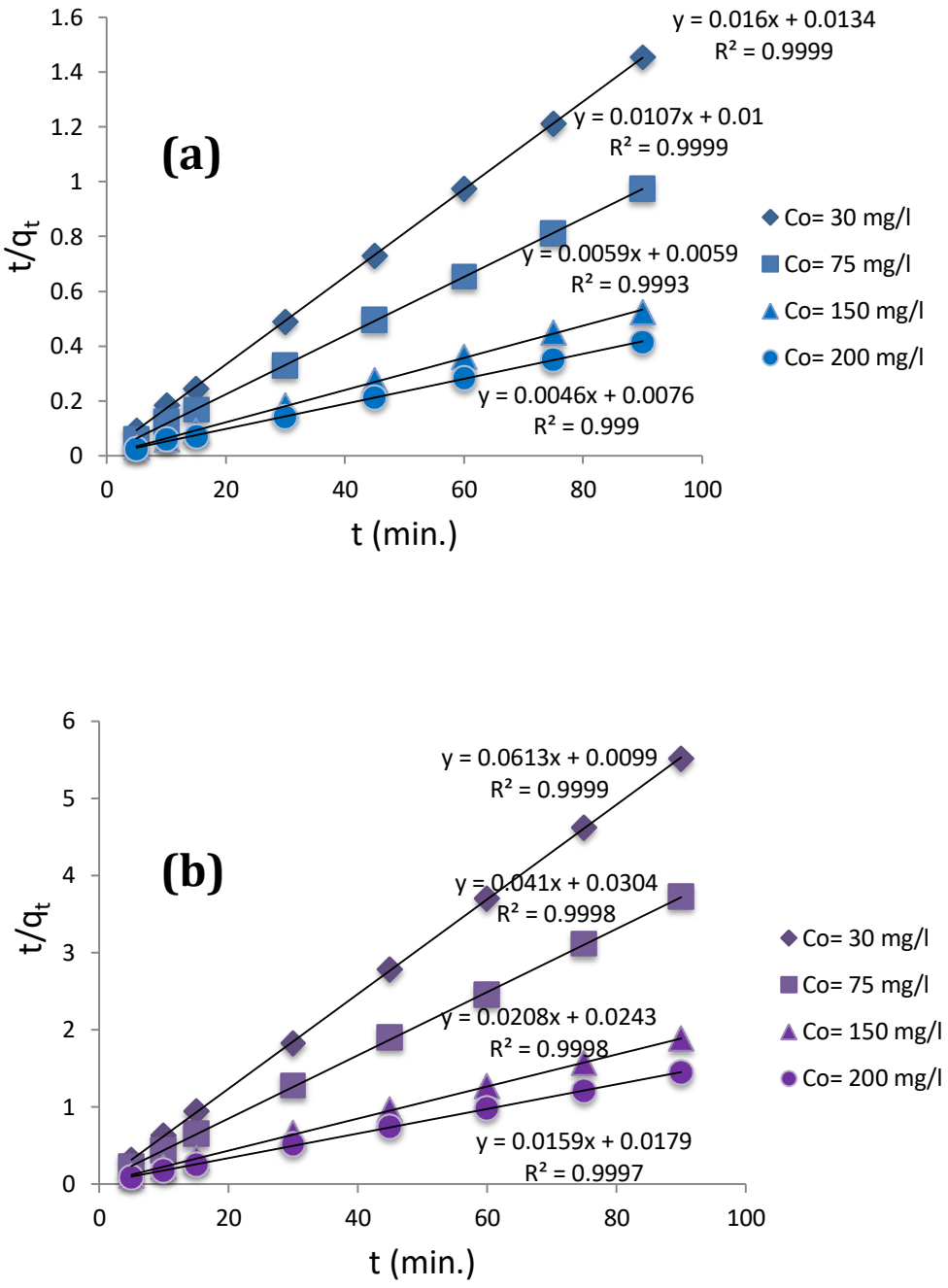

Fig. (4.15): Pseudo second-order kinetic plots for sorption of dyes onto LLSP at different initial dye concentrations: (a) for JGBD (b) for CVD at pH 9, 250 rpm using LLSP for 30 min. and 45 min. for JGBD and CVD, respectively.

4.5.3 The intraparticle diffusion model

The intraparticle diffusion model was investigated to represent the liquid-solid adsorption diffusion mechanism (Nesic et al. 2012). The data is typically graphically analyzed to visually identify the straight line segments as this model is commonly multilinear. (Malash and ElKhaiary, 2010). Where $t^{1/2}$ is the square root of time and Kip (mg g^{-1} $min^{-1/2}$) is the intraparticle diffusion rate constant. The thickness of the boundary layer is represented by the constant C_{ip} (g g^{-1}) a larger value of C_{ip} denotes a greater effect on the rate regulation of surface adsorption (Alkan et al. 2007; Li et al. 2012).

The slope and intercept of the graph of $t^{1/2}$ vs qe were utilized to determine the proper parameters. Figure (4.16a, b) explains linear intraparticle diffusion kinetic model of JGBD and CVD onto LLSP biosorbent at different dye concentrations. The conforming model fitting parameters for each dye are itemized in Table (4.11) and (4.12) for JGBD and CVD, respectively. High k_{ip} values indicate a greater intra-particle diffusion rate, this is advantageous and increases with time for the biosorption, suggesting that the thickness of the boundary layer increases and has an impact on the pace at which JGBD and CVD dyes are absorbed. (Siddiqui et al., 2019). With increased concentrations at all levels, the k_{ip} values for JGBD and CVD improved.

The C_{ip} values increased when dye concentration was raised, which may be related to the impact of the boundary layer. Similar results were obtained by the studies of ultrafine nickel/carbon nanoparticles for organic dye removal (Kim et al., 2018), Methylene Violet dye adsorption using onion skins (Naser et al., 2021), natural safiot clay to remove industrial dyes from aqueous media (Kassimi et al., 2021), kinetic studies of dyes on pure and structurally modified poly (methyl methacrylate) electrospun nanofibers (Philip et al , 2021).

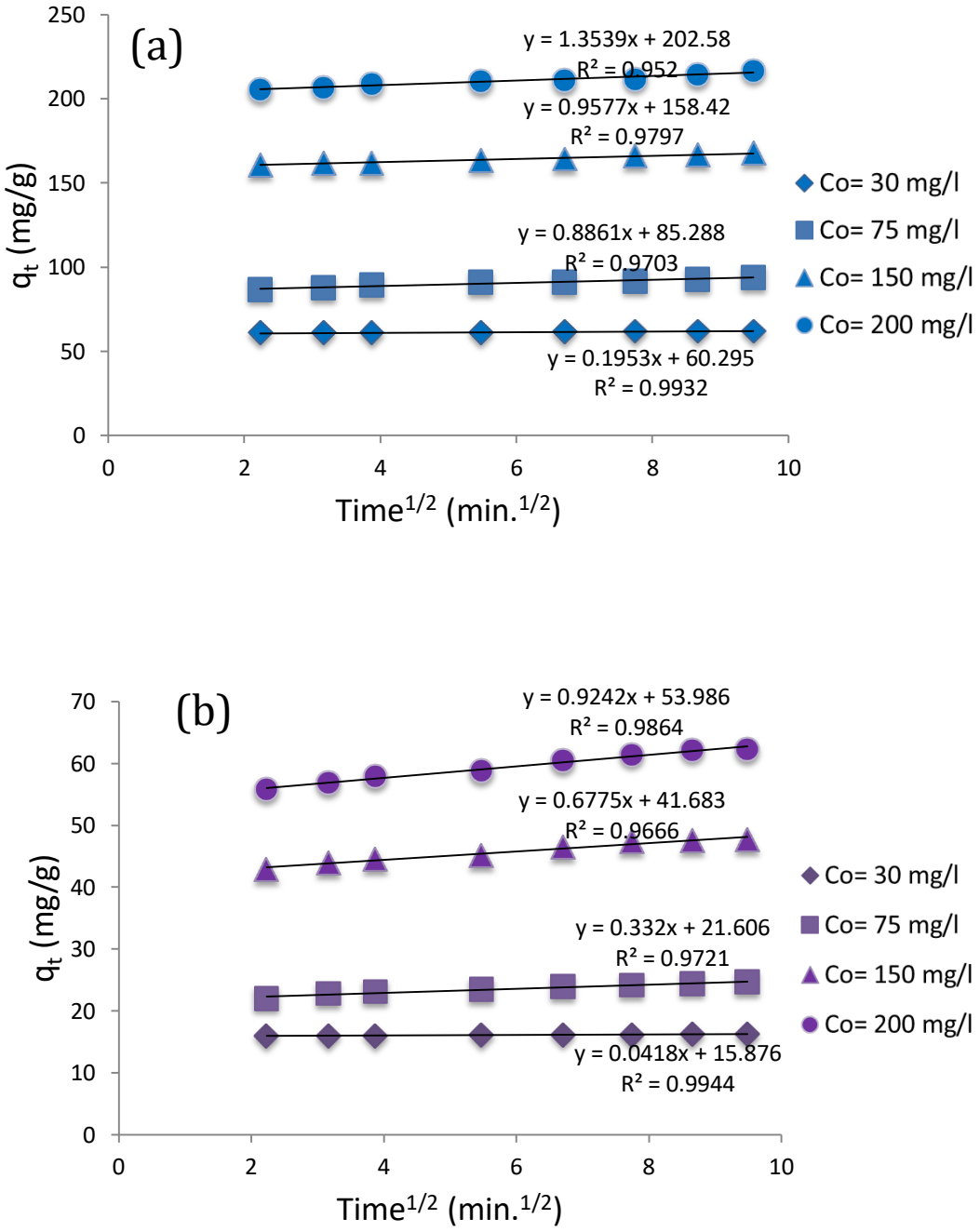

Fig. (4.16): Linear intraparticle diffusion kinetic model of dyes using LLSP at different initial dye concentrations : (a) for JGBD (b) for CVD pH 9, 250 rpm using LLSP for 30 min. and 45 min. for JGBD and CVD, respectively.

4.5.4 Elovich model for adsorption

The Elovich equation is satisfied in chemical adsorption processes and is suitable for systems with heterogeneous adsorbing surfaces, thus describing many dyes adsorption systems (Wu et al., 2009). Herein, the Elovich model fitted in good agreement for JGBD and CVD kinetic adsorption onto LLSP. In the linear model at pH 9, initial adsorption rate (α) presented erratic behavior with some very high values through increasing JGBD and CVD concentrations. Nonetheless, the linear model resulted as good to predict adsorption at equilibrium. The desorption constant (β) was observed to decrease with increase dyes concentration, as the tendency of LLSP to be desorbed is higher in the systems with lower concentrations (Pintor et al., 2018). The parameter β is also related to the extent of surface coverage and chemisorption activation energy, thus assuming a heterogeneous distribution of sites whose activation energies vary with surface coverage (Asadi et al., 2018). As a general trend, active sites values demonstrated better fit at pH 9 for linear models, the initial adsorption rate, desorption constant and predicted equilibrium adsorption capacity being almost identical. Thus, it seems that better Elovich fit was achieved with low JGBD and CVD concentrations.

Tables (4.11) and (4.12) show the R^2, a and b values for JGBD and CVD, respectively. The Elovich equation is useful to represent adsorption behavior that is compatible with the nature of adsorption, as demonstrated in figures (4.17). In engineering practice, determining an effective operating period of adsorption for adsorption systems represented appropriately by the Elovich equation is critical (Marcu, et al.,2020). Over the whole range, the experimental findings on JGBD and CVD conformed to a straight line, suggesting that the Elovich kinetic model accurately predicts the sorption of the two dyes on the LLSP surface.

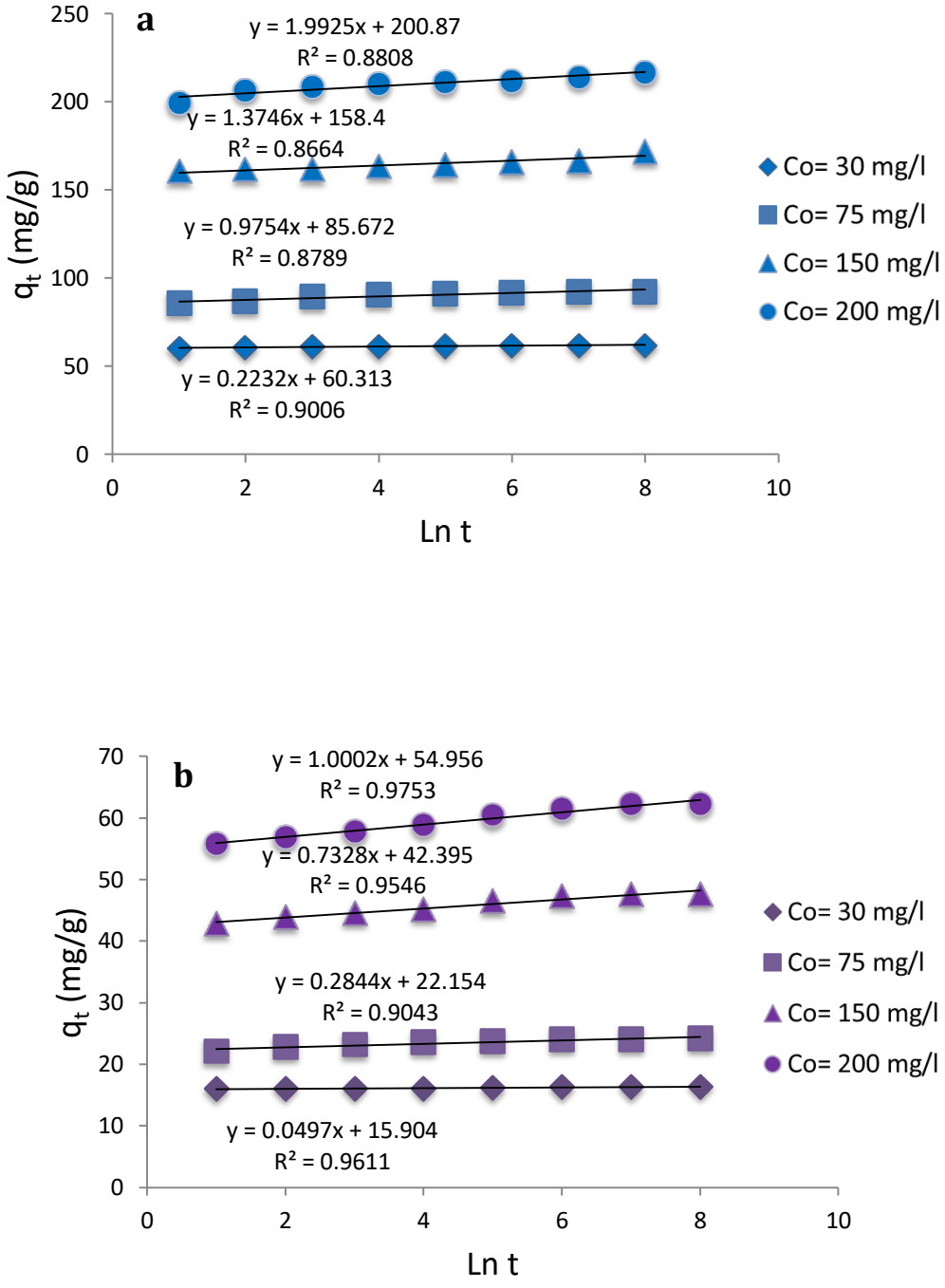

Fig. (4.17): Elovich kinetic model of dyes onto LLSP at different initial dye concentrations: (a) for JGBD (b) for CVD at pH 9, 250 rpm for 30 min. and 45 min. for JGBD and CVD, respectively.

Table(4.11): Kinetic parameters of various models fitted to JGBD sorption experimental data using LLSP.

Kinetic models	**JGBD concentration(mg/l)**			
	30	**75**	**150**	**200**
Pseudo- first- order				
q_e, exp (mg/g)	61.92	92.50	171.96	216.62
q_e, calc.(mg/g)	59.69	92.76	160.04	209.30
K_1 (min^{-1})	0.0386	0.0413	0.0111	0.0246
R^2	0.9864	0.9639	0.9596	0.9463
Pseudo –second- order				
q_e, calc. (mg/g)	62.50	93.45	169.49	217.39
K_2 (g mg^{-1} min^{-1})	0.0191	0.0114	0.0059	0.0038
h (mg $g^{-1}min^{-1}$)	74.61	99.55	169.48	181.82
R^2	0.9999	0.9999	0.9993	0.9990
Intraparticle diffusion				
K_{ip} (mg g^{-1} $min^{-0.5}$)	0.1953	0.8861	0.9577	1.3539
C (mg/g)	60.295	85.288	158.42	202.58
R^2	0.9932	0.9703	0.9797	0.9520
Elovich model				
a (mg/g min)	60.313	85.672	158.4	200.87
b (g/mg)	1/0.2232	1/0.9754	1/1.3746	1/1.9925
R^2	0.8808	0.8664	0.8789	0.9006

Table(4.12): Kinetic parameters of various models fitted to CVD sorption experimental data using LLSP.

Kinetic models	**CVD concentration(mg/l)**			
	30	**75**	**150**	**200**
Pseudo- first- order				
q_e, exp (mg/g)	16.32	24.16	47.60	62.26
q_e, calc.(mg/g)	15.89	22.60	47.81	60.90
K_1 (min^{-1})	0.019	0.0402	0.0357	0.0613
R^2	0.9886	0.9863	0.9690	0.9679
Pseudo –second- order				
q_e, calc. (mg/g)	16.39	24.40	48.07	62.89
K_2 (g mg^{-1} min^{-1})	0.0376	0.0552	0.0178	0.0141
h (mg $g^{-1}min^{-1}$)	10.1	32.86	41.13	55.76
R^2	0.9999	0.9998	0.9998	0.9980
Intraparticle diffusion				
K_{ip} (mg g^{-1} $min^{-0.5}$)	0.0418	0.332	0.6775	0.9242
C_{ip} (mg/g)	15.876	21.606	41.683	53.986
R^2	0.9944	0.9721	0.9666	0.9864
Elovich model				
a (mg/g min)	15.904	22.154	42.395	54.956
b (g/mg)	1/0.0497	1/0.2844	1/0.7328	1/1.0002
R^2	0.9753	0.9546	0.9043	0.9611

4.6 Mechanism study

The sorption kinetic of JGBD and CVD dye sorption was examined using the intraparticle diffusion model. Figure (4.18a, b) for JGBD and CVD, respectively, shows the plots of the intraparticle diffusion model with multi-linear profiles at varied starting dye concentrations. The initial linear sharp distance on the plots might be caused by boundary layer solute molecule diffusion or dye sorption on the adsorbent's external surface. It could be due to the dye intense electrostatic attraction to the biosorbent. Intraparticle diffusion was the rate-limiting process in the second phase, it called the progressive adsorption phase. Due to the strong affinity of the adsorbate that has been deposited on the biosorbent surface, the third was chosen to represent the ultimate equilibrium stage, at which the adsorption process starts to slow down.

The fact that there are non-zero intercepts in each of the three phases demonstrates that intraparticle diffusion is not the sole stage in the sorption process that is rate-limiting. It was confirmed from previous studies that the third part is static (Nal et al., 2006). The k_{ip} values for each dye increased as concentration increased. Because of the boundary layer effect, the value of intercept, C_{ip} increased when the initial dye concentration of each dye was increased as shown in Table (4.13).

The entire adsorption mechanism was described by surface adsorption and intraparticle diffusion. The LLSP samples surfaces are negatively charged at a functional pH 9 due to the deprotonated acidic groups. Oxygen atoms have a strong attraction to positively charged molecules and cations because of strong electrostatic interactions. Because JGBD and CVD are cationic dyes, electrostatic interactions are certain to play a role in their sorption on LLSP. JGBD and CVD, on the other hand, have numerous aromatic rings and cationic

atoms in their chemical structure, making them excellent for sorption on the surface of LLSP via ionic contact (Liu et al., 2019).

Cations can help anionic species sorption in some cases by increasing the binding of negatively charged anions. In some circumstances, cation loading of biomass might promote sorption of another cation due to pH buffering effects (Cheriti et al., 2011).

As a result, (1) chemical interaction between JGBD and CVD molecules and surface functional groups be involved in JGBD and CVD sorption onto LLSP. (2) weak physical forces and van der Waals contacts between the biosorbent and JGBD and CVD molecules, and (3) electrostatic interaction between the electron-rich spots on the biosorbent surface and JGBD and CVD molecules. Thus, both physical and chemical sorption were involved in JGBD and CVD sorption on the LLSP surface.

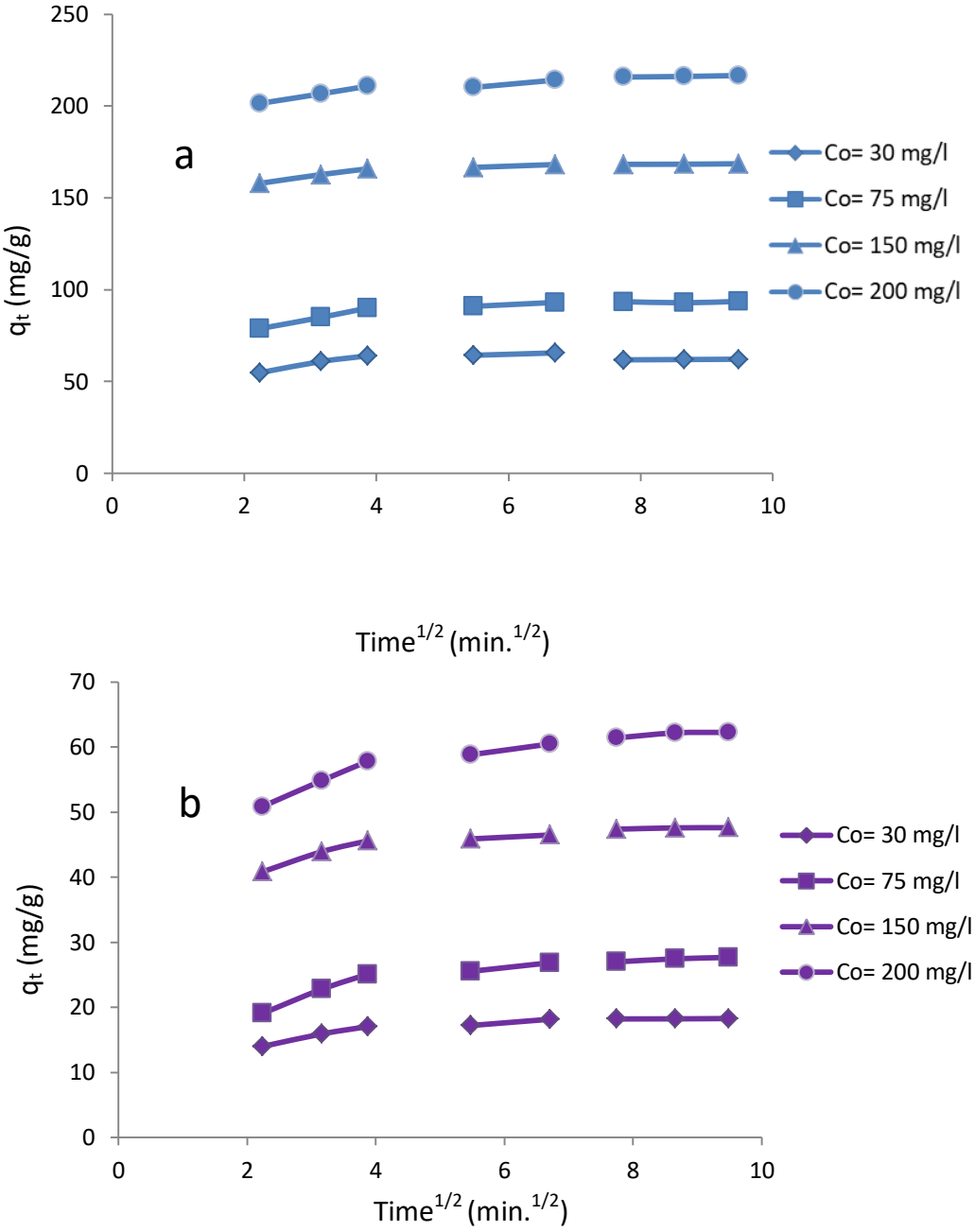

Fig. (4.18): Multi- linearity graph of intraparticle diffusion model of dyes : (a) for JGBD onto sorbent at different dye concentrations (0.08 g, pH 9 and 250 rpm) (b) for CVD onto sorbent at different dye concentrations (0.3 g, pH 9 and 250 rpm.

Table (4.13): Multi-linearity parameters of intraparticle model based sorption mechanism study of JGBD and CVD onto LLSP.

Dye	C_o (mg/l)	K_{ip1} (mg g^{-1} $min^{-0.5}$)	C_1 (mg/g)	R_1^2	K_{ip2} (mg g^{-1} $min^{-0.5}$)	C_2 (mg/g)	R_2^2
JGBD	25	0.0306	2.81	0.9985	0.0255	2.84	0.9979
	50	0.2662	4.07	0.9836	0.1942	4.41	0.9823
	100	0.9593	7.88	0.9927	0.1184	10.96	0.9738
	200	1.7145	11.71	0.9997	1.0868	13.36	0.9928
CVD	25	0.0306	2.81	0.9985	0.0255	2.84	0.9979
	50	0.2662	4.07	0.9836	0.1942	4.41	0.9823
	100	0.9593	7.88	0.9927	0.1184	10.96	0.9738
	200	1.7145	11.71	0.9997	1.0868	13.36	0.9928

4.7 Continuous sorption system for LLSP

The study of continuous sorption is an essential step to understand the behavior, mechanism of sorption, its prediction and to know the capabilities of the adsorbents and the time of dye to reach the breakthrough curve, so it was necessary to understand the continuous of sorption. Among all the column configurations, the packed bed column has been shown to be the most efficient, economical and most suitable for sorption processes (Basu and Juha, 2022).

In this study, the nature of the break through curves was calculated and the break time at which the concentration of JGBD and CVD reached the limit values for the different operating parameters. These parameters are the flow rate of inlet dye solution, the bed height of biosorbet and the initial dye concentration. The effluent amount of JGBD and CVD was examined using a spectrophotometer determined with a specified wavelength of each dye, C/C_o is

set to 0.05, which means that 5% of initial dye concentration is applied as the time needed to reach the breakpoint.

4.7.1 Effect of inlet flow rate of JGBD and CVD on breakthrough curves

As shown in Figure (4.20 a, b) and Table (4.14), the impact of flow rate (Q) on the breakthrough curves of continuous sorption was investigated at flow rates of 8, 16, and 25 ml/min at a fixed bed height of 10 cm and an initial concentration of each dye of 25 mg/l. The breakthrough time in a continuouswith constant bed height rises as the flow rate is decreased. This phenomenon may be explained by the fact that at greater flow rates. JGBD or CVD molecules have less time to diffuse into the LLSP pores (Ahmad and Hameed, 2010). In other words, because the residence time of the adsorbate in the column was insufficient to achieve adsorption equilibrium at the designated flow rate, the dye molecules left the column before they had a chance to reach the active sites of adsorbent particles.

Additionally, it is likely that high flow rates will desorb some dye molecules that have been adsorbed but have reversible or loose bonds to the adsorbent surface (Marzbali and Esmaieli, 2017). As a result, the concentration of JGBD or CVD in the effluent grew quickly, which led to an early breakthrough time (Chen et al., 2012). The low flow rate was helpful for dyes adsorption in the fixed bed utilizing LLSP because of its greater adsorption capacity. These outcomes matched those that were seen in other investigations (Han et al., 2009; Lignin et al., 2012; Marzbali and Esmaieli, 2017).

Higher flow rates lead the LLSP column to swiftly approach its maximum capacity as more dye ions exchange with functional group sites more quickly (Yunnen, et al., 2017; Patel, 2020). The breakthrough sorption capacity for JGBD and CVD, respectively, drops from 16.03 to 14.97 mg/g and from 14.94 to 11.51 mg/g when the flow rate is increased from 8 to 25 ml/min, as shown in

Table (4.14). As a result, the mass transfer zone (MTZ) moves deeper into the bed until it reaches the dye-saturated LLSP top layer (Topare and Bokil, 2021).

The pollutant concentration curve becomes S-shaped with time and starts to rapidly grow near the point of breakthrough (Vinodhini and Das, 2010; Vickers, 2017; Das , 2021). Effect of flow rate causing removal efficiency to decline from 83.08 to 71.18% for JGBD and from 81.93 to 70.82% for CVD, as the flow rate rises to 25 ml/min from 8 ml/min. Additionally, Figure 4.20 demonstrates that at higher flow rates, breakthrough curves have a steeper contour, indicating a stronger intra-particle diffusion effect and a narrower mass transfer zone. Lower flow rates are linked to flatter breakthrough curves, which suggest that film transfer resistance has a stronger impact, there is a larger mass transfer zone, and the column will last longer at longer contact durations (Aranda-García and Cristiani-Urbina, 2020).

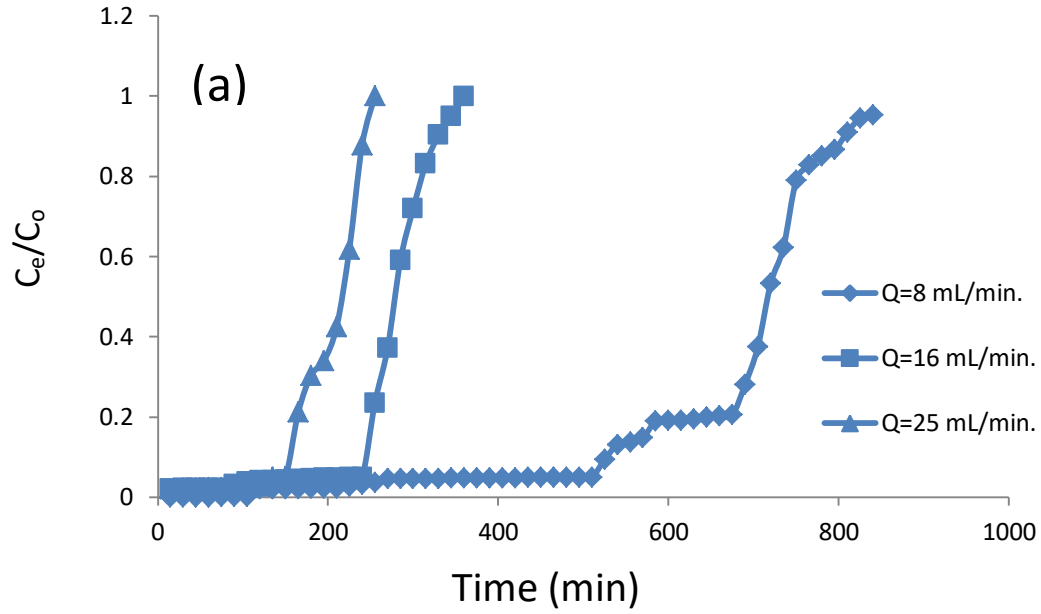

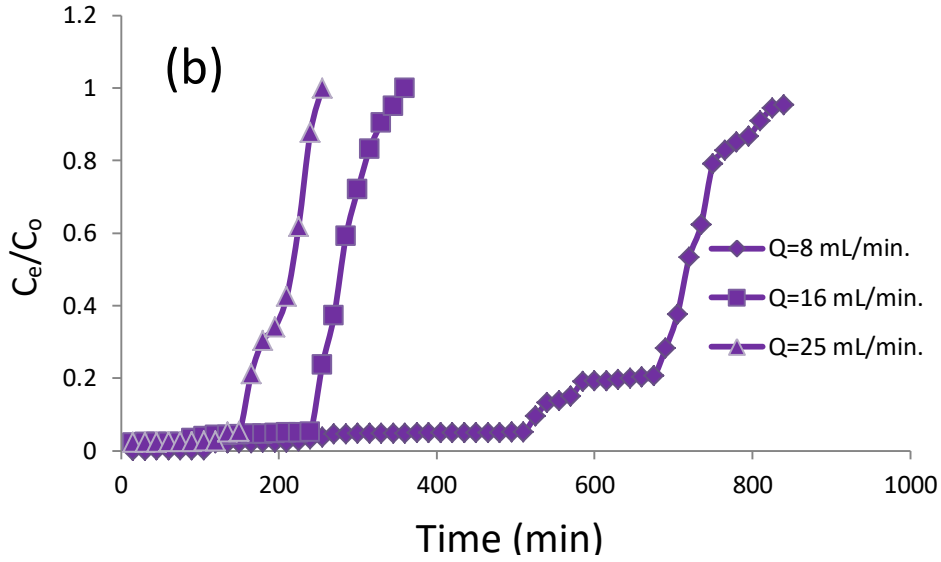

Fig. (4.19): Breakthrough curves for dyes sorption at different flow rates: (a) for JGBD, (b) for CVD, where the initial concentration for two dyes = 25 mg/l, the LLSP bed height = 10 cm, the dye solution pH 9.

Table (4.14): breakthrough curve parameters of JGBD and CVD, onto LLSP in a fixed-bed column mode at different operating conditions and breakthrough point of C/C_o was 0.05.

Dyes	Operation conditions			Breakthrough parameter							
	C_o (mg/l)	Q_v (ml/min)	H (cm)	t_b (min)	t_e (min)	m_{total} (mg)	q_{exp} (mg/g)	q_{total} (mg)	V_b (ml)	V_{eff} (ml)	Total removal (R%)
JGBD	25	8	10	585	1110	222	16.03	184.45	4680	8880	83.08
	25	16	10	285	525	210	15.76	154.55	4560	8400	73.59
	25	25	10	180	330	206.25	14.97	146.81	4500	8250	71.18
	25	8	15	690	1295	259	17.01	223.25	5520	10360	86.19
	25	8	25	765	1695	339	18.04	299.15	6120	13560	88.24
	50	8	10	360	810	324	24.52	240.47	2880	6480	74.21
	75	8	10	255	600	360	25.32	248.31	2040	4800	68.97
CVD	25	8	10	510	885	177	14.94	145.02	4080	7080	81.93
	25	16	10	240	420	168	12.47	122.29	3840	6720	72.79
	25	25	10	135	255	159.37	11.51	112.87	3375	6375	70.82
	25	8	15	585	1185	237	15.24	200.02	4680	9480	84.39
	25	8	25	675	1540	308	16.05	266.15	5400	12320	86.41
	50	8	10	300	570	228	16.52	162.01	2400	4560	71.05
	75	8	10	195	480	288	18.83	184.66	1560	3840	64.12

4.7.2 Effect of LLSP bed height on breakthrough curves

The height of the bed, which is straight related to the amount of LLSP sorption in the adsorption column, determines how much of a dye is absorbed in the fixed bed sorption column. At constant flow rates of 8 ml/min, 10, 15, and 25 cm, the sorption was examined with an intake dye concentration of 25 mg/l for each dye. Table (4.12) lists the continuous parameters for JGBD or CVD sorption using LLSP.

Figure (4.20a, b) shows that as bed depth was raised, both breakthrough time and effluent volume rose as well. In a continuous sorption experiment, there is a concept known as "exhaust time," When this happens, the influent solution leaves the experimental column with little to no treatment since the adsorbent is no longer able to remove solute molecules. The total sorption capacities of the LLSP were 184.45, 223.25, and 299.15 mg for JGBD and 145.02, 200.02, and 266.15 mg/g for CVD, as shown in Figure (4.20a,b). The exhaust time of 10, 15 and 25 cm bed depth was 1110, 1295, and 1695 min, respectively, for JGBD and was 885, 1185, and 1540 min, respectively, for CVD. This is because there are more LLSP particles, or more active sites for biosorption, at the deeper bed depth. Because the sorption molecules have more time to infiltrate into the pores of the particles, the number of dye molecules that are biosorbed by LLSP increases as bed depth increases (Marzbali and Esmaieli, 2017).

Because of the higher bed depth, increasing exhaust time results in an increase in effluent volume. These findings are consistent with research from earlier years. (Goel et al., 2005; Taty et al., 2005; Chowdhury and Saha, 2010; Vickers, 2017; Aranda-García and Cristiani-Urbina, 2020; Das, 2021).

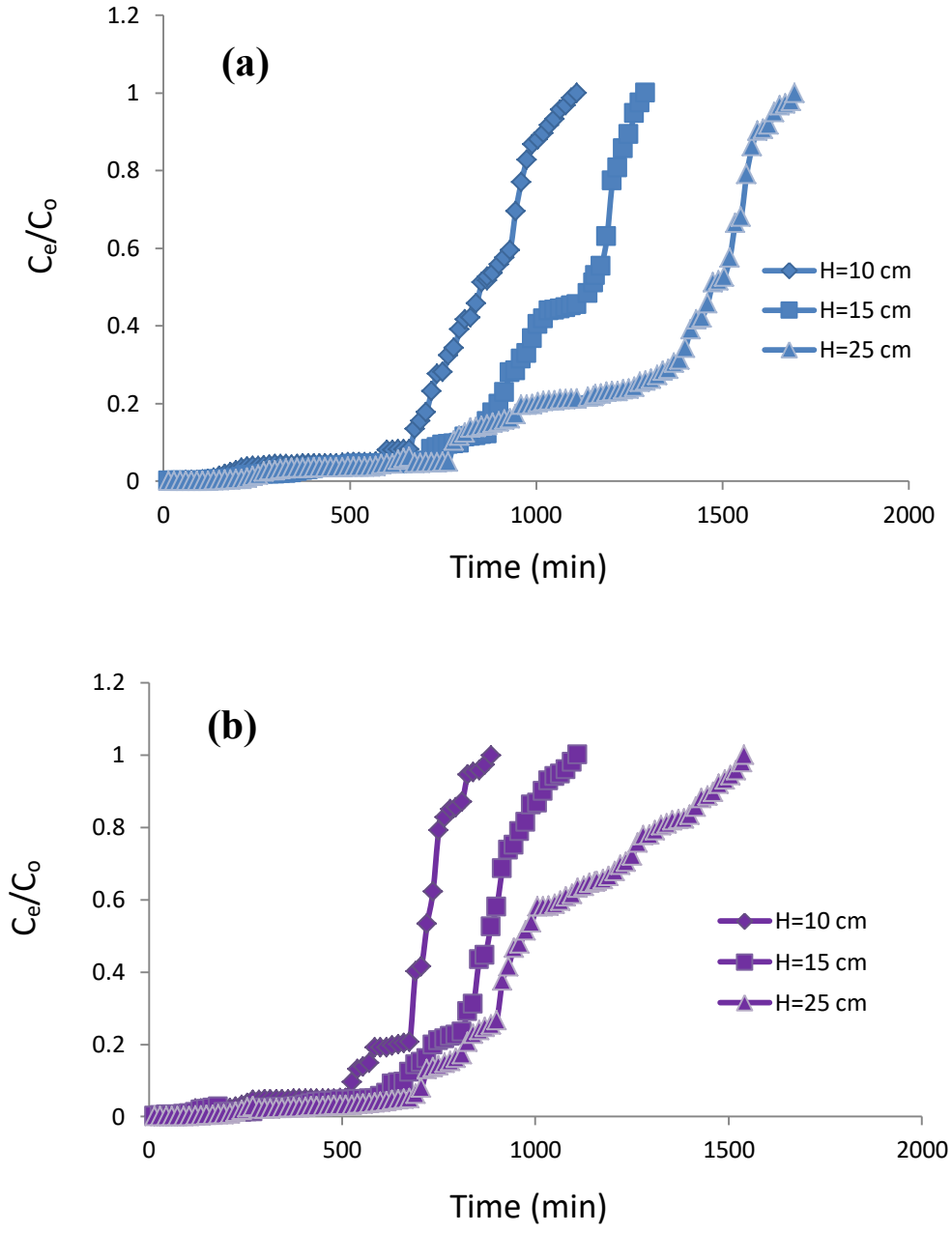

Fig. (4.20): Breakthrough curves for two dyes sorption: (a) for JGBD (b) for CVD, at different column bed heights, where the initial concentration of two dyes = 25 mg/l, the flow rate = 8 ml/min, the dye solution pH 9.

4.7.3 Influence of initial JGBD and CVD concentration on breakthrough curves

Figure (4.21 a, b) shows the impact of various influent JGBD and CVD concentrations between 25 and 75 mg/l at a constant LLSP bed height of 10 cm and solution flow rate of 8 ml/min .When increasing the influent concentration, the volume of effluent treated decreases from 8880 ml to 4800 ml for JGBD and from 7080 ml to 3840ml for CVD as shown in Table (4.12).

The numbers of solute molecules compete for the active sites of LLSP increases on increasing the influent concentration, which results in quicker exhaustion of the column. The concentration gradient solid liquid interface is more at higher concentration that drives the solute molecules to enter into the sorption sites. The amount of bioadsorbed dye increased when the concentration of the dye concentration increased, while the removal efficiency R% decreased, because all the active sites were occupied with the dye in a short time. The sorption process achieved saturation more quickly at higher influent concentrations, as expected, and the breakthrough times for JGBD and CVD were observed to drop from 585 to 255 min and 510 to 195 min, respectively, as shown in Table (4.12).

This shows that the saturation rate and breakthrough curve are impacted by the change in concentration. This may be because the mass transfer of dye molecules is accelerated by the stronger driving force produced by the bigger concentration gradient, covering the sorption sites more quickly (Liao et al., 2013). These results are concur with earlier research on a class of pigments that have the same behavior as these pigments (Marzbali and Esmaieli, 2017; Thillainayagam, et al., 2021)

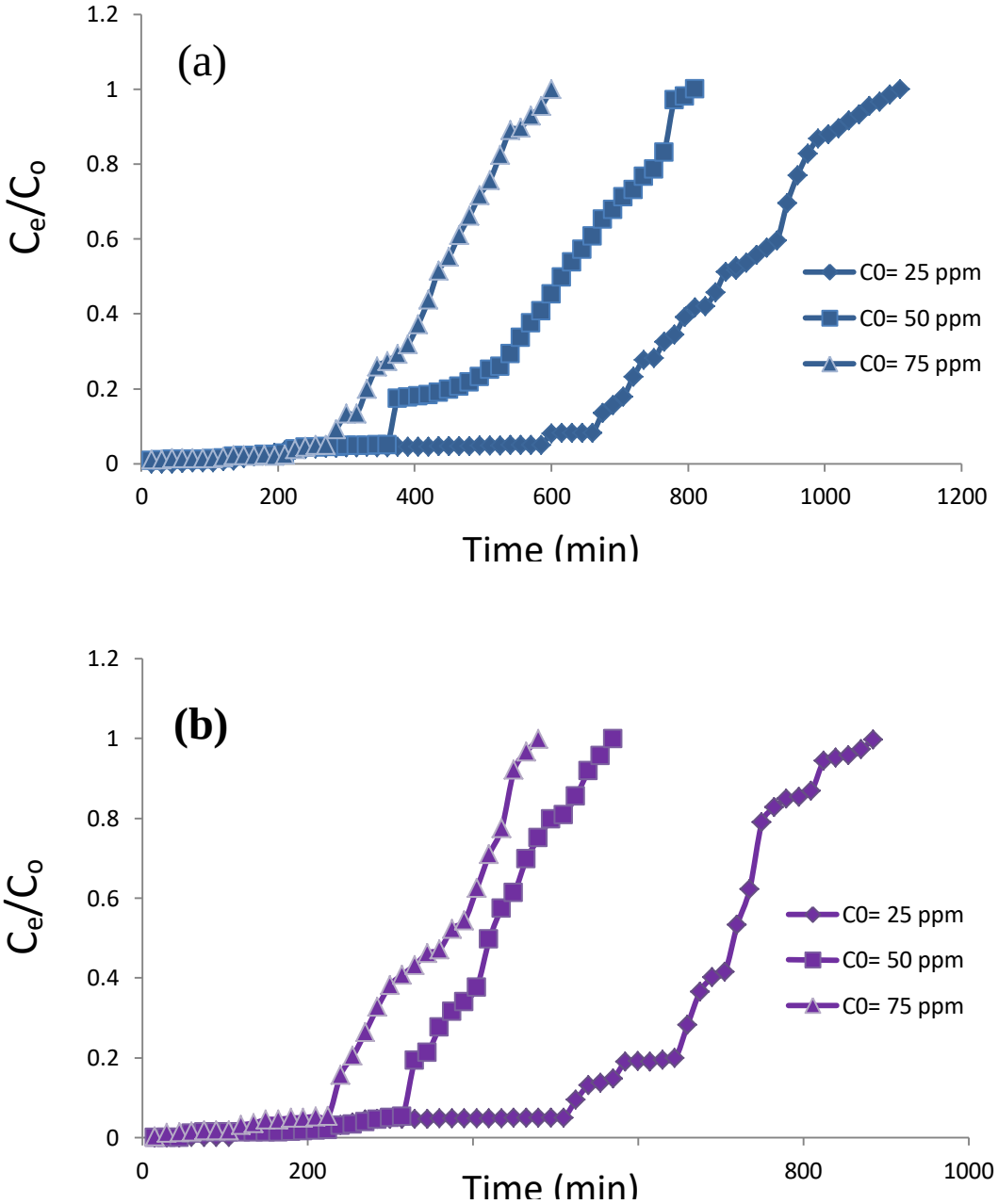

Fig. (4.21): Breakthrough curves for two dyes biosorption: (a) for JGBD (b) for CVD at different initial concentrations when LLSP bed height = 10 cm, the flow rate = 8 ml/min, the dye solution pH 9.

4.8 fixed-bed sorption column dynamic modeling for LLSP

A fixed-bed column performance and successful design are explained using the breakthrough curve. Two essential characteristics that govern the functioning and dynamic responsiveness of a fixed-bed sorption column are the breakthrough time and the shape of the breakthrough curve. To predict the breakthrough curves seen under various experimental settings, three models are included in this study, Bed Depth Service Time (BDST), Thomas models, and Yoon-Nelson models.

4.8.1 The BDST (Bed Depth Service Time) model application

The BDST model was applied to the experimental data concerning column bed depth. The linearized form of the BDST model was plotted according to Equation (2.24). The BDST plot (C_t /C_0 = 0.05, 0.1, 0.20, 0.40, 0.60 and 0.80) for sorption of JGBD and CVD onto LLSP at various bed depth with a flow rate of 8 ml/min. and initial concentration of each dye 25 mg/l was presented in Figure (4.22).

BDST model validity on the basis of the current system was proved by a linear plot, R^2= 0.9912, 0.9812 for JGBD and CVD, respectively drawn between service time and bed height at 8 ml/min flow rate as shown in Figure (4.22). The sorption capacity of the bed per unit bed volume, q_B, was determined from the slope of the BDST plot, with assuming initial concentration C_0, and linear velocity U_f, as constant at the time of operating the column. K_B, the rate constant, was determined from the intercept of the BDST plot and it corresponds to the solute transfer rate from the fluid phase to the solid phase.

The constants computed q_B and K_B were found to be from 2.51 to 4.31 mg/g, 0.000236 to -0.000065 l/mg. min for JGBD, respectively, and 2.28 to 3.92 mg/g, from 0.00027 to -0.000074 l/mg. min for CVD, respectively. BDST model parameters help increase the process and test it for other rates of flow and

there is no need for more experimental runs. The q_B and K_B parameters can be obtained from the linear plot and the values are listed in Table (4.15).

From Table (4.15), it was observed that the sorption capacity (q_B) increased with an increase in the breakthrough point (C_e /C_0) from 0.05–0.80 for both dyes. The increase in adsorption capacity may be due to the column's saturation with the each dye and less active sites for further biosorption. The K_B represents the transfer rate of the binary dye mixture from the liquid phase to the column bed solid phase.

The value of K_B was found to be either positive or negative for both the dyes. Also, it was clear that the value of K_B decreased with an increased breakthrough point (Jayalakshmi and Jeyanthi, 2021). As a result of each dye continuing sorption onto the sorption surface. Because certain active sites of the LLSP are still unoccupied by JGBD and CVD at lower breakthrough values, the biosorbent remains unsaturated (Kumar and Chakraborty, 2009). According to the assumptions, the BDST model performance is found to be good and provides better equations to model any system parameter changes (Ko et al., 2000; Thillainayagam et al., 2021).

Since the BDST model is used to forecast the relationship between service time (t) and bed height (Z), it also serves as a well accomplished model for dye sorption in systems involving fixed beds (Walker et al., 2000; Thillainayagam et al., 2021). It also revealed that short critical bed depth is required for a lower flow rate, whereas the longer bed is higher (Singh et al., 2017). This showed a positive correlation between the K_B and C_e /C_0 and the column's inclining capacity to further remove the JGBD and CVD. The time it takes for all of an biosorbent active binding sites to become fully filled by adsorbate molecules until regeneration is required is known as column service time. Table (4.16) shows the low deviation between the experimental and calculated time using this model.

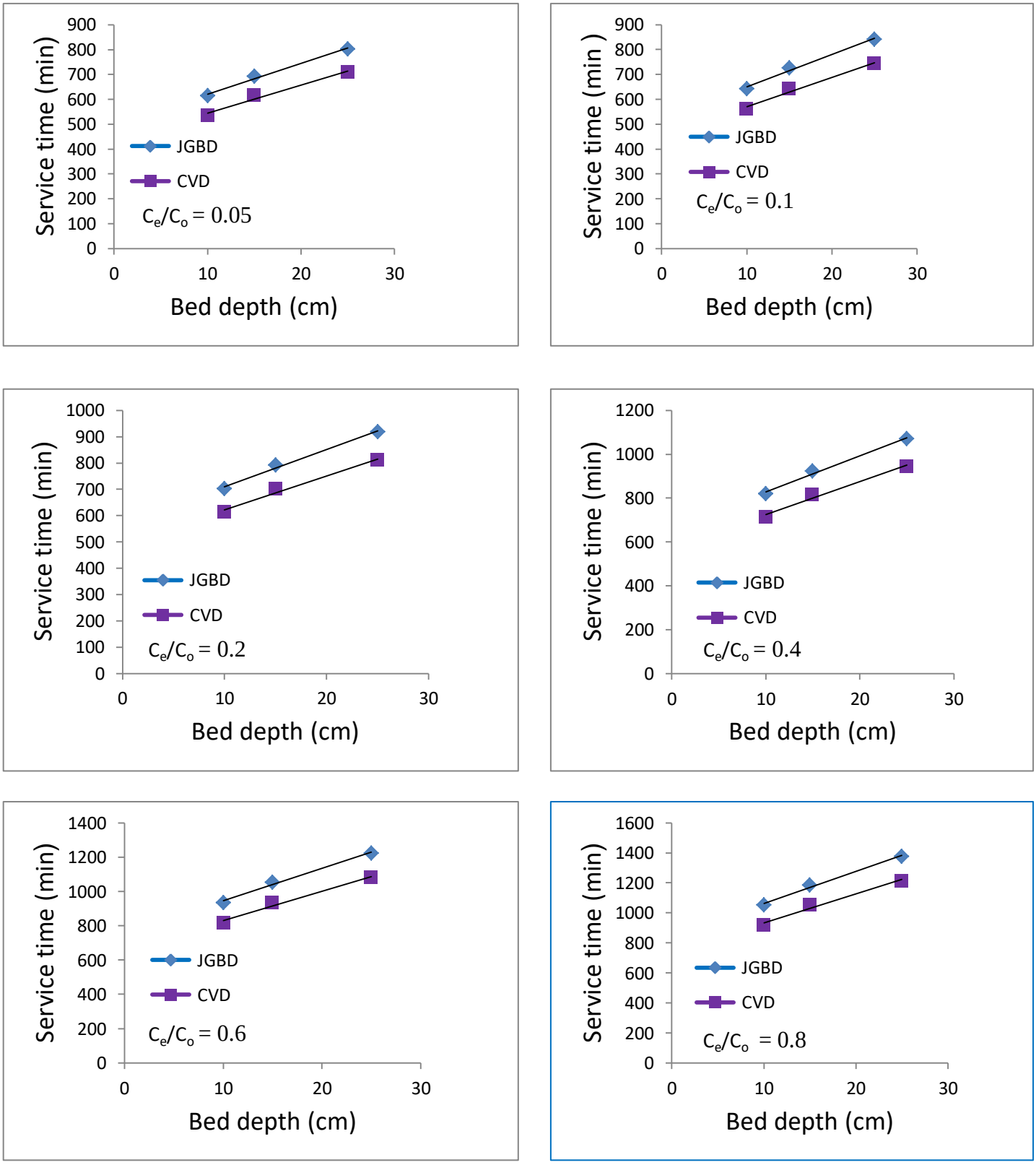

Fig. (4.22): BDST model plot at different values of C_e/C_o in fixed-bed column for JGBD and CVD sorption onto LLSP (C_o =25 mg/l, flow rate =8 ml/min).

Table (4.15): Estimated BDST model parameters at different bed depth height with Q = 8 ml/min and C_o =25 mg/l for JGBD sorption onto LLSP column.

BDST model parameters for JGBD sorption onto LLSP						
Parameters	q_B (mg/l)	q_B (mg/g)	K_B(l/mg.min)	U_f (cm/min)	Z_c (cm)	R^2
C_e/C_o = 0.05	785.81	3.72	0.000236	2.54	40.32	0.9912
C_e/C_o = 0.1	823.02	3.89	0.00016	2.54	42.38	0.9909
C_e/C_o=0.2	897.69	4.25	0.000097	2.54	40.43	0.9908
C_e/C_o=0.4	1047.75	4.96	0.000024	2.54	40.95	0.9911
C_e/C_o=0.6	1199.26	5.67	-0.000021	2.54	40.89	0.9926
C_e/C_o=0.8	1348.04	6.38	-0.000065	2.54	40.18	0.9918
BDST model parameters for CVD sorption onto LLSP						
C_e/C_o = 0.05	714.37	3.38	0.00027	2.54	38.77	0.9812
C_e/C_o = 0.1	748.34	3.54	0.00019	2.54	39.25	0.981
C_e/C_o=0.2	816.229	3.86	0.00011	2.54	39.21	0.9808
C_e/C_o=0.4	956.11	4.52	0.000028	2.54	38.46	0.9862
C_e/C_o=0.6	1089.47	5.15	-0.000024	2.54	39.38	0.9823
C_e/C_o=0.8	1225.42	5.80	-0.000074	2.54	38.83	0.9821

Table (4.16): Comparison between $t_{cal.}$ & $t_{exp.}$ for JGBD and CVD sorption onto LLSP at different breakthrough point (C/C_o) using estimated BDST model parameters at different bed depth height with Q =8 ml/min and C_o= 25 mg/l for column.

Parameters	Bed depth, H (cm)	Flow rate, Q_v (ml/min	Initial MBD concentration, C_o (mg/l)	$t_{cal.}$(min.)	t_{exp}(min.)
Comparison between $t_{cal.}$ and $t_{exp.}$ for JGBD					
C/C_o=0.05	10	8	25	622.80	585
	15	8	25	684.68	690
	25	8	25	808.43	765
C/C_o=0.1	10	8	25	678.91	643.5
	15	8	25	743.72	726.2
	25	8	25	873.32	841.5
C/C_o=0.2	10	8	25	713.03	702
	15	8	25	783.72	792.38
	25	8	25	925.08	918
C/C_o=0.4	10	8	25	840.77	819
	15	8	25	923.27	924.02
	25	8	25	1088.27	1071
C/C_o=0.6	10	8	25	961.17	936
	15	8	25	1055.60	1054
	25	8	25	1244.46	1224
C/C_o=0.8	10	8	25	1065.39	1053
	15	8	25	1171.53	1187
	25	8	25	1383.82	1377
Comparison between $t_{cal.}$ and $t_{exp.}$ for CVD					
C/C_o=0.05	10	8	25	548.71	510
	15	8	25	604.96	585
	25	8	25	717.46	675
C/C_o=0.1	10	8	25	580.42	561
	15	8	25	639.34	643.57
	25	8	25	757.19	742.5
C/C_o=0.2	10	8	25	632.64	612
	15	8	25	696.91	702.23
	25	8	25	825.45	810
C/C_o=0.4	10	8	25	729.80	714
	15	8	25	805.08	815
	25	8	25	955.65	945
C/C_o=0.6	10	8	25	847.34	816
	15	8	25	933.13	935
	25	8	25	1104.70	1080
C/C_o=0.8	10	8	25	942.32	918
	15	8	25	1038.81	1052.13
	25	8	25	1231.79	1215

4.8.2 Thomas model

Thomas model is a popular model used in a packed bed column. In this model, an assumption is made, i.e., Langmuir adsorption-desorption kinetics and no axial dispersion whereas the rate driving force is found to be following the second order reversible reaction kinetics.

In the Thomas model, it is deemed that the separation factor remains to be constant and seems to remain valid for favorable and unfavorable isotherms (Aksu and Gönen, 2004). This model determines the adsorption rate constant and the solid-phase dye concentration on the adsorbent. It is that analyses using the Thomas model were conducted for a wide range of flow rates at diffrent bed heights.

In Table (4.17), there is a summary of the Thomas model parameters that were attained at a wide range of flow rates. Figure (4.23) and (4.24) shows the fitted linear plot of $\ln [(C_o/C_e) - 1)]$ versus time (t) for various bed heights and flow rates for JGBD and CVD, respectively. In the results shown, the Thomas model constant k_{Th} was increased when increased flow rate from 8 ml/min to 25 ml/min, when change the bed heights from 10 to 25 cm, K_{Th} was decreased.

When the flow rate was increased for each dye, the adsorption capacity was decreased. The obtained results showed that Thomas model best described the experimental data. The calculated q_{Th} and K_{Th} are given in Table(4.17). For all the bed heights, high correlation coefficients were observed (R^2 ~ 0.98 to 0.99) for each dye. Therefore, it can be concluded that (i) Thomas constant decreased with height and increased with flow rate while (ii) the calculated adsorption capacity substantial decreased with flow rate and increased with height to fit the experimental adsorption results. This proved that Thomas model fitted the experimental data from the current column-based adsorption on LLSP (Khalfa

et al., 2021). Adsorbed amounts (q_{Th}) calculated from the model were very close to the experimental values (qe_{exp}), further confirming the best fit.

Furthermore, high coefficients of determination indicated an adequate model. However, the model cannot strictly follow the sorption in the column, nor determine the minimum height of the sorption front and thus allows a better knowledge of the performance. Such an outcome reveals the existence of a good fit of the Thomas model (Thillainayagam et al., 2021).

Based on the findings displayed in the figures, it is evident that both the Thomas model and the BDST model are found to be fit for column sorption data. The LLSP is easily available, cheap, and ecofriendly which makes it the best suitable alternative for dye bearing wastewater treatment.

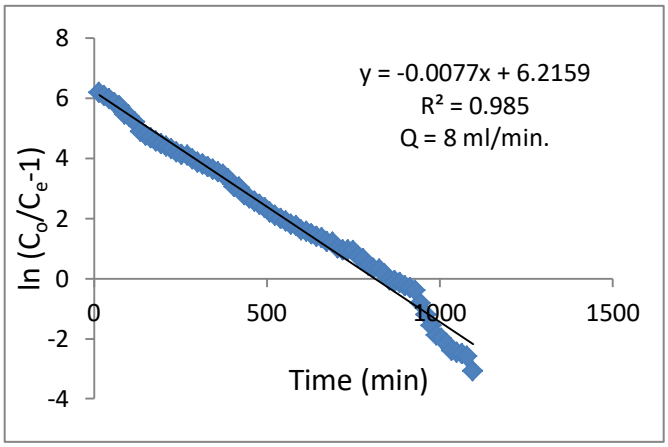

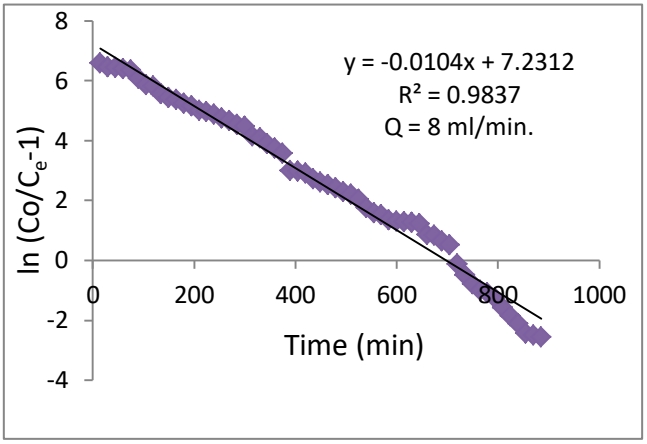

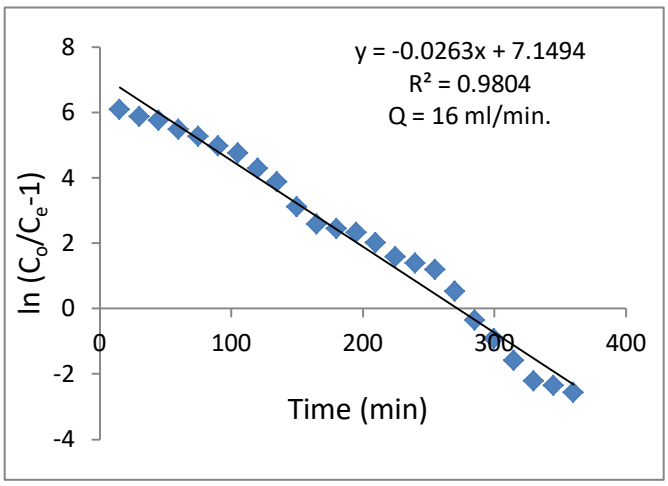

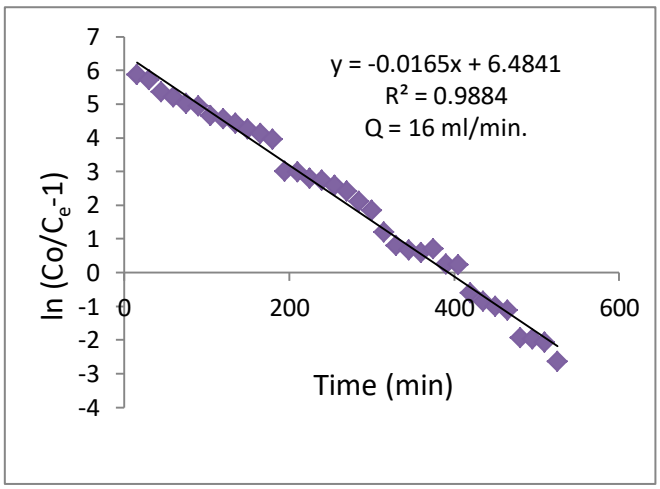

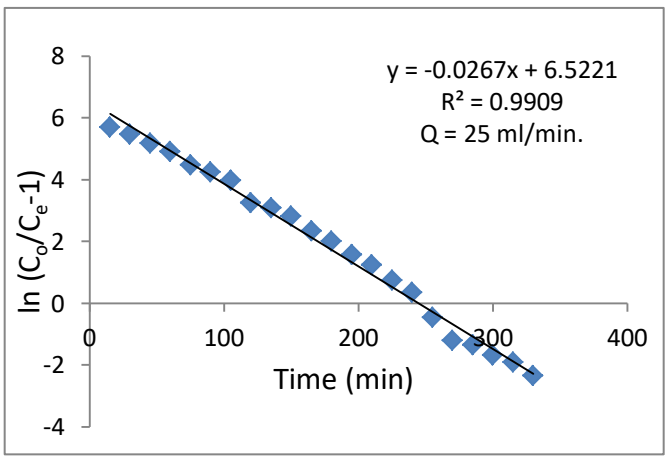

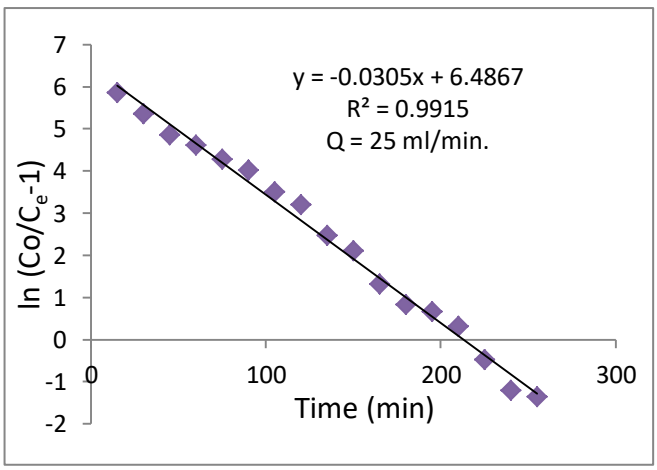

Fig. (4.23): Thomas kinetic plots for sorption of JGBD and CVD under various effect flow rate (Co=25 mg/l, H=15 cm, pH 9).

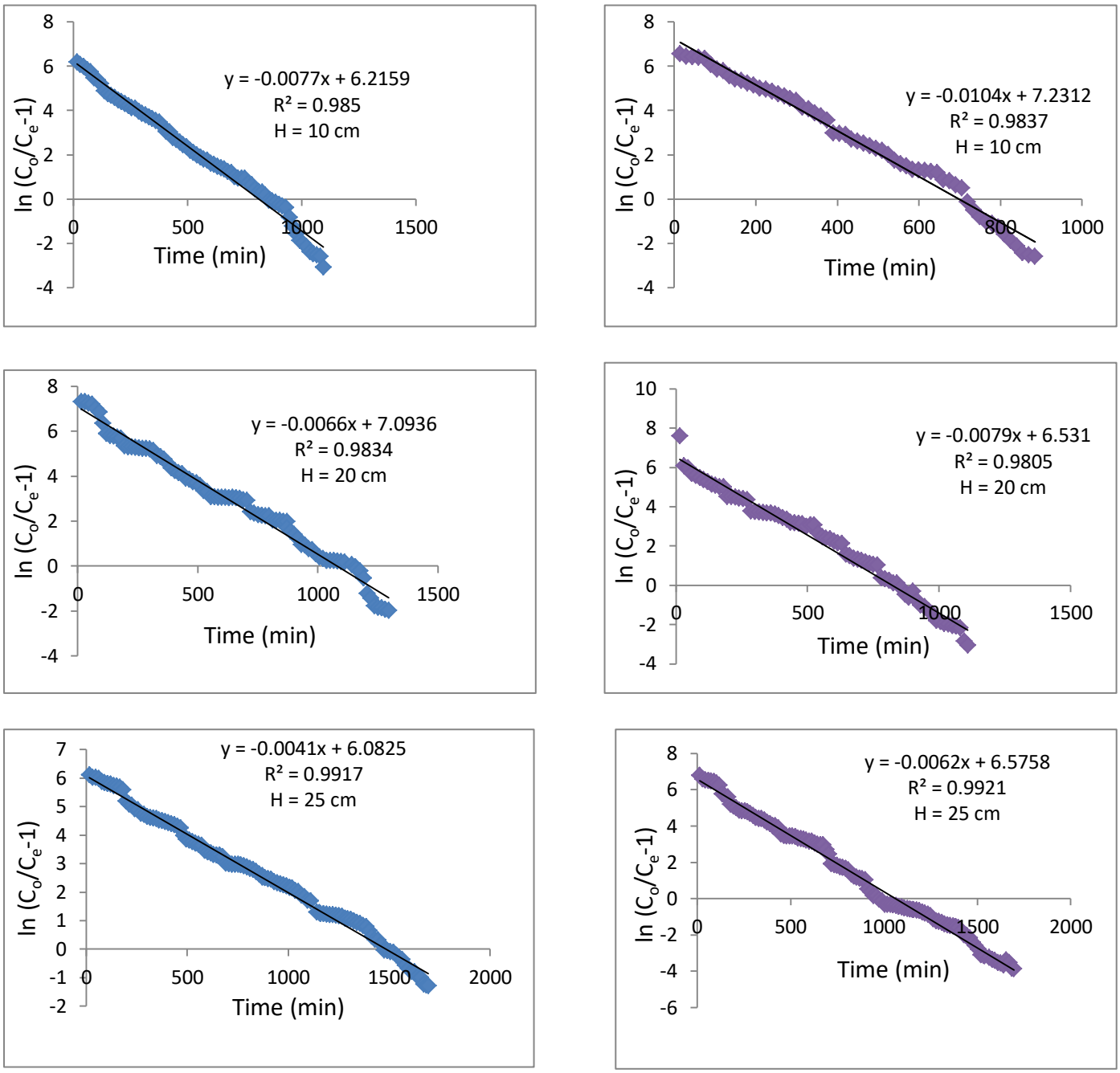

Fig. (4.24): Thomas kinetic plots for sorption of JGBD and CVD under various effect bed depth (H=8 ml/min, C_o= 25 mg/l).

4.8.3 Yoon and Nelson model

It is the simplest model as it does not concern with the physicochemical characteristics of LLSP, type of sorbent and properties of the sorption column (Yagub et al., 2014).The application of Yoon and Nelson model to the experimental data resulted in K_{YN} and t_{50} values that adequately described the fixed bed adsorption of each dye onto the LLSP layer Table (4.17).

Figure (4.25) and Figure (4.26) show graphs of ln (C_e/C_o-C_e) against time for various bed heights and inlet flow rates derived from equation (2.26) and shows the fit of this model for JGBD and CVD adsorption using LLSP at 8, 16 and 25 ml/min. t_{50} decreased with the flow rate because of the faster column saturation. Previous studies have successfully used the Yoon and Nelson model for the description of pollutants adsorption in a fixed-bed design (Calero et al., 2009; Liu et al., 2011).

The effect of bed depth on the breakthrough curve for different flow rates is evaluated using the Yoon Nelson model. (min) and K_{YN} (min^{-1}) values are summarized in Table (4.17). Table (4.17) shows the value of correlation coefficients (R^2) demonstrated the model applicability ($R^2 > 0.98$ for each dye) to the experimental data under various conditions for the removal of JGBD and CVD using LLSP (Jayalakshmi and Jeyanthi , 2021). For all the ranges of bed depth and flow rates, the qe_{cal} and qe_{exp} were very close, which validates the fitness of Yoon Nelson. The time required for 50% adsorbent breakthrough (τ) increases on increasing the bed depth.

Correspondingly, the quantity of treated effluent increased. The increase in bed depth provides more number of adsorption sites, which increased the τ value (Gopal et al., 2016). The decreased τ value due to increase in flow rate was attributed to the rapid saturation of bed depth. The values of K_{YN} decreased with an increased bed depth and increased with an increased flow rate for each dye. The time taken for dye molecules to travel through the bed have increased

as the bed depth increases, which resulted in a increased of the adsorption rate, decreased the adsorption rate due to increased flow rate (Vieira et al., 2018). All these established findings ensured the Yoon-Nelson model's better fitness for the removal of each dye using LLSP (Sivakumar and Palanisamy, 2009; Javanbakht and Shafiei, 2020).

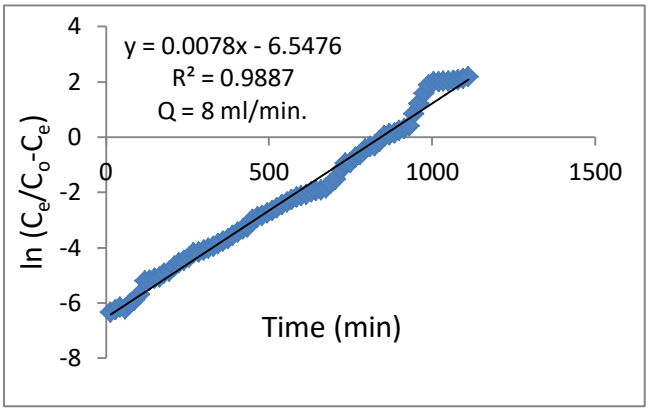

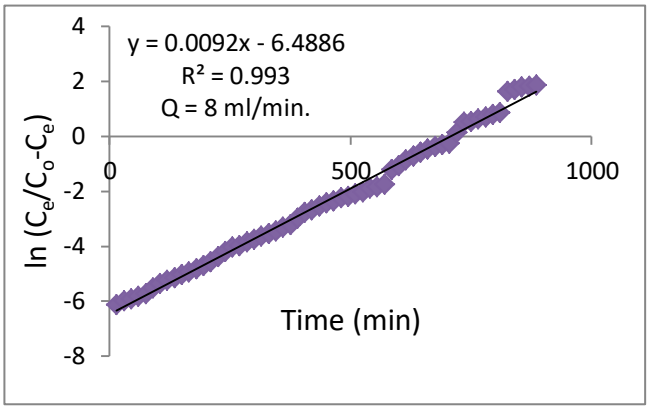

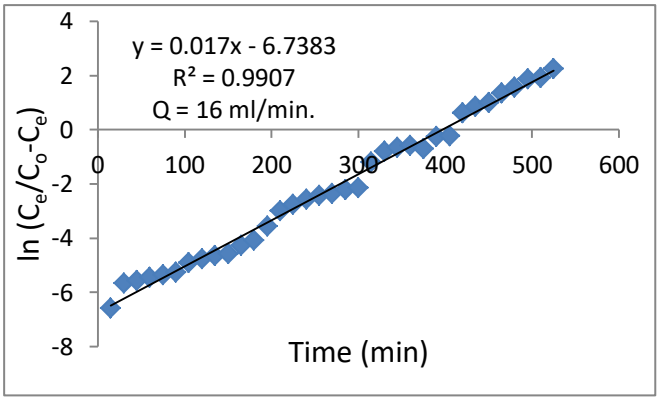

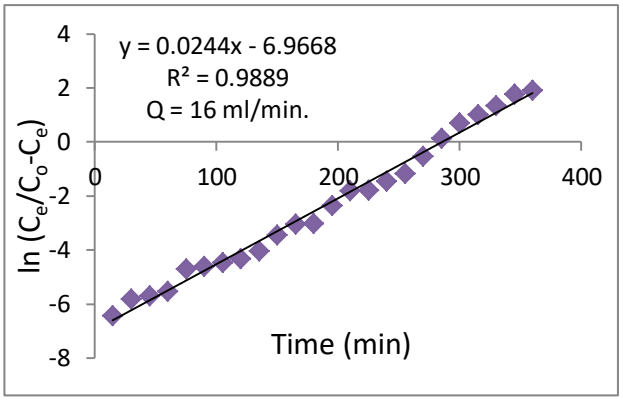

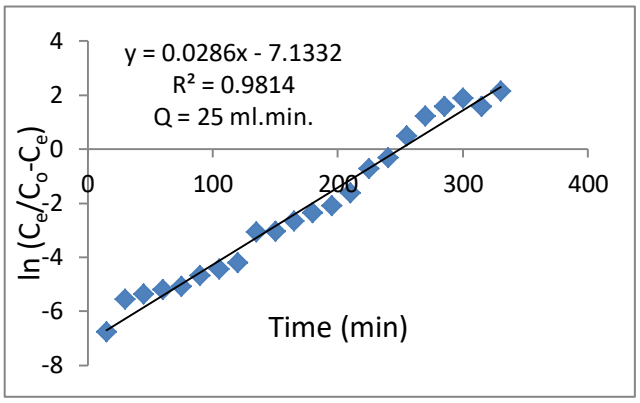

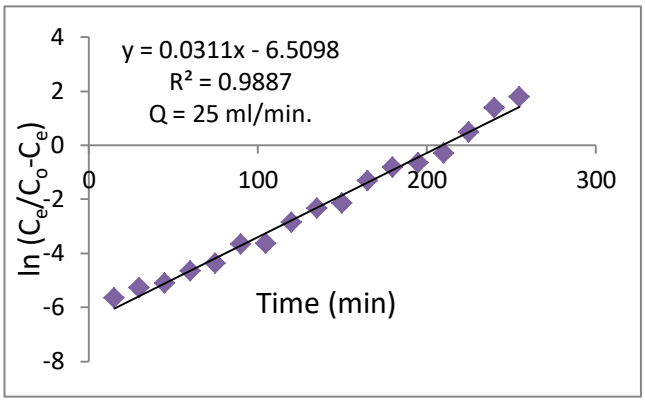

Fig. (4.25): Yoon-Nelson kinetics plots for the sorption of JGBD and CVD on JGBD under different effect of flow rate (C_o = 25 mg/l, H = 10 cm, pH 9).

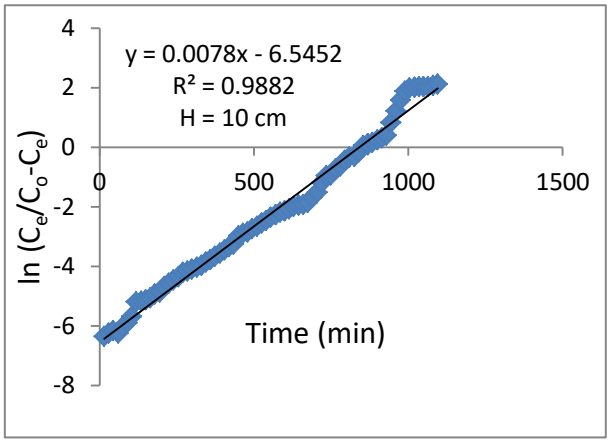

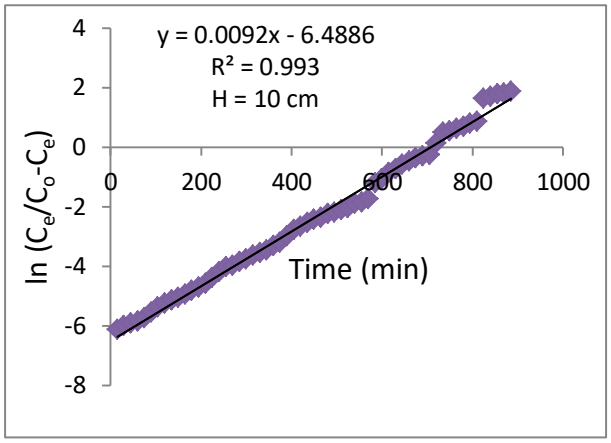

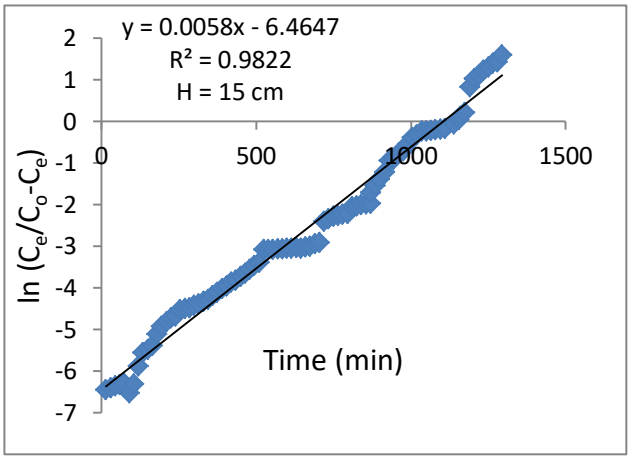

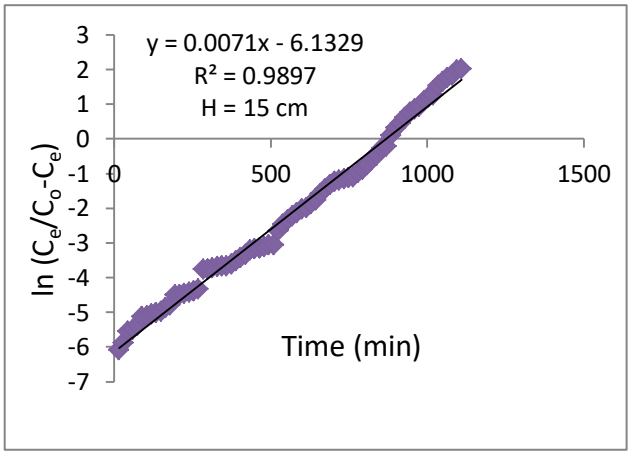

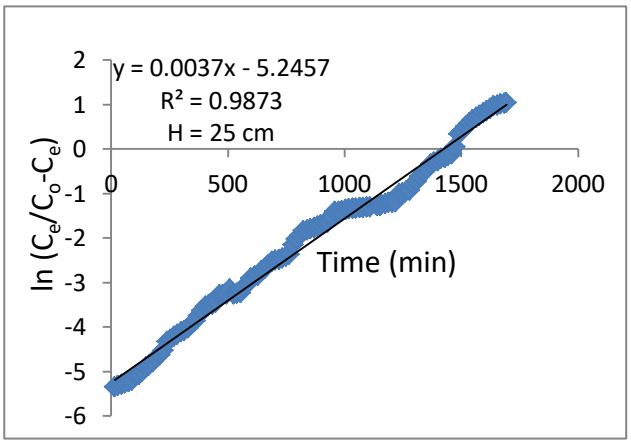

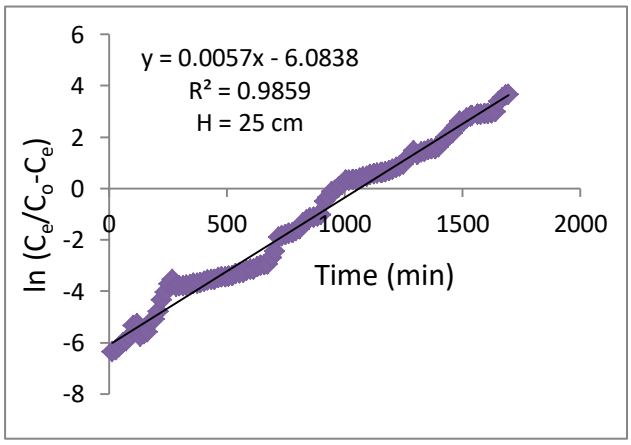

Fig. (4.26): Yoon-Nelson kinetics plots for the sorption of JGBD and CVD on JGBD under different effect of bed depth (C_o = 25 mg/l, Q = 8 ml/min, pH 9).

Table (4.17): Kinetic models parameters for sorption of JGBD and CVD onto LLSP continuous at different feed flow rate and bed height.

Experimental conditions							
Flow rate, Q_v(ml/min)		8	16	25	8	8	8
Bed depth (cm)		10	10	10	10	15	25
Initial concentration (mg/l)		25	25	25	25	25	25
qe_{exp} (mg/g)	JGBD	16.03	15.76	14.97	16.03	17.01	18.04
	CVD	14.94	12.47	11.51	14.94	15.24	16.05
Thomas Model Parameters							
JGBD	K_{TH} (l/mg.min)	0.000308	0.00066	0.001068	0.000308	0.00026	0.000164
	q_{TH}(mg/g)	16.46	16.02	15.56	16.46	17.39	17.89
	R^2	0.985	0.9804	0.9909	0.985	0.9834	0.9917
CVD	K_{TH} (l/mg.min)	0.00042	0.00105	0.00122	0.00042	0.00032	0.00025
	q_{TH}(mg/g)	14.04	11.10	13.55	14.04	15.37	16.69
	R^2	0.9837	0.9884	0.9915	0.9837	0.9805	0.9921
Yoon-Nelson Model Parameters							
JGBD	$K_{YN}(min^{-1})$	0.0092	0.0244	0.0311	0.0092	0.0071	0.0057
	τ_{exp}(min)	877.5	427.5	270	877.5	1035	1147.5
	τ_{cal}(min)	839.45	396.37	249.41	839.45	1114.6	1417.75
	q_{YN}(mg/g)	16.46	15.48	15.28	16.46	17.67	18.78
	R^2	0.9887	0.9907	0.9814	0.9887	0.9822	0.9873
CVD	$K_{YN}(min^{-1})$	0.0078	0.017	0.0286	0.0078	0.0058	0.0037
	τ_{exp}(min)	765	360	202.5	765	877.5	1012.5
	τ_{cal}(min)	705.28	285.52	209.31	705.28	856.87	1067.33
	q_{YN}(mg/g)	13.83	11.20	12.82	13.83	17.67	18.78
	R^2	0.993	0.9889	0.9887	0.993	0.9897	0.9859

Chapter Five

Conclusions and Recommendations

Chapter Five

Conclusions and Recommendations

5.1 Conclusions

On the basis of the data, the findings are as follows:

1. It was concluded that LLSP prepared from natural plant is an effective biosorbent and alternative for removing JGBD and CVD from aqueous solutions.
2. Several operational factors have been studied on dye solution, like pH, contact time, dose of LLSP and initial concentration, where the percentage of removal efficiency increased with the increase of first three factors, while decreased with the increase of fourth factor.
3. The sorption of each dye was reached to equilibrium time at 30 min. and 45 min. for JGBD and CVD, respectively.
4. Each dye had a uniform monolayer covering on the LLSP surface confirm that the Langmuir isotherm model is good match to the equilibrium sorption of each dye by using MAE and MSAE. For JGBD and CVD, the maximal sorption potential was reported to be 142.85 mg/g and 45.45 mg/g, respectively. The beneficial sorption process is also shown by the dimensionless separation factor (R_L).
5. The study of kinetic showed that the sorption mechanism of each dye followed a pseudo-second-order model, where R^2 value 99.95% and 99.93% was for JGBD and CVD, respectively indicating the occurrence of chemical sorption on the surface of LLSP.
6. The multi-linearity of the intraparticle diffusion kinetic model demonstrated that JGBD and CVD sorption are controlled by two or more processes, including intraparticle diffusion.
7. The produced LLSP was found to be feasible media for using as a column bed for removal of JGBD and CVD from colored water.

8. The breakthrough curves were projected under various situations using the kinetic model of BDST, Thomas, and Yoon Nelson, and the parameters of column kinetic were discovered by the kinetic investigation. The obtained findings demonstrated that all three models had excellent R^2 to represent a breakthrough curve completely. According to the results, LLSP may be utilized as a biosorbent in the form of a continuous to successfully remove JGBD and CVD continuously from aqueous solutions.
9. The proposed place to place this treatment for the wastewater treatment plant is in the stage of advanced treatments.

5.2 Recommendations for future study

Future studies should consider the following recommendations:

1. The production of biomass-based biosorbent using other locally accessible biomass solid wastes, such as Willow Leaves (Salix alba), Ziziphus spina-christi Seeds, Acacia Bark Leaves and Palma Seeds and so on, might be studied similarly under comparable working circumstances.
2. This research may be expanded to examine the competitive sorption in batch and continuous flow modes in the presence of additional dye or heavy metal ions.
3. Wastewater samples can be used as biosorbates to evaluate the efficiency of biosorbents since real industrial effluents simultaneously produce a wide range of organic pollutants.
4. Both batch and continuous flow methods of heavy metal removal can be investigated using the natural plants.

References

References

- Abdolali, A., Guo, W. S., Ngo, H. H., Chen, S. S., Nguyen, N. C., & Tung, K. L. (2014). Typical lignocellulosic wastes and by-products for sorption process in water and wastewater treatment: a critical review. Bioresource technology, 160, 57-66.
- Abdolali, A., Ngo, H. H., Guo, W., Zhou, J. L., Zhang, J., Liang, S., ... & Liu, Y. (2017). Application of a breakthrough biosorbent for removing heavy metals from synthetic and real wastewaters in a lab-scale continuous fixed-bed column. Bioresource technology, 229, 78-87.
- Abebe, B., Murthy, H. A., & Amare, E. (2018). Summary on adsorption and photocatalysis for pollutant remediation: Mini review. Journal of Encapsulation and Adsorption Sciences, 8(4), 225-255.
- Abed, F., Aksas, H., Abai, N., & Babakhouya, N. (2019). Study of the adsorption of methylene blue by natural materials (olive stone, date pit and their mixture) in continuous. Algerian Journal of Environmental Science and Technology, 5(2).
- Abrouki, Y., Mabrouki, J., Anouzla, A., Rifi, S. K., Zahiri, Y., Nehhal, S., ... & Souabi, S. (2021). Optimization and modeling of a fixed-bed sorption of textile dye using agricultural biomass from the Moroccan Sahara. Desalin Water Treat, 240, 144-151.
- Ahmad, A. A., & Hameed, B. H. (2010). Fixed-bed adsorption of reactive azo dye onto granular activated carbon prepared from waste. Journal of hazardous materials, 175(1-3), 298-303.
- Ahmad, A., Bhat, A. H., & Buang, A. (2018). Sorption of transition metals by freely suspended and Ca-alginate immobilised with Chlorella vulgaris: Kinetic and equilibrium modeling. Journal of Cleaner Production, 171, 1361-1375.

- Ahmad, M. A., Puad, N. A. A., & Bello, O. S. (2014). Kinetic, equilibrium and thermodynamic studies of synthetic dye removal using pomegranate peel activated carbon prepared by microwave-induced KOH activation. Water Resources and industry, 6, 18-35.
- Ahmed, A.M., and Samaka, S. S. (2018). Bentonite coated with magnetite Fe3O4 nanoparticles as a novel adsorbent for copper (II) ions removal from water/wastewater. Environmental Technology & Innovation, 10, 162-174.
- Ajiboye, T. O., Oyewo, O. A., & Onwudiwe, D. C. (2021). Simultaneous removal of organics and heavy metals from industrial wastewater: A review. Chemosphere, 262, 128379.
- Ajmal, M., Rao, R. A. K., & Khan, M. A. (2005). Adsorption of copper from aqueous solution on Brassica cumpestris (mustard oil cake). Journal of hazardous materials, 122(1-2), 177-183.
- Akar, S. T., Özcan, A. S., Akar, T., Özcan, A., & Kaynak, Z. (2009). Sorption of a reactive textile dye from aqueous solutions utilizing an agro-waste. Desalination, 249(2), 757-761.
- Aksu, Gönen, and Z. Demircan (2002). Sorption of chromium(VI) ions by Mowital®B30H resin immobilized activated sludge in a packed bed: Comparison with granular activated carbon, Process Biochem., vol. 38, no. 2, pp. 175–186, 2002.
- Aksu, Z., & Gönen, F. (2004). Sorption of phenol by immobilized activated sludge in a continuous packed bed: prediction of breakthrough curves. Process biochemistry, 39(5), 599-613.
- Al-Ghamdi, Y. O., Jabli, M., Soury, R., & Ali Khan, S. (2020). A cellulosic fruit derived from nerium oleander biomaterial: Chemical characterization and its valuable use in the sorption of methylene blue in a batch mode. Polymers, 12(11), 2539.

- Al-Ghouti, M. A., & Da'ana, D. A. (2020). Guidelines for the use and interpretation of adsorption isotherm models: A review. Journal of hazardous materials, 393, 122383.
- Ali, I., Asim, M., & Khan, T. A. (2012). Low cost adsorbents for the removal of organic pollutants from wastewater. Journal of environmental management, 113, 170-183.
- Ali, N., Hameed, A., & Ahmed, S. (2009). Physicochemical characterization and bioremediation perspective of textile effluent, dyes and metals by indigenous bacteria. Journal of hazardous materials, 164(1), 322-328.
- Aljeboree, A. M., Alshirifi, A. N., & Alkaim, A. F. (2017). Kinetics and equilibrium study for the adsorption of textile dyes on coconut shell activated carbon. Arabian journal of chemistry, 10, S3381-S3393.
- Al-Saadi, A. A., Saleh, T. A., & Gupta, V. K. (2013). Spectroscopic and computational evaluation of cadmium adsorption using activated carbon produced from rubber tires. Journal of Molecular Liquids, 188, 136-142.
- Al-Saraj, M., Abdel-Latif, M. S., El-Nahal, I., & Baraka, R. (1999). Bioaccumulation of some hazardous metals by sol–gel entrapped microorganisms. Journal of non-crystalline solids, 248(2-3), 137-140.
- Alshabib, M., Oluwadamilare, M. A., Tanimu, A., Abdulazeez, I., Alhooshani, K., & Ganiyu, S. A. (2021). Experimental and DFT investigation of ceria-nanocomposite decorated AC derived from groundnut shell for efficient removal of methylene-blue from wastewater effluent. Applied Surface Science, 536, 147749.
- Anwar, J., Shafique, U., Salman, M., Dar, A., & Anwar, S. (2010). Removal of Pb (II) and Cd (II) from water by adsorption on peels of banana. Bioresource technology, 101(6), 1752-1755.

- Aranda-García, E., & Cristiani-Urbina, E. (2020). Hexavalent chromium removal and total chromium sorption from aqueous solution by Quercus crassipes acorn shell in a continuous up-flow fixed-bed column: Influencing parameters, kinetics, and mechanism. PLos One, 15(1), e0227953.
- Aravind, M., & Amalanathan, M. (2021). Structural, morphological, and optical properties of country egg shell derived activated carbon for dye removal. Materials Today: Proceedings, 43, 1491-1495.
- Archin, S., Sharifi, S. H., & Asadpour, G. (2019). Optimization and modeling of simultaneous ultrasound-assisted adsorption of binary dyes using activated carbon from tobacco residues: response surface methodology. Journal of Cleaner Production, 239, 118136.
- Aryal, N., Ottosen, L. D. M., Kofoed, M. V. W., & Pant, D. (Eds.). (2021). Emerging Technologies and Biological Systems for Biogas Upgrading. Academic Press.
- Asfaram, A., Ghaedi, M., Agarwal, S., Tyagi, I., & Gupta, V. K. (2015). Removal of basic dye Auramine-O by ZnS: Cu nanoparticles loaded on activated carbon: optimization of parameters using response surface methodology with central composite design. RSC advances, 5(24), 18438-18450.
- Asfaram, A., Ghaedi, M., Dashtian, K., & Ghezelbash, G. R. (2018). Preparation and characterization of Mn0. 4Zn0. 6Fe2O4 nanoparticles supported on dead cells of Yarrowia lipolytica as a novel and efficient adsorbent/biosorbent composite for the removal of azo food dyes: central composite design optimization study. ACS Sustainable Chemistry & Engineering, 6(4), 4549-4563.

- Atar, N., Olgun, A., Wang, S., & Liu, S. (2011). Adsorption of anionic dyes on boron industry waste in single and binary solutions using batch and fixed-bed systems. Journal of Chemical & Engineering Data, 56(3), 508-516.
- Ayawei, N., Ebelegi, A. N., & Wankasi, D. (2017). Modelling and interpretation of adsorption isotherms. Journal of chemistry, 2017.
- Bachmann, S. A. L., Calvete, T., & Féris, L. A. (2021). Caffeine removal from aqueous media by adsorption: an overview of adsorbents evolution and the kinetic, equilibrium and thermodynamic studies. Science of the Total Environment, 767, 144229.
- Bachmann, S. A. L., Calvete, T., & Féris, L. A. (2021). Caffeine removal from aqueous media by adsorption: an overview of adsorbents evolution and the kinetic, equilibrium and thermodynamic studies. Science of the Total Environment, 767, 144229.
- Badr, S. M., & Isra'a, S. (2021). Using agricultural waste as biosorbent for hazardous brilliant green dye removal from aqueous solutions. Journal of Engineering Science & Technology, 16(4), 3435-3454.
- Baral, S. S., Das, N., Ramulu, T. S., Sahoo, S. K., Das, S. N., & Chaudhury, G. R. (2009). Removal of Cr (VI) by thermally activated weed Salvinia cucullata in a fixed-bed column. Journal of Hazardous Materials, 161(2-3), 1427-1435.
- Basu, M., & Guha, A. K. (2022). Analysis of continuous bioadsorptive removal of cadmium in the light of circular economy and sustainability. Bioresource Technology Reports, 101101.

- Bayes, G. S., Raut, S. S., Patil, V. R., & Lokhande, R. S. (2012). Formation of diazepam–lanthanides (III) complexes in the 50–50 volume% ethanol– water solvent system and study of the effect of temperature on the complex formation constants. Journal of solution chemistry, 41(2), 241-248.
- Behloul, M., Lounici, H., Abdi, N., Drouiche, N., & Mameri, N. (2017). Adsorption study of metribuzin pesticide on fungus Pleurotus mutilus. International Biodeterioration & Biodegradation, 119, 687-695.
- Belhouchat, N., Zaghouane-Boudiaf, H.,Viseras, C., 2017, "Removal of anionic and cationic dyes from aqueous solution with activated organo-bentonite/sodium alginate encapsulated beads", Applied Clay Science, 135, 9–15.
- Bello, O. S., Ahmad, M. A., & Ahmad, N. (2012). Adsorptive features of banana (Musa paradisiaca) stalk-based activated carbon for malachite green dye removal. Chemistry and Ecology, 28(2), 153-167.
- Belmabrouk, H., Selmi, M., Alshahrani, T., Bajahzar, A., & Jabli, M. (2022). Experimental and theoretical study of methylene blue sorption using a new biomaterial Pergularia tomentosa L. fruit. International Journal of Environmental Science and Technology, 1-18.
- Bharathi, K. S., & Ramesh, S. P. T. (2013). Fixed-bed column studies on sorption of crystal violet from aqueous solution by Citrullus lanatus rind and Cyperus rotundus. Applied Water Science, 3(4), 673-687.
- Boudechiche, N., Mokaddem, H., Sadaoui, Z., & Trari, M. (2016). Sorption of cationic dye from aqueous solutions onto lignocellulosic biomass (Luffa cylindrica): characterization, equilibrium, kinetic and thermodynamic studies. International Journal of Industrial Chemistry, 7(2), 167-180.

- Bouras, H. D., Yeddou, A. R., Bouras, N., Hellel, D., Holtz, M. D., Sabaou, N., & Nadjemi, B. (2017). Sorption of Congo red dye by Aspergillus carbonarius M333 and Penicillium glabrum Pg1: Kinetics, equilibrium and thermodynamic studies. Journal of the Taiwan Institute of Chemical Engineers, 80, 915-923.
- Brandani, S. (2021). Kinetics of liquid phase batch adsorption experiments. Adsorption, 27(3), 353-368.
- Brigden, K., Labunska, I., House, E., Santillo, D., & Johnston, P. (2012). Hazardous chemicals in branded textile products on sale in 27 countries during 2012. Greenpeace Research Laboratories Technical Report 06−2012.
- Brito, M. J. P., Veloso, C. M., Santos, L. S., Bonomo, R. C. F., & Fontan, R. D. C. I. (2018). Adsorption of the textile dye Dianix® royal blue CC onto carbons obtained from yellow mombin fruit stones and activated with KOH and H3PO4: kinetics, adsorption equilibrium and thermodynamic studies. Powder technology, 339, 334-343.
- Bushra, R., Mohamad, S., Alias, Y., Jin, Y., & Ahmad, M. (2021). Current approaches and methodologies to explore the perceptive adsorption mechanism of dyes on low-cost agricultural waste: A review. Microporous and Mesoporous Materials, 319, 111040.
- Calero, M., Hernáinz, F., Blázquez, G., Tenorio, G., & Martín-Lara, M. A. (2009). Study of Cr (III) sorption in a fixed-bed column. Journal of Hazardous Materials, 171(1-3), 886-893.
- Calero, M., Iáñez-Rodríguez, I., Pérez, A., Martín-Lara, M. A., & Blázquez, G. (2018). Neural fuzzy modelization of copper removal from water by sorption in fixed-bed columns using olive stone and pinion shell. Bioresource technology, 252, 100-109.

- Cameselle C, Gouveia S, Akretche DE, Belhadj B (2013) Advances in electrokinetic remediation for the removal of organic contaminants in soil. In: Rashed MN (ed.), Soils, Organic Pollutants-Monitoring, Risk and Treatment.
- Chakraborty, S., Chowdhury, S., & Saha, P. D. (2012). Insight into sorption equilibrium, kinetics and thermocontinuous of crystal violet onto Ananas comosus (pineapple) leaf powder. Applied Water Science, 2(2), 135-141.
- Charola, S., Yadav, R., Das, P., & Maiti, S. (2018). Fixed-bed adsorption of Reactive Orange 84 dye onto activated carbon prepared from empty cotton flower agro-waste. Sustainable Environment Research, 28(6), 298-308.
- Chavan, R. B. (2011). Environmentally friendly dyes. Handbook of textile and industrial dyeing, 515-561.
- Chebli, D., Bouguettoucha, A., Mekhalef, T., Nacef, S., & Amrane, A. (2015). Valorization of an agricultural waste, Stipa tenassicima fibers, by sorption of an anionic azo dye, Congo red. Desalination and Water Treatment, 54(1), 245-254.
- Chen, B. Y., Chen, C. Y., Guo, W. Q., Chang, H. W., Chen, W. M., Lee, D. J., ... & Chang, J. S. (2014). Fixed-bed sorption of cadmium using immobilized Scenedesmus obliquus CNW-N cells on loofa (Luffa cylindrica) sponge. Bioresource technology, 160, 175-181.
- Chen, S., Qin, C., Wang, T., Chen, F., Li, X., Hou, H., & Zhou, M. (2019). Study on the adsorption of dyestuffs with different properties by sludge-rice husk biochar: adsorption capacity, isotherm, kinetic, thermocontinuous and mechanism. Journal of Molecular Liquids, 285, 62-74.

- Chen, S., Yue, Q., Gao, B., Li, Q., Xu, X., & Fu, K. (2012). Adsorption of hexavalent chromium from aqueous solution by modified corn stalk: a fixed-bed column study. Bioresource technology, 113, 114-120.
- Chen, T., Zhou, Z., Han, R., Meng, R., Wang, H., & Lu, W. (2015). Adsorption of cadmium by biochar derived from municipal sewage sludge: impact factors and adsorption mechanism. Chemosphere, 134, 286-293.
- Cheriti, A., Talhi, M. F., Belboukhari, N., & Taleb, S. (2011). Copper ions sorption properties of biomass derived from Algerian Sahara plants. Expanding issues in desalination. Intech, 319-338.
- Chew, T. L., & Husni, H. (2019). Oil palm frond for the adsorption of Janus Green dye. Materials Today: Proceedings, 16, 1766-1771.
- Choudhary, A. Removal of Oil from Seawater Using Charcoal and Rice Hull. IOP Conf. Ser. Mater. Sci. Eng. 2017, 263, 032007.
- Chowdhury, S., & Saha, P. (2010). Sea shell powder as a new adsorbent to remove Basic Green 4 (Malachite Green) from aqueous solutions: Equilibrium, kinetic and thermodynamic studies. Chemical Engineering Journal, 164(1), 168-177.
- Chowdhury, S., & Saha, P. D. (2013). Adsorption of malachite green from aqueous solution by naoh-modified rice husk: Fixed-bed column studies. Environmental Progress & Sustainable Energy, 32(3), 633-639.
- Cimá-Mukul, C. A., Abdellaoui, Y., Abatal, M., Vargas, J., Santiago, A. A., & Barrón-Zambrano, J. A. (2019). Eco-efficient biosorbent based on leucaena leucocephala residues for the simultaneous removal of Pb (II) and Cd (II) ions from water system: sorption and mechanism. Bioinorganic chemistry and applications, 2019.

- Cimá-Mukul, C. A., Olguín, M. T., Abatal, M., Vargas, J., Barrón-Zambrano, J. A., Avila-Ortega, A., & Santiago, A. A. (2020). Assessment of leucaena leucocephala as bio-based adsorbent for the removal of pb2+, cd2+ and ni2+ from water. Desalin Water Treat, 173, 331-342.
- Cojocaru, C., Samoila, P., & Pascariu, P. (2019). Chitosan-based magnetic adsorbent for removal of water-soluble anionic dye: artificial neural network modeling and molecular docking insights. International journal of biological macromolecules, 123, 587-599.
- Coman, G., Blattner, C. M., Blickenstaff, N. R., Andersen, R., & Maibach, H. I. (2014). Textile allergic contact dermatitis: current status. Reviews on Environmental Health, 29(3), 163-168.
- Costa, F. M. A. S., Seolatto, A. A., Fontoura, R. S., & Freitas, F. F. (2021). Use of brewery spent grains as a biosorbent for reactive blue 5G dye removal: batch and continuous flow studies. Chemical Engineering Communications, 1-18.
- Crini, G. (2005). Recent developments in polysaccharide-based materials used as adsorbents in wastewater treatment. Progress in polymer science, 30(1), 38-70.
- Crini, G. (2006). Non-conventional low-cost adsorbents for dye removal: a review. Bioresource technology, 97(9), 1061-1085.
- Crini, G., Lichtfouse, E., Wilson, L. D., & Morin-Crini, N. (2019). Conventional and non-conventional adsorbents for wastewater treatment. Environmental Chemistry Letters, 17(1), 195-213.
- Cruz, C. C., Da Costa, A. C. A., Henriques, C. A., & Luna, A. S. (2004). Kinetic modeling and equilibrium studies during cadmium sorption by dead Sargassum sp. biomass. Bioresource technology, 91(3), 249-257.

- Da Silva, D. C. C., & de Abreu Pietrobelli, J. M. T. (2019). Residual biomass of chia seeds (Salvia hispanica) oil extraction as low cost and eco-friendly biosorbent for effective reactive yellow B2R textile dye removal: characterization, kinetic, thermodynamic and isotherm studies. Journal of Environmental Chemical Engineering, 7(2), 103008.
- Darwesh, O. M., El-Latief, A., Aya, H., Abuarab, M. E., & Kasem, M. A. (2021). Enhancing the efficiency of some agricultural wastes as low-cost absorbents to remove textile dyes from their contaminated solutions. Biomass Conversion and Biorefinery, 1-10.
- Das, L., Sengupta, S., Das, P., Bhowal, A., & Bhattacharjee, C. (2021). Experimental and Numerical modeling on dye adsorption using pyrolyzed mesoporous biochar in Batch and fixed-bed column reactor: Isotherm, Thermocontinuous, Mass transfer, Kinetic analysis. Surfaces and Interfaces, 23, 100985.
- Das, N., Das, D., (2013), "Recovery of rare earth metals through biosorption: An overview", Journal of Rare Earths, 31(10), 933– 943.
- Dawood, S., Sen, TK, Phan, C. , (2016). Adsorption removal of Methylen prepared from Eucalyptus sheathiana bark: kinetic, equilibrium, mechanism, thermodynamic and process design", Desal. Water Treat., 57: PP. 28964-28980.
- De Lima, C. R. M., Gomes, D. N., Pereira, M. R., & Fonseca, J. L. C. (2018). Anionic and cationic drug sorption on interpolyelectrolyte complexes. Colloids and Surfaces B: Biointerfaces, 170, 210-218.
- De Sá, I. C., De Oliveira,, Borges, P. H. S., Lepri, F. G., Semaan, F. S., ... & Pacheco, W. F. (2022). Modified dry bean pod waste (Phaseolus vulgaris) as a biosorbent for fluorescein removal from aqueous media: Batch and fixed bed studies. Journal of Hazardous Materials, 424, 127723.

- Dehghani, M. H., Salari, M., Karri, R. R., Hamidi, F., & Bahadori, R. (2021). Process modeling of municipal solid waste compost ash for reactive red 198 dye adsorption from wastewater using data driven approaches. Scientific Reports, 11(1), 1-20.
- Desore, A., & Narula, S. A. (2018). An overview on corporate response towards sustainability issues in textile industry. Environment, Development and Sustainability, 20(4), 1439-1459.
- Deveci, H., & Kar, Y. (2013). Adsorption of hexavalent chromium from aqueous solutions by bio-chars obtained during biomass pyrolysis. Journal of Industrial and Engineering Chemistry, 19(1), 190-196.
- Ebrahimian Pirbazari. A, Saberikhah. E., Habibzadeh Kozani S.S., (2014). Fe3O4–wheat straw: preparation, characterization and its application for methylene blue adsorption, Water Resources and Industry, Volumes 7–8, , Pages 23-37,ISSN 2212-3717.
- El Maguana, Y., Elhadiri, N., Bouchdoug, M., Benchanaa, M., & Jaouad, A. (2019). Activated carbon from prickly pear seed cake: optimization of preparation conditions using experimental design and its application in dye removal. International Journal of Chemical Engineering, 2019.
- Elhadiri, N., Bouchdoug, M., Benchanaa, M., & Boussetta, A. (2018). Optimization of preparation conditions of novel adsorbent from sugar scum using response surface methodology for removal of methylene blue. Journal of Chemistry, 2018.
- Elmholt, S., Schjønning, P., Munkholm, L. J., & Debosz, K. (2008). Soil management effects on aggregate stability and biological binding. Geoderma, 144(3-4), 455-467.

- Eloussaief, M., Kallel, N., Yaacoubi, A., & Benzina, M. (2011). Mineralogical identification, spectroscopic characterization, and potential environmental use of natural clay materials on chromate removal from aqueous solutions. Chemical Engineering Journal, 168(3), 1024-1031.
- El-Sayed, G. O., Dessouki, H. A., & Ibrahim, S. S. (2010). Sorption of Ni (II) and Cd (II) ions from aqueous solutions onto rice straw. Chemical Sciences Journal.
- Essawy, A. A., Ali, A. E. H., & Abdel-Mottaleb, M. S. A. (2008). Application of novel copolymer-TiO2 membranes for some textile dyes adsorptive removal from aqueous solution and photocatalytic decolorization. Journal of Hazardous Materials, 157(2-3), 547-552.
- Farhood, A. S., Ali, L. A. M., Majeed, A. S., & Taha, D. N. (2021). Batch Adsorption Technique for the Removal of Janus Green B Dye from Industrial Waste Water by Using Walnut Kernel Shell as Adsorbent. Annals of the Romanian Society for Cell Biology, 25(7), 154-168.
- Fat'hi, M. R., Asfaram, A., Hadipour, A., & Roosta, M. (2014). Kinetics and thermodynamic studies for removal of acid blue 129 from aqueous solution by almond shell. Journal of Environmental Health Science and Engineering, 12(1), 1-7.
- Fernandez, M. E., Nunell, G. V., Bonelli, P. R., & Cukierman, A. L. (2012). Batch and dynamic sorption of basic dyes from binary solutions by alkaline-treated cypress cone chips. Bioresource Technology, 106, 55-62.
- Fideles, R. A., Ferreira, G. M. D., Teodoro, F. S., Adarme, O. F. H., da Silva, L. H. M., Gil, L. F., & Gurgel, L. V. A. (2018). Trimellitated sugarcane bagasse: A versatile adsorbent for removal of cationic dyes from aqueous solution. Part I: Batch adsorption in a monocomponent system. Journal of colloid and interface science, 515, 172-188.

- Fontana, I. B., Peterson, M., & Cechinel, M. A. P. (2018). Application of brewing waste as biosorbent for the removal of metallic ions present in groundwater and surface waters from coal regions. Journal of environmental chemical engineering, 6(1), 660-670.
- Freundlich, H. M. F. (1906). Over the adsorption in solution. J. Phys. chem, 57(385471), 1100-1107.
- Fu, L., Li, J., Wang, G., Luan, Y., & Dai, W. (2021). Adsorption behavior of organic pollutants on microplastics. Ecotoxicology and Environmental Safety, 217, 112207.
- Fu, L., Li, J., Wang, G., Luan, Y., & Dai, W. (2021). Adsorption behavior of organic pollutants on microplastics. Ecotoxicology and Environmental Safety, 217, 112207.
- Gan, P. P., & Li, S. F. Y. (2012). Potential of plant as a biological factory to synthesize gold and silver nanoparticles and their applications. Reviews in Environmental Science and Bio/Technology, 11(2), 169-206.
- Gao, Y., Xu, S., Yue & Gao, B. (2016). Chemical preparation of crab shell-based activated carbon with superior adsorption performance for dye removal from wastewater. Journal of the Taiwan institute of chemical engineers, 61, 327-335.
- Ghaedi, M., Ghaedi, Ansari, A., Vafaei, A., & Rajabi, M. (2014). Random forest model for removal of bromophenol blue using activated carbon obtained from Astragalus bisulcatus tree. Journal of Industrial and Engineering Chemistry, 20(4), 1793-1803.
- Ghaedi, M., Khafri & Goudarzi, A. (2016). Response surface methodology approach for optimization of adsorption of Janus Green B Acta Part A: Molecular and Biomolecular Spectroscopy, 152, 233-240.

- Ghasemi, M., Keshtkar, A. R., Dabbagh, R., & Safdari, S. J. (2011). Sorption of uranium (VI) from aqueous solutions by Ca-pretreated Cystoseira indica alga: breakthrough curves studies and modeling. Journal of hazardous materials, 189(1-2), 141-149.
- Ghosh, K., Bar, N., Biswas, A. B., & Das, S. K. (2022). Removal of methylene blue by H3PO4Treated eucalyptus leaves: Study of continuous and GA-ANN modeling. Sustainable Chemistry and Pharmacy, 29, 100774.
- Goel, J., Kadirvelu, K., Rajagopal, C., & Garg, V. K. (2005). Removal of lead (II) by adsorption using treated granular activated carbon: batch and column studies. Journal of hazardous materials, 125(1-3), 211-220.
- Gopal, N., & Asaithambi, M. (2015). Fixed bed adsorption studies of Rhodamine-B dye using polymer bound adsorbent. Advances in Applied Science Research, 6(7), 65-73.
- Gopal, N., Asaithambi, M., Sivakumar, P., & Sivakumar, V. (2016). Continuous fixed bed adsorption studies of Rhodamine-B dye using polymer bound adsorbent, 23, 53-58.
- Grabi, H., Lemlikchi, W., Derridj, F., Lemlikchi, S., & Trari, M. (2021). Efficient native biosorbent derived from agricultural waste precursor for anionic dye adsorption in synthetic wastewater. Biomass Conversion and Biorefinery, 1-18.
- Guo, X., & Wang, J. (2019). A general kinetic model for adsorption: theoretical analysis and modeling. Journal of Molecular Liquids, 288, 111100.
- Gupta, K., Gupta, D., & Khatri, O. P. (2019). Graphene-like porous carbon nanostructure from Bengal gram bean husk and its application for fast and efficient adsorption of organic dyes. Applied Surface Science, 476, 647-657.

- Gupta, V. K., & Ali, I. (2012). Environmental water: advances in treatment, remediation and recycling, Chapter 2-Water treatment for inorganic pollutants by adsorption technology.
- Gupta, V. K., Ali, I., & Saini, V. K. (2007). Defluoridation of wastewaters using waste carbon slurry. Water Research, 41(15), 3307-3316.
- Gupta, V. K., Mittal, A., Krishnan, L., & Gajbe, V. (2004). Adsorption kinetics and column operations for the removal and recovery of malachite green from wastewater using bottom ash. Separation and purification technology, 40(1), 87-96.
- Gupta, V. K., Mohan, D., Suhas,† and, & Singh, K. P. (2006). Removal of 2-aminophenol using novel adsorbents. Industrial & engineering chemistry research, 45(3), 1113-1122.
- Haddad, K., Jellali, S., Jaouadi, S., Benltifa, M., Mlayah, A., & Hamzaoui, A. H. (2015). Raw and treated marble wastes reuse as low cost materials for phosphorus removal from aqueous solutions: Efficiencies and mechanisms. Comptes Rendus Chimie, 18(1), 75-87.
- Hadi, M., Samarghandi, M. R., & McKay, G. (2011). Simplified fixed bed design models for the adsorption of acid dyes on novel pine cone derived activated carbon. Water, Air, & Soil Pollution, 218(1), 197-212.
- Hall, K. R., Eagleton, L. C., Acrivos, A., & Vermeulen, T. (1966). Pore- and solid-diffusion kinetics in fixed-bed adsorption under constant-pattern conditions. Industrial & engineering chemistry fundamentals, 5(2), 212-223.
- Hamza, W., Chtara, C., & Benzina, M. (2015). Characterization and application of Fe and iso-Ti-pillared bentonite on retention of organic matter contained in wet industrial phosphoric acid (54%): kinetic study. Research on Chemical Intermediates, 41(9), 6117-6140.

- Hamza, W., Dammak, N., Hadjltaief, H. B., Eloussaief, M., & Benzina, M. (2018). Sono-assisted adsorption of Cristal Violet dye onto Tunisian Smectite Clay: Characterization, kinetics and adsorption isotherms. Ecotoxicology and Environmental Safety, 163, 365–371.
- Han, R., Wang, Y., Yu, W., Zou, W., Shi, J., & Liu, H. (2007). Sorption of methylene blue from aqueous solution by rice husk in a fixed-bed column. Journal of hazardous materials, 141(3), 713-718.
- Han, R., Wang, Y., Zhao, X., Wang, Y., Xie, F., Cheng, J., & Tang, M. (2009). Adsorption of methylene blue by phoenix tree leaf powder in a fixed-bed column: experiments and prediction of breakthrough curves. Desalination, 245(1-3), 284-297.
- Hanafiah, M. A. K. M., Mansur, N. F., Wan Ab Rahman, W. M. N., & Ismail, M. (2015). Methylene Blue Adsorption onto NaOH Treated Leucaena leucocephala Leaf Power. In Applied Mechanics and Materials (Vol. 752, pp. 251-256). Trans Tech Publications Ltd.
- Hasanzadeh, M., Ansari, R., & Ostovar, F. (2016). Synthesis and application of CeO2/sawdust nanocomposite for removal of As (III) ions from aqueous solutions using a continuous system. Glob. Nest J, 19, 7-16.
- Hashim, K. S., Shaw, A., Al Khaddar, R., Pedrola, M. O., & Phipps, D. (2017). Defluoridation of drinking water using a new flow column-electrocoagulation reactor (FCER)-Experimental, statistical, and economic approach. Journal of environmental management, 197, 80-88.
- Ho, Y. S., & McKay, G. (1998). A comparison of chemisorption kinetic models applied to pollutant removal on various sorbents. Process safety and environmental protection, 76(4), 332-340.
- Hossain, M. Y., Zhu,Sarker, S., Hassan, M. Cai, Y. (2021). Adsorption, kinetics, and thermodynamic studies of cacao husk extracts in waterless sustainable dyeing of cotton fabric. Cellulose, 28(4), 2521–2536.

- Hu, L., Peng, Y., Wu, F., Peng, S., Li, J., & Liu, Z. (2017). Tubular activated carbons made from cotton stalk for dynamic adsorption of airborne toluene. Journal of the Taiwan Institute of Chemical Engineers, 80, 399-405.
- Hu, Q., Pang, S., & Wang, D. (2021). In-depth Insights into Mathematical Characteristics, Selection Criteria and Common Mistakes of Adsorption Kinetic Models: A Critical Review. Separation & Purification Reviews, 1–19.
- Hu, X., Liu, S., Zhou, G., Huang, Y., Xie, Z., & Jing, X. (2014). Electrospinning of polymeric nanofibers for drug delivery applications. Journal of controlled release, 185, 12-21.
- Hunger, K. (Ed.). (2007). Industrial dyes: chemistry, properties, applications. John Wiley & Sons.
- Ibrahim, S., Shuy, W. Z., Ang, H. M., & Wang, S. (2010). Preparation of bioadsorbents for effective adsorption of a reactive dye in aqueous solution. Asia-Pacific Journal of Chemical Engineering, 5(4), 563-569.
- Ilyas, R. A., Sapuan, S. M., & Ishak, M. R. (2018). Isolation and characterization of nanocrystalline cellulose from sugar palm fibres (Arenga Pinnata). Carbohydrate polymers, 181, 1038-1051.
- Iqbal, J., Wattoo, F. H., Wattoo, M. H. S., Malik, R., Tirmizi, S. A., Imran, M., & Ghangro, A. B. (2011). Adsorption of acid yellow dye on flakes of chitosan prepared from fishery wastes. Arabian Journal of Chemistry, 4(4), 389-395.
- Jaafar, S. N. S. (2006). Adsorption study-dye removal using clay
- Jabar, J. M., Odusote, Y. A., Alabi, K. A., & Ahmed, I. B. (2020). Kinetics and mechanisms of congo-red dye removal from aqueous solution using activated Moringa oleifera seed coat as adsorbent. Applied Water Science, 10(6), 1-11.

- Jacob, J. M., Karthik, C., Saratale, R. G., Kumar, S. S., Prabakar, D., Kadirvelu, K., & Pugazhendhi, A. (2018). Biological approaches to tackle heavy metal pollution: a survey of literature. Journal of environmental management, 217, 56-70.
- Jain, H., Yadav, V., Rajput, V. D., Minkina, T., Agarwal, S., & Garg, M. C. (2022). An Eco-sustainable Green Approach for Sorption of Methylene Blue Dye from Textile Industry Wastewater by Sugarcane Bagasse, Peanut Hull, and Orange Peel: A Comparative Study Through Response Surface Methodology, Isotherms, Kinetic, and Thermocontinuous. Water, Air, & Soil Pollution, 233(6), 1-24.
- Jain, S. N., Tamboli, S. R., Sutar, D. S., Jadhav, S. R., Marathe, J. V., Shaikh, A. A., & Prajapati, A. A. (2020). Batch and continuous studies for adsorption of anionic dye onto waste tea residue: kinetic, equilibrium, breakthrough and reusability studies. Journal of Cleaner Production, 252, 119778.
- Javanbakht, V., & Shafiei, R. (2020). Preparation and performance of alginate/basil seed mucilage biocomposite for removal of eriochrome black T dye from aqueous solution. International journal of biological macromolecules, 152, 990-1001.
- Jawad, A. H& Radzun, K. A. (2018). Utilization of watermelon (Citrullus lanatus) rinds as a natural low-cost biosorbent for adsorption of methylene blue: kinetic, equilibrium and thermodynamic studies. Journal of Taibah University for Science, 12(4), 371-381.
- Jayalakshmi, R., & Jeyanthi, J. (2021). Dynamic modelling of Alginate-Cobalt ferrite nanocomposite for removal of binary dyes from textile effluent. Journal of Environmental Chemical Engineering, 9(1), 104924.

- Juela D. M., (2020). Comparison of the adsorption capacity of acetaminophen on sugarcane bagasse and corn cob by dynamic simulation.
- Kai Shen, M.A. Gondal, Removal of hazardous Rhodamine dye from water by adsorption onto exhausted coffee ground, (2017) ujJournal of Saudi Chemical Society, Volume 21, Supplement 1, Pages S120-S127,ISSN 1319-6103.
- Kajjumba, G. W. , Emik, S., Öngen, A., & Aydın, H. K. Ö. S. (2018). Modelling of Adsorption Kinetic Processes—Errors, Theory and Application. In (Ed.), Advanced Sorption Process Applications. IntechOpen. https://doi.org/10.5772/intechopen.80495.
- Kanda, M., Sridevi, V., Pamu, S. H., Tukaram Bai, M., & Prasad, K. S. N. (2022). Adsorption of Malachite Green from Aqueous Solution using Hen Feathers -Application of Different Mathematical Models to Continuous Biosorption. Journal of Environmental Treatment Techniques, 10(1), 116-123.
- Kassimi, A. E., Achour, Y., Himri, M. E., Laamari, M. R., & Haddad, M. E. (2021). High efficiency of natural Safiot Clay to remove industrial dyes from aqueous media: Kinetic, isotherm adsorption and thermodynamic studies. Biointerface Res. Appl. Chem, 11, 12717-12731.
- Kausar, A., Iqbal, M., Javed, A., Aftab, K., Bhatti, H. N., & Nouren, S. (2018). Dyes adsorption using clay and modified clay: a review. Journal of Molecular Liquids, 256, 395-407.
- Khalfa, L., Sdiri, A., Bagane, M., & Cervera, M. L. (2021). A calcined clay fixed bed adsorption studies for the removal of heavy metals from aqueous solutions. Journal of Cleaner Production, 278, 123935.

- Khan, S., & Malik, A. (2014). Environmental and health effects of textile industry wastewater. In Environmental deterioration and human health (pp. 55-71). Springer, Dordrecht.
- Khasri, A., Jamir, M. R. M., Ahmad, A. A., & Ahmad, M. A. (2021). Adsorption of Remazol Brilliant Violet 5R dye from aqueous solution onto melunak and rubberwood sawdust based activated carbon: interaction mechanism, isotherm, kinetic and thermodynamic properties. DWT, 216, 401-411.
- Kim, T. S., Song, H. J., Dar, M. A., Lee, H. J., & Kim, D. W. (2018). Fast adsorption kinetics of highly dispersed ultrafine nickel/carbon nanoparticles for organic dye removal. Applied Surface Science, 439, 364-370.
- Ko, D. C., Porter, J. F., & McKay, G. (2000). Optimised correlations for the fixed-bed adsorption of metal ions on bone char. Chemical engineering science, 55(23), 5819-5829.
- Kostić, M., Radović, M., Mitrović, J., Antonijević, M., Bojić, D., Petrović, M., & Bojić, A. (2014). Using xanthated Lagenaria vulgaris shell biosorbent for removal of Pb (II) ions from wastewater. Journal of the Iranian Chemical Society, 11(2), 565-578.
- Kuila, U., & Prasad, M. (2013). Specific surface area and pore-size distribution in clays and shales. Geophysical Prospecting, 61(2-Rock Physics for Reservoir Exploration, Characterisation and Monitoring), 341-362.
- Kumar, P. A., Chakraborty, S., (2009). "Fixed-bed column study for hexavalent chromium removal and recovery by short-chain polyaniline synthesized on jute fiber", Journal of Hazardous Materials, 162(2-3), 1086–1098.

- Kumar, P., Agnihotri, R., Wasewar, K. L., Uslu, H., & Yoo, C. (2012). Status of adsorptive removal of dye from textile industry effluent. Desalination and Water Treatment, 50(1-3), 226-244
- Kumar, R., & Ahmad, R. (2011). Sorption of hazardous crystal violet dye from aqueous solution onto treated ginger waste (TGW). Desalination, 265(1-3), 112-118.
- Kumari, R., & Dey, S. (2019). A breakthrough column study for removal of malachite green using coco-peat. International journal of phytoremediation, 21(12), 1263-1271.
- Kunz, A., Peralta-Zamora, P., Moraes, S. G. D., & Durán, N. (2002). New tendencies on textile effluent treatment. Quimica Nova, 25, 78-82.
- Kuppusamy, S., Thavamani, P., Megharaj, M., & Naidu, R. (2015). Bioremediation potential of natural polyphenol rich green wastes: a review of current research and recommendations for future directions. Environmental Technology & Innovation, 4, 17-28.
- Kyi, P. P., Quansah, J. O., Lee, C. G., Moon, J. K., & Park, S. J. (2020). The removal of crystal violet from textile wastewater using palm kernel shell-derived biochar. Applied Sciences, 10(7), 2251.
- Langmuir, I. (1918). The adsorption of gases on plane surfaces of glass, mica and platinum. Journal of the American Chemical society, 40(9), 1361-1403.
- Lee, C. C., & Lin, S. D. (2000). Handbook of environmental engineering calculations. New York: McGraw-Hill.
- Lellis, B., Fávaro-Polonio, C. Z., Pamphile, J. A., & Polonio, J. C. (2019). Effects of textile dyes on health and the environment and bioremediation potential of living organisms. Biotechnology Research and Innovation 3: 275–290.

- León, O., Muñoz-Bonilla, A., Soto, D., Pérez, D., Rangel, M., Colina, M., & Fernández-García, M. (2018). Removal of anionic and cationic dyes with bioadsorbent oxidized chitosans. Carbohydrate polymers, 194, 375-383.
- Li, F. T., Yang, H., Zhao, Y., & Xu, R. (2007). Novel modified pectin for heavy metal adsorption. Chinese Chemical Letters, 18(3), 325-328.
- Li, L., Wu, M., Song, C., Liu, L., Gong, W., Ding, Y., & Yao, J. (2021). Efficient removal of cationic dyes via activated carbon with ultrahigh specific surface derived from vinasse wastes. Bioresource Technology, 322, 124540 .
- Li, W., Zheng, P., Guo, J., Ji, J., Zhang, M., Zhang, Z., ... & Abbas, G. (2014). Characteristics of self-alkalization in high-rate denitrifying automatic circulation (DAC) reactor fed with methanol and sodium acetate. Bioresource technology, 154, 44-50.
- Liang, Z., Wang, J., Zhang, Y., Han, C., Ma, S., Chen, J., ... & An, T. (2020). Removal of volatile organic compounds (VOCs) emitted from a textile dyeing wastewater treatment plant and the attenuation of respiratory health risks using a pilot-scale biofilter. Journal of Cleaner Production, 253, 120019.
- Lignin, O. A., Albadarin, A. B., Mangwandi, C., Al-muhtaseb, A. H., Walker, G. M., Allen, S. J., & Ahmad, M. N. M. (2012). Modelling and continuous adsorption of Cr (VI) onto. Chinese Journal of Chemical Engineering, 20(3), 469–477. http://dx.doi.org/10.1016/S1004-9541(11)60208-5
- Liu, C. C., Li, Y. S., Chen, Y. M., Wang, M. K., San Chiou, C., Yang, C. Y., & Lin, Y. A. (2011). Sorption of chromium, copper and zinc on rice wine processing waste sludge in fixed bed. Desalination, 267(1), 20-24.

- Liu, M., Hou, L. A., Yu, S., Xi, B., Zhao, Y., & Xia, X. (2013). MCM-41 impregnated with A zeolite precursor: Synthesis, characterization and tetracycline antibiotics removal from aqueous solution. Chemical engineering journal, 223, 678-687.
- Liu, Q. X., Zhou, Y. R., Wang, M., Zhang, Q., Ji, T., Chen, T. Y., & Yu, D. C. (2019). Adsorption of methylene blue from aqueous solution onto viscose-based activated carbon fiber felts: Kinetics and equilibrium studies. Adsorption Science & Technology, 37(3-4), 312-332.
- López-Cervantes, J., Sánchez-Machado, D. I., Sánchez-Duarte, R. G., & Correa-Murrieta, M. A. (2018). Study of a fixed-bed column in the adsorption of an azo dye from an aqueous medium using a chitosan–glutaraldehyde biosorbent. Adsorption Science & Technology, 36(1-2), 215-232.
- Loulidi, I., Boukhlifi, F., Ouchabi, M., Amar, A., Jabri, M., Kali, A., ... & Aziz, F. (2020). Adsorption of crystal violet onto an agricultural waste residue: kinetics, isotherm, thermocontinuous, and mechanism of adsorption. The Scientific World Journal, 2020.
- Lu, F., & Astruc, D. (2020). Nanocatalysts and other nanomaterials for water remediation from organic pollutants. Coordination Chemistry Reviews, 408, 213180.)
- Luongo, G., Thorsén, G., & Östman, C. (2014). Quinolines in clothing textiles—a source of human exposure and wastewater pollution?. Analytical and bioanalytical chemistry, 406(12), 2747-2756..
- Ma, C. M., Hong, G. B., & Wang, Y. K. (2020). Performance evaluation and optimization of dyes removal using Rice bran-based magnetic composite adsorbent. Materials, 13(12), 2764.

- Mahamadi, C., & Nharingo, T. (2010). Competitive adsorption of Pb2+, Cd2+ and Zn2+ ions onto Eichhornia crassipes in binary and ternary systems. Bioresource technology, 101(3), 859-864.
- Malinauskiene, L., Bruze, M., Ryberg, K., Zimerson, E., & Isaksson, M. (2013). Contact allergy from disperse dyes in textiles–a review. Contact Dermatitis, 68(2), 65-75.
- Mansur, N. F., Megat Hanafiah, M. A. K., & Ismail, M. (2020). Pb (II) Adsorption onto Urea Treated Leucaena leucocephala Leaf Powder: Characterization, Kinetics and Isotherm Studies. Nature Environment & Pollution Technology, 19(1).
- Manzoor, J., & Sharma, M. (2020). Impact of textile dyes on human health and environment. In Impact of textile dyes on public health and the environment (pp. 162-169). IGI Global.
- Marcu, C., Varodi, C., & Balla, A. (2020). Adsorption Kinetics of Chromium (VI) from Aqueous Solution Using an Anion Exchange Resin. Analytical Letters, 54(1-2), 140–149.
- Marzbali, M. H., & Esmaieli, M. (2017). Fixed bed adsorption of tetracycline on a mesoporous activated carbon: Experimental study and neuro-fuzzy modeling. Journal of applied research and technology, 15(5), 454-463.
- Mashkoor, F., & Nasar, A. (2019). Preparation, characterization and adsorption studies of the chemically modified Luffa aegyptica peel as a potential adsorbent for the removal of malachite green from aqueous solution. Journal of Molecular Liquids, 274, 315-327.
- Mehta, D., Mondal, P., & George, S. (2016). Utilization of marble waste powder as a novel adsorbent for removal of fluoride ions from aqueous solution. Journal of Environmental Chemical Engineering, 4(1), 932-942.

- Mehta, S. K., & Gaur, J. P. (2005). Use of algae for removing heavy metal ions from wastewater: progress and prospects. Critical reviews in biotechnology, 25(3), 113-152.
- Milenković, D. D., Bojić, A. L., & Veljković, V. B. (2013). Ultrasound-assisted adsorption of 4-dodecylbenzene sulfonate from aqueous solutions by corn cob activated carbon. Ultrasonics sonochemistry, 20(3), 955-962.
- Mohammad Razi, M. A., Mohd Hishammudin, M. N. A., & Hamdan, R. (2017). Factor Affecting Textile Dye Removal Using Adsorbent From Activated Carbon: A Review. MATEC Web of Conferences, 103, 06015.
- Mohammed, A. A. (2015). Sorption of Lead, Cadmium, and Zinc onto Sunflower Shell: Equilibrium, Kinetic, and Thermodynamic Studies. Iraqi Journal of Chemical and Petroleum Engineering, 16(1), 91-105
- Mohammed, A. A., & Isra'a, S. S. (2018). Bentonite coated with magnetite Fe3O4 nanoparticles as a novel adsorbent for copper (II) ions removal from water/wastewater. Environmental Technology & Innovation, 10, 162-174.
- Mohammed, N. A., Abu-Zurayk, R. A., Hamadneh, I., & Al-Dujaili, A. H. (2018). Phenol adsorption on biochar prepared from the pine fruit shells: Equilibrium, kinetic and thermocontinuous studies. Journal of environmental management, 226, 377-385.
- Mohseni-Bandpi, A., Al-Musawi, T. J., Ghahramani, E., Zarrabi, M., Mohebi, S., & Vahed, S. A. (2016). Improvement of zeolite adsorption capacity for cephalexin by coating with magnetic Fe3O4 nanoparticles. Journal of Molecular Liquids, 218, 615-624.
- Moosavi, S., Gan, S. I. N. Y. E. E., & Zakaria, S. (2019). Functionalized cellulose beads with activated carbon Fe 3 O 4/CoFe 2 O 4 for cationic dye removal. Cellul. Chem. Technol, 53, 815-825.

- Moosavi, S., Lai, C. W., Akbarzadeh, O., & Johan, M. R. (2021). Recycled Activated Carbon-Based Materials for the Removal of Organic Pollutants from Wastewater. In Waste Recycling Technologies for Nanomaterials Manufacturing (pp. 513-539). Springer, Cham.
- Moosavi, S., Lai, C. W., Gan, S., Zamiri, G., Akbarzadeh Pivehzhani, O., & Johan, M. R. (2020). Application of efficient magnetic particles and activated carbon for dye removal from wastewater. ACS omega, 5(33), 20684-20697.
- Moosavi, S., Li, R. Y. M., Lai, C. W., Yusof, Y., Gan, S., Akbarzadeh, O., ... & Johan, M. R. (2020). Methylene blue dye photocatalytic degradation over synthesised Fe3O4/AC/TiO2 nano-catalyst: degradation and reusability studies. Nanomaterials, 10(12), 2360.
- Moyo, M., Pakade, V. E., & Modise, S. J. (2017). Sorption of lead (II) by chemically modified Mangifera indica seed shells: adsorbent preparation, characterization and performance assessment. Process Safety and Environmental Protection, 111, 40-51.
- Muhammad Farhan Hanafi, Norzahir Sapawe, (2020). A review on the water problem associate with organic pollutants derived from phenol, methyl orange, and remazol brilliant blue dyes, Materials Today: Proceedings, Volume 31, Part 1, Pages A141-A150, ISSN 2214-7853.
- Munagapati, V. S., Yarramuthi, V., Nadavala, S. K., Alla, S. R., & Abburi, K. (2010). Sorption of Cu (II), Cd (II) and Pb (II) by Acacia leucocephala bark powder: kinetics, equilibrium and thermocontinuous. Chemical Engineering Journal, 157(2-3), 357-365.

- Naderipour, A., Abdul-Malek, Z., Ahmad, N. A., Kamyab, H., Ashokkumar, V., Ngamcharussrivichai, C., & Chelliapan, S. (2020). Effect of COVID-19 virus on reducing GHG emission and increasing energy generated by renewable energy sources: A brief study in Malaysian context. Environmental technology & innovation, 20, 101151.
- Nagda, G. K., & Ghole, V. S. (2011). Removal of Janus Green dye from aqueous solution by phosphoric acid carbonized agro-industrial waste. Sci Asia, 37, 38-42.
- Nageeb, M. (2013). Adsorption Technique for the Removal of Organic Pollutants from Water and Wastewater. Organic Pollutants - Monitoring, Risk and Treatment. doi:10.5772/54048 url to share this paper: sci-hub.se/10.5772/54048
- Nakkeeran, E., Patra, C., Shahnaz, T., Rangabhashiyam, S., & Selvaraju, N. J. B. T. R. (2018). Continuous sorption assessment for the removal of hexavalent chromium from aqueous solutions using Strychnos nux vomica fruit shell. Bioresource Technology Reports, 3, 256-260.
- Naser, Dakhil, I. H., Ali, A. H., & Taha, A. H. (2021). Methylene Violet Dye Adsorption Using Onion Skins: Kinetics and Isotherm Studies. IOP Conference Series: Materials Science and Engineering, 1090(1), 012047.
- Nawaz, S., Bhatti, H. N., Bokhari, T. H., & Sadaf, S. (2014). Removal of Novacron Golden Yellow dye from aqueous solutions by low-cost agricultural waste: Batch and fixed bed study. Chemistry and Ecology, 30(1), 52-65.
- Nazifa, T. H., Habba, N., Aris, A., & Hadibarata, T. (2018). Adsorption of Procion Red MX-5B and Crystal Violet Dyes from Aqueous Solution onto Corncob Activated Carbon. Journal of the Chinese Chemical Society, 65(2), 259-270.

- Neag, E., Moldovan, A., Băbălău-Fuss, V., Török, A., Cadar, O., & Roman, C. (2019). Kinetic, Equilibrium and Phytotoxicity Studies for Dyes Removal by Low Cost Natural Activated Plant-Based Carbon. Acta Chimica Slovenica, 66(4), 850-858.
- Nishikawa, E., da Silva, M. G. C., & Vieira, M. G. A. (2018). Cadmium sorption by alginate extraction waste and process overview in life cycle assessment context. Journal of Cleaner Production, 178, 166-175.
- Noble, R. D., Noble, R. D., & Terry, P. A. (2004). Principles of chemical separations with environmental applications. Cambridge University Press.
- Novais, R. M., Ascensao, G., Tobaldi, D. M., Seabra, M. P., & Labrincha, J. A. (2018). Biomass fly ash geopolymer monoliths for effective methylene blue removal from wastewaters. Journal of Cleaner Production, 171, 783-794.
- Önal, Y., Akmil-Başar, C., Eren, D., Sarıcı-Özdemir, Ç., & Depci, T. (2006). Adsorption kinetics of malachite green onto activated carbon prepared from Tunçbilek lignite. Journal of hazardous materials, 128(2-3), 150-157.
- Ospina Álvarez, S. P., Ramírez Cadavid, D. A., Escobar Sierra, D. M., Ossa Orozco, C. P., Rojas Vahos, D. F., Zapata Ocampo, P., & Atehortúa, L. (2014). Comparison of extraction methods of chitin from Ganoderma lucidum mushroom obtained in submerged culture. BioMed research international, 2014.
- Özdemir, S., Mohamedsaid, S. A., Kılınç, E., & Soylak, M. (2019). Magnetic solid phase extractions of Co (II) and Hg (II) by using magnetized C. micaceus from water and food samples. Food chemistry, 271, 232-238.

- Padmesh, T. V. N., Vijayaraghavan, K., Sekaran, G., & Velan, M. (2005). Batch and column studies on sorption of acid dyes on fresh water macro alga Azolla filiculoides. Journal of Hazardous Materials, 125(1-3), 121-129.
- Pal, P. (2017). Industry-specific water treatment. Industrial Water Treatment Process Technology, 243-511.
- Parimelazhagan, V., Jeppu, G., & Rampal, N. (2021). Continuous Fixed-Bed Column Studies on Congo Red Dye Adsorption-Desorption Using Free and Immobilized Nelumbo nucifera Leaf Adsorbent. Polymers, 14(1), 54.
- Park, D., Yun, Y. S., & Park, J. M. (2010). The past, present, and future trends of biosorption. Biotechnology and Bioprocess Engineering, 15(1), 86-102.
- Parvathi, K., Nagendran, R., & Nareshkumar, R. (2007). Lead sorption onto waste beer yeast by-product: a means to decontaminate effluent generated from battery manufacturing industry. Electronic Journal of Biotechnology, 10(1), 92-105.
- Patel, H. (2020). Batch and continuous fixed bed adsorption of heavy metals removal using activated charcoal from neem (Azadirachta indica) leaf powder. Scientific Reports, 10(1), 1-12.
- Patel, H. (2021). Comparison of batch and continuous adsorption: a critical review. International Journal of Environmental Science and Technology, 1-18.
- Patil, A.K., Shrivastava, V.S., (2012). Kinetic and equilibrium studies on the adsorption of crystal violet dye using leucacena leucocephala (Subabul) seed pods as an adsorbent", Journal of Applied Research, 6 (4): 24-36.

- Pattnaik, P., Dangayach, G. S., & Bhardwaj, A. K. (2018). A review on the sustainability of textile industries wastewater with and without treatment methodologies. Reviews on Environmental Health, 33(2), 163-203.
- Pearce, C. I., Lloyd, J. R., & Guthrie, J. T. (2003). The removal of colour from textile wastewater using whole bacterial cells: a review. Dyes and pigments, 58(3), 179-196.
- Pernyeszi, T., Farkas, R., & Kovács, J. (2019). Methylene blue adsorption study on microcline particles in the function of particle size range and temperature. Minerals, 9(9), 555.
- Philip, P., Jose, T., Mathew, J. T., & Kuthanapillil, J. M. (2021). Multilayer adsorption and kinetic studies of dyes on pure and structurally modified poly (methyl methacrylate) electrospun nanofibers. Nano Futures, 5(2), 025005.
- Pholosi, A., Naidoo, E. B., & Ofomaja, A. E. (2020). Batch and continuous flow studies of Cr (VI) adsorption from synthetic and real wastewater by magnetic pine cone composite. Chemical Engineering Research and Design, 153, 806-818.
- Phuong, D. T. M., Loc, N. X., & Miyanishi, T. (2019). Efficiency of dye adsorption by biochars produced from residues of two rice varieties, Japanese Koshihikari and Vietnamese IR50404. Desalin. Water Treat, 165, 333-351.
- Picardo, M. C., de Melo Ferreira, A. C., & da Costa, A. C. A. (2009). Continuous thorium biosorption–Dynamic study for critical bed depth determination in a fixed-bed reactor. Bioresource Technology, 100(1), 208-210.

- Pirbazari, A. E., Saberikhah, E., & Kozani, S. H. (2014). Fe3O4–wheat straw: preparation, characterization and its application for methylene blue adsorption. Water Resources and Industry, 7, 23-37.
- Popa, S., Radulescu-Grad, M. E., Perdivara, A., & Mosoarca, G. (2021). Aspects regarding colour fastness and adsorption studies of a new azo-stilbene dye for acrylic resins. Scientific reports, 11(1), 1-9.
- Posner, S., & Jönsson, C. (2014). Chemicals in textiles-Risks to human health and the environment: Report from a government assignment.
- Qi, X., Wei, W., Li, J., Zuo, G., Pan, X., Su, T., ... & Dong, W. (2017). Salecan-based pH-sensitive hydrogels for insulin delivery. Molecular pharmaceutics, 14(2), 431-440.
- Qi, Y., Zhu, J., Fu, Q., Hu, H., & Huang, Q. (2017). Sorption of Cu by humic acid from the decomposition of rice straw in the absence and presence of clay minerals. Journal of Environmental Management, 200, 304-311.
- Rafatullah, M., Sulaiman, O., Hashim, R., & Ahmad, A. (2010). Adsorption of methylene blue on low-cost adsorbents: a review. Journal of hazardous materials, 177(1-3), 70-80.
- Rafique, T., Naseem, S., Usmani, T. H., Bashir, E., Khan, F. A., & Bhanger, M. I. (2009). Geochemical factors controlling the occurrence of high fluoride groundwater in the Nagar Parkar area, Sindh, Pakistan. Journal of Hazardous Materials, 171(1-3), 424-430.
- Raj, K. R., Kardam, A., Arora, J. K., Srivastava, S., & Srivastava, M. M. (2013). Adsorption behavior of dyes from aqueous solution using agricultural waste: modeling approach. Clean Technologies and Environmental Policy, 15(1), 73-80.

- Rápó, E., & Tonk, S. (2021). Factors affecting synthetic dye adsorption; desorption studies: A review of results from the last five years (2017–2021). Molecules, 26(17), 5419. (Rápó and Tonk, 2021)
- Rápó, E., Szép, R., Keresztesi, Á., Suciu, M., & Tonk, S. (2018). Adsorptive removal of cationic and anionic dyes from aqueous solutions by using eggshell household waste as biosorbent. Acta Chimica Slovenica, 65(3), 709-717.
- Ray, S. S., Gusain, R., & Kumar, N. (2020). Adsorption equilibrium isotherms, kinetics and thermocontinuous. Carbon Nanomaterial-Based Adsorbents for Water Purification, 101-118.,
- Reddy, M. S., Sivaramakrishna, L., & Reddy, A. V. (2012). The use of an agricultural waste material, Jujuba seeds for the removal of anionic dye (Congo red) from aqueous medium. Journal of hazardous materials, 203, 118-127.
- Regti, A., Laamari, M. R., Stiriba, S. E., & El Haddad, M. (2017). Use of response factorial design for process optimization of basic dye adsorption onto activated carbon derived from Persea species. Microchemical Journal, 130, 129-136.
- Rivera-Utrilla J, Sanchez-Polo M, Ferro-Garcia M, et al. (2013) Pharmaceuticals as emerging con-taminants and their removal from water: a review.Chemosphere93(7): 1268–1287.
- Roosta, M. A., Ghaedi, M. A., Shokri, N., Daneshfar, A., Sahraei, R., & Asghari, A. (2014). Optimization of the combined ultrasonic assisted/adsorption method for the removal of malachite green by gold nanoparticles loaded on activated carbon: experimental design. Spectrochimica Acta Part A: Molecular and Biomolecular Spectroscopy, 118, 55-65.

- Ryberg, K., Goossens, A., Isaksson, M., Gruvberger, B., Zimerson, E., Nilsson, F., ... & Bruze, M. (2009). Is contact allergy to disperse dyes and related substances associated with textile dermatitis?. British Journal of Dermatology, 160(1), 107-115.
- Ryberg, K., Isaksson, M., Gruvberger, B., Hindsén, M., Zimerson, E., & Bruze, M. (2006). Contact allergy to textile dyes in southern Sweden. Contact Dermatitis, 54(6), 313-321.
- Saad, M., Tahir, H., Khan, J., Hameed, U., & Saud, A. (2017). Synthesis of polyaniline nanoparticles and their application for the removal of crystal violet dye by ultrasonicated adsorption process based on response surface methodology. Ultrasonics sonochemistry, 34, 600-608.
- Sáez-Navarrete, C., Zamorano, A., Ferrada, C., & Rodriguez, L. (2009). Sulphate reduction and biomass growth rates for Desulfobacterium autotrophicum in yeast extract–Supplemented media at 38° C. Desalination, 248(1-3), 377-383.
- Salahshoor, Z., & Shahbazi, A. (2016). Modeling and optimization of cationic dye adsorption onto modified SBA-15 by application of response surface methodology. Desalination and Water Treatment, 57(29), 13615-13631.
- Sarı, A., & Tuzen, M. (2008). Sorption of cadmium (II) from aqueous solution by red algae (Ceramium virgatum): equilibrium, kinetic and thermodynamic studies. Journal of hazardous materials, 157(2-3), 448-454.
- Seader, J. D., Henley, E. J., & Roper, D. K. (1998). Separation process principles.

- Sebeia, N., Jabli, M., Ghith, A., & Saleh, T. A. (2020). Eco-friendly synthesis of Cynomorium coccineum extract for controlled production of copper nanoparticles for sorption of methylene blue dye. Arabian Journal of Chemistry, 13(2), 4263-4274.
- Şentürk, İ., & Alzein, M. (2020). Adsorption of acid violet 17 onto acid-activated pistachio shell: isotherm, kinetic and thermodynamic studies. Acta Chimica Slovenica, 67(1), 55-69.
- Shakoor, S., & Nasar, A. (2018). Adsorptive decontamination of synthetic wastewater containing crystal violet dye by employing Terminalia arjuna sawdust waste. Groundwater for Sustainable Development, 7, 30-38.
- Sharma, S. K. (Ed.). (2015). Green chemistry for dyes removal from waste water: research trends and applications.
- Sheng, L., Zhang, Y., Tang, F., & Liu, S. (2018). Mesoporous/microporous silica materials: preparation from natural sands and highly efficient fixed-bed adsorption of methylene blue in wastewater. Microporous and Mesoporous Materials, 257, 9-18.
- Siddiqui, S. I., Manzoor, O., Mohsin, M., & Chaudhry, S. A. (2019). Nigella sativa seed based nanocomposite-MnO2/BC: An antibacterial material for photocatalytic degradation, and adsorptive removal of Methylene blue from water. Environmental research, 171, 328-340.
- Silva, F., Nascimento, L., Brito, M., da Silva, K., Paschoal Jr, W., & Fujiyama, R. (2019). Sorption of methylene blue dye using natural biosorbents made from weeds. Materials, 12(15), 2486.
- Silva, W. L. L. D., & Oliveira, S. P. D. (2012). Modification of the adsorption characteristics of the sugarcane bagasse for the removal of methylene blue from aqueous solutions. Sci. Plena, 8, 1-9.

- Singh, D. K., Kumar, V., Mohan, S., Bano, D., & Hasan, S. H. (2017). Breakthrough curve modeling of graphene oxide aerogel packed continuous for the removal of Cr (VI) from water. Journal of water process engineering, 18, 150-158.
- Singh, K. J. N. P. A. (2018). TS Suresh Kumar M. Chem. Eng. J, 348, 67-73.
- Singh, P., Singh, S. K., Bajpai, J., Bajpai, A. K., & Shrivastava, R. B. (2014). Iron crosslinked alginate as novel nanosorbents for removal of arsenic ions and bacteriological contamination from water. Journal of Materials Research and Technology, 3(3), 195-202.
- Singh, S., Kapoor, D., Khasnabis, S., Singh, J., & Ramamurthy, P. C. (2021). Mechanism and kinetics of adsorption and removal of heavy metals from wastewater using nanomaterials. Environmental Chemistry Letters, 19(3), 2351–2381.
- Sivakumar, P., & Palanisamy, P. N. (2009). Packed bed column studies for the removal of Acid blue 92 and Basic red 29 using non-conventional adsorbent,16, 301-307
- Sivashankar, R., Thirunavukkarasu, A., Nithya, R., Kanimozhi, J., Sathya, A. B., & Sivasubramanian, V. (2020). Sequestration of methylene blue dye from aqueous solution by magnetic biocomposite: three level Box–Behnken experimental design optimization and kinetic studies. Separation Science and Technology, 55(10), 1752-1765.
- Sivashankar, R., Thirunavukkarasu, A., Nithya, R., Kanimozhi, J., Sathya, A. B., & Sivasubramanian, V. (2020). Sequestration of methylene blue dye from aqueous solution by magnetic biocomposite: three level Box–Behnken experimental design optimization and kinetic studies. Separation Science and Technology, 55(10), 1752-1765.

- Šljivić-Ivanović, M., & Smičiklas, I. (2020). Utilization of C&D waste in radioactive waste treatment—Current knowledge and perspectives. In Advances in Construction and Demolition Waste Recycling (pp. 475-500). Woodhead Publishing.
- Souza, N. K. (2013). Adsorption of Cationic and Anionic Dyes in Aqueous Solution Using New Bi-Functional Materials of Sugarcane Bagasse (Doctoral dissertation, Federal University of Ouro Preto).
- Soylak, M., Unsal, Y. E., & Tuzen, M. (2011). Spectrophotometric determination of trace levels of allura red in water samples after separation and preconcentration. Food and chemical toxicology, 49(5), 1183-1187.
- Suganya, S., Saravanan, A., & Ravikumar, C. (2017). Computation of adsorption parameters for the removal of dye from wastewater by microwave assisted sawdust: theoretical and experimental analysis. Environmental Toxicology and Pharmacology, 50, 45-57.
- Sun, H., Cao, L., & Lu, L. (2011). Magnetite/reduced graphene oxide nanocomposites: one step solvothermal synthesis and use as a novel platform for removal of dye pollutants. Nano Research, 4(6), 550-562.
- Sun, Q., & Yang, L. (2003). The adsorption of basic dyes from aqueous solution on modified peat–resin particle. Water research, 37(7), 1535-1544.
- Szende, T., Eszter, R. Környezeti Szennyez˝ok, Környezeti Problémák, Környezeti Remediáció, 1st ed. (2020). EXIT Kiadó: Cluj Napoca, Romania,; ISBN 978-606-9091-23-4.
- Taha, D. N., Mohammed, L. A., Farhood, A. S., & Ali, I. N. A. (2014). Adsorption of Janus green B dye from industrial waste water on the pistachio shells. life, 1, 2.

- Tan, K. L., & Hameed, B. H. (2017). Insight into the adsorption kinetics models for the removal of contaminants from aqueous solutions. Journal of the Taiwan Institute of Chemical Engineers, 74, 25-48.
- Temesgen, F., Gabbiye, N., & Sahu, O. (2018). Sorption of reactive red dye (RRD) on activated surface of banana and orange peels: economical alternative for textile effluent. Surfaces and interfaces, 12, 151-159.
- Ternes TA and Richardson SD (2018) Water analysis: Emerging contaminants and current issues.Analytical Chemistry90(1): 398–428.
- Thamer, B. M., Aldalbahi, A., Moydeen, M., El-Hamshary, H., Al-Enizi, A. M., & El-Newehy, M. H. (2019). Effective adsorption of Coomassie brilliant blue dye using poly (phenylene diamine) grafted electrospun carbon nanofibers as a novel adsorbent. Materials Chemistry and Physics, 234, 133-145.
- Thillainayagam, B. P., Saravanan, P., Ravindiran, G., & Josephraj, J. (2021). Continuous sorption of methylene blue dye from aqueous solution using effective microorganisms-based water hyacinth waste compost in a packed column. Biomass Conversion and Biorefinery, 1-10.
- Thirunavukkarasu, A., & Nithya, R. (2011). Response surface optimization of critical extraction parameters for anthocyanin from Solanum melongena. J Bioprocess Biotechniq, 1, 103.
- Thirunavukkarasu, A., & Nithya, R. (2019). Response surface optimization of Cu (II) sorption onto Candida tropicalis immobilized strontium alginate beads by Box-Behnken experimental design. J Environ Biotechnol Res, 8(2), 14-21.

- Thirunavukkarasu, A., Muthukumaran, K., & Nithya, R. (2018). Adsorption of acid yellow 36 onto green nanoceria and amine functionalized green nanoceria: comparative studies on kinetics, isotherm, thermocontinuous, and diffusion analysis. Journal of the Taiwan Institute of Chemical Engineers, 93, 211-225
- Thirunavukkarasu, A., Nithya, R., & Sivashankar, R. (2021). Continuous fixed-bed sorption process: a review. Chemical Engineering Journal Advances, 8, 100188.
- Thuong, N. T., Nhi, N. T. T., Nhung, V. T. C., Bich, H. N., Quynh, B. T. P., Bach, L. G., & Trinh, N. D. (2019). A fixed-bed column study for removal of organic dyes from aqueous solution by pre-treated durian peel waste. Indonesian Journal of Chemistry, 19(2), 486-494.
- Tonato, D., Drumm, F. C., Grassi, P., Georgin, J., Gerhardt, A. E., Dotto, G. L., & Mazutti, M. A. (2019). Residual biomass of Nigrospora sp. from process of the microbial oil extraction for the sorption of procion red H–E7B dye. Journal of Water Process Engineering, 31, 100818.
- Topare, N. S., & Bokil, S. A. (2021). Adsorption of textile industry effluent in a continuous using activated carbon prepared from agro-waste materials. Materials Today: Proceedings, 43, 530-534.
- Tran, H. T., Vu, N. D., Matsukawa, M., Okajima, M., Kaneko, T., Ohki, K., & Yoshikawa, S. (2016). Heavy metal sorption from aqueous solutions by algae inhabiting rice paddies in Vietnam. Journal of Environmental Chemical Engineering, 4(2), 2529-2535
- Uddin, M. T., Rukanuzzaman, M., Khan, M. M. R., & Islam, M. A. (2009). Adsorption of methylene blue from aqueous solution by jackfruit (Artocarpus heteropyllus) leaf powder: A fixed-bed column study. Journal of environmental management, 90(11), 3443-3450.

- Vickers, N. J. (2017). Animal communication: when i'm calling you, will you answer too?. Current biology, 27(14), R713-R715.
- Vieira, M. L., Martinez, M. S., Santos, G. B., Dotto, G. L., & Pinto, L. A. (2018). Azo dyes adsorption in continuous packed with different deacetylation degrees chitosan coated glass beads. Journal of Environmental Chemical Engineering, 6(2), 3233-3241.
- Vijayaraghavan, K., & Yun, Y. S. (2008). Bacterial biosorbents and biosorption. Biotechnology advances, 26(3), 266-291.
- Vijayaraghavan, K., Rangabhashiyam, S., Ashokkumar, T., & Arockiaraj, J. (2017). Assessment of samarium sorption from aqueous solution by brown macroalga Turbinaria conoides. Journal of the Taiwan Institute of Chemical Engineers, 74, 113-120.
- Vikrant, K., Giri, B. S., Raza, N., Roy, K., Kim, K. H., Rai, B. N., & Singh, R. S. (2018). Recent advancements in bioremediation of dye: current status and challenges. Bioresource technology, 253, 355-367.
- Vinodhini, V., & Das, N. (2010). Packed bed column studies on Cr (VI) removal from tannery wastewater by neem sawdust. Desalination, 264(1-2), 9-14.
- Vital RK, Saibaba KVN, Shaik KB, R Gopinath (2016) Dye Removal by Adsorption: A Review. J Bioremediat Biodegrad 7: 371.
- Walker, G. M., & Weatherley, L. R. (2000). Biodegradation and sorption of acid anthraquinone dye. Environmental pollution, 108(2), 219-223.
- Wang, J., & Chen, C. (2009). Biosorbents for heavy metals removal and their future. Biotechnology advances, 27(2), 195-226
- Wang, W., & Wang, J. (2018). Comparative evaluation of sorption kinetics and isotherms of pyrene onto microplastics. Chemosphere, 193, 567-573.

- Wang, X. S., Li, Z. Z., & Tao, S. R. (2009). Removal of chromium (VI) from aqueous solution using walnut hull. Journal of Environmental Management, 90(2), 721-729.
- Wang, Y. X., Ngo, H. H., & Guo, W. S. (2015). Preparation of a specific bamboo based activated carbon and its application for ciprofloxacin removal. Science of the Total Environment, 533, 32-39.
- Warren, L. and Harriot, P. (1993). Unit operation of chemical engineering. McGraw-Hill.
- Weber and Chakravorti, (1974). Pore and solid diffusion models for fixed- bed adsorbers, AIChE J., vol. 20, no. 2, pp. 228–238, doi: 10.1002/aic.690200204.
- Wong, S., Yac'cob, N. A. N., Ngadi, N., Hassan, O., & Inuwa, I. M. (2018). From pollutant to solution of wastewater pollution: Synthesis of activated carbon from textile sludge for dye adsorption. Chinese Journal of Chemical Engineering, 26(4), 870-878.
- Wu, F. C., Tseng, R. L., & Juang, R. S. (2009). Characteristics of Elovich equation used for the analysis of adsorption kinetics in dye-chitosan systems. Chemical Engineering Journal, 150(2-3), 366-373.
- Xiang, X., Chen, X., Dai, R., Luo, Y., Ma, P., Ni, S., & Ma, C. (2016). Anaerobic digestion of recalcitrant textile dyeing sludge with alternative pretreatment strategies. Bioresource technology, 222, 252-260.
- Xiao, W., Garba, Z. N., Sun, S., Lawan, I., Wang, L., Lin, M., & Yuan, Z. (2020). Preparation and evaluation of an effective activated carbon from white sugar for the adsorption of rhodamine B dye. Journal of Cleaner Production, 253, 119989.
- Xiao, Y., Azaiez, J., (2018). Erroneous Application of Pseudo-Second-Order Adsorption Kinetics Model: and Spurious Correlations. Industrial & Engineering Chemistry Research, 57(7), 2705–2709.

- Xiao, Y., Azaiez, J., & Hill, J. M. (2018). Erroneous Application of Pseudo-Second-Order Adsorption Kinetics Model: Ignored Assumptions and Spurious Correlations. Industrial & Engineering Chemistry Research, 57(7), 2705–2709.
- Yadav, D., Kapur, M., Kumar, P., & Mondal, M. K. (2015). Adsorptive removal of phosphate from aqueous solution using rice husk and fruit juice residue. Process Safety and Environmental Protection, 94, 402-409.
- Yagub, M. T., Sen, T. K., Afroze, S., & Ang, H. M. (2014). Dye and its removal from aqueous solution by adsorption: a review. Advances in colloid and interface science, 209, 172-184.
- Yang, G., Wu, L., Xian, Q., Shen, F., Wu, J., & Zhang, Y. (2016). Removal of congo red and methylene blue from aqueous solutions by vermicompost-derived biochars. PLoS One, 11(5), e0154562.
- Yoon, Y. H., & Nelson, J. H. (1984). Application of gas adsorption kinetics I. A theoretical model for respirator cartridge service life. American industrial hygiene association journal, 45(8), 509-516.
- Yunnen, C., Ye, W., Chen, L., Lin, G., Jinxia, N., & Rushan, R. (2017). Continuous Fixed-Bed Column Study and Adsorption Modeling: Removal of Arsenate and Arsenite in Aqueous Solution by Organic Modified Spent Grains. Polish Journal of Environmental Studies, 26(4).
- Yusuff, A.S. (2019). Adsorption of hexavalent chromium from aqueous solution by Leucaena leucocephala seed pod activated carbon: equilibrium, kinetic and thermodynamic studies. Arab Journal of Basic and Applied Sciences, 26:1, 89-102, DOI: 10.1080/25765299.2019.1567656.
- Zeraatkar, A. K., Ahmadzadeh, H., Moheimani, N. R., & McHenry, M. P. (2016). Potential use of algae for heavy metal bioremediation, a critical review. Journal of environmental management, 181, 817-831.

- Zhang, B., Ma, Z., Yang, F., Liu, Y., & Guo, M. (2017). Adsorption properties of ion recognition rice straw lignin on PdCl42−: Equilibrium, kinetics and mechanism. Colloids and Surfaces A: Physicochemical and Engineering Aspects, 514, 260-268.
- Zhang, S., Wang, Z., Zhang, Y., Pan, H., & Tao, L. (2016). Adsorption of methylene blue on organosolv lignin from rice straw. Procedia Environmental Sciences, 31, 3-11.
- Zhao, P., Zhang, G., & Hao, L. (2020). A novel blended amine functionalized porous silica adsorbent for carbon dioxide capture. Adsorption, 26(5), 749-764.
- Zheng, Y., Cheng, B., You, W., Yu, J., & Ho, W. (2019). 3D hierarchical graphene oxide-NiFe LDH composite with enhanced adsorption affinity to Congo red, methyl orange and Cr (VI) ions. Journal of hazardous materials, 369, 214-225.
- Zulfadhly, Z., Mashitah, M. D., & Bhatia, S. (2001). Heavy metals removal in fixed-bed column by the macro fungus Pycnoporus sanguineus. Environmental Pollution, 112(3), 463-470.

اقرار لجنة المناقشة

نحن أعضاء لجنة المناقشة ، نشهد بأننا اطلعنا على رسالة الماجستير الموسومة " أزالة الصبغات العضوية من المحاليل المائية بأستخدام مخلفات نباتية " وقد ناقشنا الطالب في محتوياتها وفيما له علاقة بها ، نؤيد انها جديرة بالقبول لنيل درجة الماجستير علوم في الهندسة البيئية.

رئيس اللجنة	**عضو اللجنة**
التوقيع :	**التوقيع :**
الاسم : : أ.د. سيف صلاح مهدي القزويني	**الاسم : : أ.م.د. طارق جواد كاظم الموسوي**
التاريخ:	**التاريخ :**
عضو اللجنة	**عضو اللجنة (مشرفاً)**
التوقيع :	**التوقيع :**
الاسم : أ.م.د. حسين علي مهدي الزبيدي	**الاسم : أ.د. إسراء سعدي عبد الأمير سماكه**
التاريخ:	**التاريخ :**
مصادقة رئيس القسم	**مصادقة عميد الكلية**
التوقيع :	**التوقيع :**
الاسم : أ.م.د. حسين علي مهدي الزبيدي	**الاسم : أ.د.حاتم هادي عبيد**
التاريخ :	**التاريخ :**

اقـــــرار المشرف

اشهد ان اعداد هذه الرسالة والموسومة بـــ (أزالة الصبغات العضوية من المحاليل المائية بأستخدام مخلفات نباتية) والمقدمة من قبل الطالب (سامر حسين محمد جاسم) جرت تحت اشرافي في قسم هندسة البيئة / كلية الهندسة / جامعة بابل وهي جزء من متطلبات نيل درجة الماجستير علوم في الهندسة البيئية.

التوقيع:

المشرف: أ.د. اسراء سعدي عبد الامير سماكه

التاريخ : / /٢٠٢٣

اشهد ان هذه الرسالة المذكورة اعلاه قد استكملت في هندسة البيئة في كلية الهندسة / جامعة بابل

التوقيع:

رئيس القسم: أ.م.د. حسين علي مهدي الزبيدي

التاريخ : / /٢٠٢٣

الخلاصـــــــــة

تهدف الدراسة الحالية التحري عن امكانية تطوير قدرة النبات الطبيعي (قشور بذور نبات اللوسينيا) على الامتزاز الحيوي لصبغتي(JGBD) Janus green B dye و Crystal violate dye (CVD) من مياه الصرف الصحي، باعتبار ان هذا النبات طبيعي، منخفض الكلفة و متوفر بكثرة في العديد من مناطق العراق.

تم استخدام سلسلة من التجارب المختبرية التي انقسمت الى قسمين الاول هو تجارب الدُفعات و الثاني تجارب التدفق المستمر و ذلك من اجل تقييم المعالجات المحتملة و المتغيرات التي قد تأثر على الامتزاز الحيوي للاصباغ في المحاليل المائية باستخدام هذه المادة المازة. تم استخدام تقنيات و فحوصات عديدة من اجراء فحوصات التمييز للعينات قبل و بعد ازالة الصبغتين، من بين هذه الفحوصات هو فحص المساحة السطحية (S_{BET}) و جهاز التحليل الطيفي بالاشعة تحت الحمراء (FTIR) و المسح المجهري الإلكتروني (SEM) و مجهر المسح الضوئي (SPM) في دراسة الدُفعات تم دراسة مجموعة من العوامل المؤثرة على الامتزاز الحيوي للصبغتين في درجه حراره الغرفة.

من بين هذه العوامل تم دراسة عامل الاس الهيدروجيني pH لمحلول الصبغة، وقت التلامس، جرعة المادة المازة و تركيز الصبغة الاولي. تم اختيار انسب الظروف للامتزاز الحيوي عند pH 9 بالنسبة للصبغتين، جرعة LLSP 0.08 g/100 l لصبغة JGBD و 0.3 g/100 l لصبغة CVD، لوقت قياس 30 دقيقة، 45 دقيقة بالنسبة الى JGBD و CVD، على التوالي. تم تحليل البيانات التجريبية بواسطة نموذجي الايزوثرم Langmuir و Freundlich، من بين الموديلين تم اختيار Langmuir لأنه اكثر توافق مع البيانات التجريبية ليكون افضل نموذج لمحاكاة امتزاز الصبغتين بواسطة LLSP ، حيث وجد ثابت Langmuir للامتزاز الحيوي (q_{max}) البالغ 142.85 mg/g 45.45 mg/g, و بلغ معامل التحديد (R^2) 0.9906, 0.9996 بالنسبة الى JGBD و CVD, على التوالي. تمت محاكاة النموذج (Pseudo second order) للبيانات التجريبية بشكل افضل من النماذج الاخرى حيث كانت قيم الامتزاز الحيوي تشير الى الامتزاز الكيمياوي و كذلك عملية الانتشار داخل الجسيمات. بالنسبة لتجارب عمود الحشوة الثابتة تم تغيير معدل التدفق، ارتفاع الحشوة و تركيز الصبغة الاولي. اظهرت بيانات العمود التي تم تحليلها ان منحنيات الاختراق تأثرت كثيراً بهذه العوامل. تم استخدام نموذج (BDST) Time, Thomas Bed Depth Surface, Yoon-Nelson الحركية لتحليل بيانات العمود التجريبية. تم الحصول على قيم عالية بالنسبة الى (R^2) لجميع النماذج الحركية التي تم

استخدامها و كان الانحراف بين القيم التجريبية و القيم المقدرة بواسطة هذه النماذج قليلة جداً. في النهاية تم استنتاج بان مادة مازة ذات قدرة عالية على ازالة JGBD و CVD من المحاليل المائية.

جمهورية العراق
وزارة التعليم العالي والبحث العلمي
جامعة بابل
كلية الهندسة
قسم الهندسة البيئية

أزالة الصبغات العضوية من المحاليل المائية بأستخدام مخلفات نباتية

رسالة مقدمة الى
قسم الهندسة البيئية في كلية الهندسة
في جامعة بابل كجزء من متطلبات نيل
درجة ماجستير في الهندسة / الهندسة البيئية

اعداد

سامر حسين محمد جاسم

اشراف

أ.د. اسراء سعدي عبد الامير سماكه

1444 هـ **2023 م**